Development of coatings rich in primary amines for biomedical applications

Laurine Martocq

This dissertation is submitted for the degree of Doctor of Philosophy

April 2023

School of Engineering

Declaration

This thesis has not been submitted in support of an application for another degree at this or any other university. It is the result of my own work and includes nothing that is the outcome of work done in collaboration except where specifically indicated. Many of the ideas in this thesis were the product of discussion with my supervisors Dr. Timothy Douglas and Dr. Alexander Robson.

This multidisciplinary research was made possible with different collaborations including:

- Dr. Anna Mieszkowska from Jagiellonian University in Krakow (Poland) and Dr. Katarzyna Gurzawska-Comis from University of Birmingham (UK) for cell test studies.
- Dr. Ute Hempel from Technische Universität Dresden (Germany) for cell test studies.
- Dr. Bethany Lee Patenall from Bath University (UK) for the study of the minimum inhibitory concentration of PG.
- Prof. James Bradley, Dr. Mike Barnes, and Dr. Stephane Simon from the University of Liverpool (UK) for making and bringing plasma polymer coatings to Lancaster University for XPS analyses and chemical derivatisation to allow a comparison with samples made at Lancaster. They also performed the plasma phase study at the University of Liverpool.

Publications

Excerpts of this thesis have been published or will be published in the following academic publications.

Barnes, M.; J., Simon, S.; Martocq, L.; Robson, A.J.; Short, R.D.; Bradley, J.W., *In preparation*.

Martocq, L.; Wood, B.; Danos, L.; Robson, A.J.; Short, R.D. Functionalisation of allylamine plasma polymer coatings via TFBA derivatisation. *To be submitted in Chemcomm*.

Facchetti, D.; Hempel, U.; Martocq, L.; Smith, A.M.; Koptyug, A.; Surmenev, R.A.; Surmeneva, M.A.; Douglas, T.E.L. Heparin Enriched-WPI Coating on Ti6Al4V Increases Hydrophilicity and Improves Proliferation and Differentiation of Human Bone Marrow Stromal Cells. *International Journal of Molecular Sciences.* **2022**, *23*, 139, doi:10.3390/ijms23010139.

Martocq, L.; Douglas, T.E.L. Amine-Rich Coatings to Potentially Promote Cell Adhesion, Proliferation and Differentiation, and Reduce Microbial Colonization: Strategies for Generation and Characterization. *Coatings*. **2021**, *11*, 983, doi:10.3390/coatings11080983.

Mieszkowska, A.; Beaumont, H.; Martocq, L.; Koptyug, A.; Surmeneva, M.A.; Surmenev, R.A.; Naderi, J.; Douglas, T.E.L.; Gurzawska-Comis, K.A. Phenolic-Enriched Collagen Fibrillar Coatings on Titanium Alloy to Promote Osteogenic Differentiation and Reduce Inflammation. *International Journal of Molecular Sciences.* **2020**, *21*, 6406, doi:10.3390/ijms21176406.

Rabe, R.; Hempel, U.; Martocq, L.; Keppler, J.K.; Aveyard, J.; Douglas, T.E.L. Dairy-Inspired Coatings for Bone Implants from Whey Protein Isolate-Derived Self-Assembled Fibrils. *International Journal of Molecular Sciences.* **2020**, *21*, 5544, doi:10.3390/ijms21155544.

Presentations

Oral presentations

"Development of amine-rich coatings for antimicrobial surfaces", Engineering Postgraduate Research Conference (1-4th July 2020), Lancaster University, online.

"Titanium alloy coated with phloroglucinol-enriched collagen fibrils regulates osteogenic differentiation and inflammation", 29th Annual Conference Biomaterials in Medicine and Veterinary Medicine (15-18th October 2020), Poland, online.

"Development of amine-rich coatings for antimicrobial applications", UK-Poland Bioinspired Materials Conference (23-24th November 2020), Lancaster University, online.

"Development of amine-rich coatings for antimicrobial applications", Engineering Postgraduate Research Conference (30-1st July 2021), Lancaster University, online.

"Development of whey protein fibrillar coatings on biomaterials for antimicrobial applications", Material Science Institute PhD Conference (7th October 2021), Lancaster University, UK.

"Development of whey protein fibrillar coatings on biomaterials for antimicrobial applications", UK-Russia Conference "Advanced biomaterials to combat cancer" (8-10th December 2021), Lancaster, UK.

"Development of amine-rich coatings for biomedical applications", Engineering Postgraduate Conference (6-7th July 2022), Lancaster University, UK. (award: 2nd Prize of the 3rd-year PGRs)

"*Development of coatings rich in primary amines for biomedical application*s", UK-Poland-Ukraine Bioinspired Materials Conference (29-30th November 2022), online.

"*Development of coatings rich in primary amines for biomedical application*s", 20 minutes of Engineering (7th December 2022), Lancaster University, UK.

Poster presentations

"Development of phloroglucinol enriched-collagen fibril coatings for antimicrobial applications", 11th World Biomaterials Congress (11-15th December 2020), online.

"Development of whey protein fibrillar coatings enriched with phloroglucinol to fight microbial contamination", Postgraduate Research Conference (17th July 2021), Lancaster University, online.

"Development of coatings made of self-assembled whey protein fibrils for biomedical applications", Bordeaux Polymer Conference (13-16th June 2022), Bordeaux, France.

"Allylamine plasma polymer coatings for biomedical applications", International Conference on Plasma Medicine (26-1st July 2022), Utrecht, The Netherlands.

Abstract

Biomaterials, such as hip prostheses or dental implants, must be well tolerated by the recipient, i.e., they must not cause inflammation, allergy, or a rejection reaction. The long-term success of a biomaterial largely depends on its integration into the body tissues due to adhesion of tissue-forming cells on the biomaterial's surface, their proliferation, and differentiation to form tissue-specific extracellular matrix. Biomaterial surfaces govern their interaction with surrounding tissues, which can be tailored by modifying the surfaces. Microbial infection must also be prevented due to the growing threat of antibiotic-resistant bacteria. In this project, coatings rich in primary amine groups (-NH_2) were developed via two different strategies.

The first method involved plasma polymerisation. Allylamine plasma polymer coatings (AApp) were deposited with the usual collisionless α regime vs. the collisional γ regime. The atomic composition of the coatings was characterised by XPS. -NH_2 groups were quantified by a chemical derivatisation technique. Results showed that AApp coatings produced with the γ regime led to a higher degree of -NH_2 retention. Therefore, the γ regime may be suitable to use during plasma polymerisation to obtain coatings rich in -NH_2.

The second method involved deposition of whey protein isolate (WPI) fibrillar coatings. Fibrils withstood autoclave sterilisation and were used as a matrix to incorporate biomolecules such as phloroglucinol (PG) and tannic acids (TAs). The presence of the coatings was attested by SEM images and XPS analyses. WPI/PG coatings improved bone forming-cell behaviour by increasing gene expression relative to matrix formation and mineralisation as well as by reducing the inflammatory response. WPI/TAs coatings did not have a negative impact on cell viability and might improve osteogenic differentiation.

These amine-rich coatings may be applied on biomaterials such as bone implants to improve cell behaviour, but further work needs to be done to endow them with antimicrobial properties.

Acknowledgements

This multidisciplinary research was made possible by funding from Lancaster University and the Engineering and Physical Sciences Research Council, as well as the many people involved to whom I would like to express my gratitude.

First of all, I would like to thank my supervisors Dr. Tim Douglas and Dr. Alex Robson for giving me the opportunity to do this PhD, as well as for their support and guidance throughout my PhD. Thank you very much for all the time and advice you have given me.

I would like to thank Prof. Rob Short for his guidance regarding plasma polymers and XPS analyses. I would also like to thank Dr. John Hardy for taking part in the appraisal panel and providing support and guidance during these three years.

I would also like to thank all the people involved, including Dr. Sara Baldock for the SEM images, Dr. Roman Surmenev for providing Ti alloy substrates, Dr. Bethany Pathenall for the microbiology work, Dr. Jackie Parry for her training on microbiology basics and the opportunity to work in her lab, Amy Crisp and Dr. Craig Williams for giving me the opportunity to work at the Department of Pathology of the Royal Infirmary Hospital at Lancaster.

I would also like to thank Ben Wood and Dr. Lefteris Danos for their collaboration in using their glovebox, as well as Prof. James Bradley, Dr. Mike Barnes, and Dr. Stephane Simon for bringing samples from Liverpool to Lancaster for analyses and their plasma phase analyses. I would like to thank all the people involved in cell tests including Dr. Anna Mieskowska, Dr. Katarzyna Gurzawska-Comis and Dr. Ute Hempel.

Thank you to Charles Weir of Lancaster University, UK and to Kayla Friedman and Malcolm Morgan of the University of Cambridge for producing the Microsoft Word thesis template used to produce this document.

Finally, a big thank you to my family and friends who always support me. Merci à tous mes amis de longue date que j'ai la chance d'avoir : Camille.B, Julie, Lucy,

Marina, Léna, Camille.G, Myriam, Alex, Raf, Richard, Rémi, toujours partants pour se retrouver à mes retours en France. Je remercie énormément Romain pour son soutien durant ces trois ans sans qui rien aurait été pareil, et maintenant bientôt ton tour... Et le meilleur pour la fin, merci à mes parents pour leur soutien tout le long de mes études, sans vous je n'aurai pas pu atteindre ce niveau, c'est grâce à vous alors merci x1000. Merci aussi à mon frère pour son soutien et si tu veux savoir si j'ai trouvé, je t'invite à lire les prochaines pages... Good luck bro! Maman, Papa, Flo, cette thèse est pour vous !

Contents

List of Tables

List of Figures

List of Abbreviations and Acronyms

AApp	Allylamine plasma polymer
ADECA	Amino density estimation by colorimetric assay
AgNPs	Silver nanoparticles
AL2	ALSOK2
AL4	ALSOK4
ALDpp	Aldehyde plasma polymer
ALP	Alkaline phosphatase
AFM	Atomic force microscopy
AS	Artificial saliva
BGLAP	Bone gamma-carboxyglutamate protein
BM-MSCs	Human bone marrow-derived mesenchymal stem cells
BRW	Brewtan F
CA	Contact angle
COL1A1	Collagen type I alpha 1 chain
CPS	Counts per second
CS	Chondroitin sulphate
DST	Diagnostic Sensitivity Test
EBM®	Electron beam melting
EGF	Epidermal growth factor
EPS	Extracellular polymeric substances
ESCA	Electron spectroscopy for chemical analysis
FEG-SEM	Field Emission Scanning Electron Microscope
FN	Fibronectin

FTIR	Fourier-transform infrared spectroscopy
hBMSCs	Human bone marrow stromal cells
HCAI	Healthcare-associated infection
hMSCs	Human mesenchymal stromal cells
HMDS	Hexamethyldisilizane
IL1a	Interleukin 1 alpha
IL1b	Interleukin 1 beta
IL8	Interleukin 8
LB	Luria-Bertani
N6	Nylon 6
OP	Osteopontin
PBS	Phosphate-buffered saline
PDA	Polydopamine
PEG	Polyethylene glycol
PEI	Polyethyleneimine
PET	Polyethylene terephthalate
PG	Phloroglucinol
PGG	Pentagalloyl glucose
PP	Plasma polymerisation
PS	Polystyrene
PTFE	Polytetrafluoroethylene
RF	Radiofrequency
RUNX	Runt-related transcription factor
SEM	Scanning electron microscopy

SF	Silk fibroin
TAs	Tannic acids
TFBA	4-trifluoromethyl-benzaldehyde
TNAP	Tissue non-specific alkaline phosphatase
VSMCs	Vascular smooth muscle cells
WCA	Water contact angle
WPI	Whey protein isolate
XPS	X-ray photoelectron spectroscopy
ZOI	Zone of inhibition

List of Appendices

Chapter 1. Introduction and thesis objectives

Biomaterials are materials that can be used for medical purposes to replace a part or function of an organ or tissue (for example hip prostheses, dental implants, etc). They must be well tolerated by the recipient, i.e., they must not cause infection, inflammation, allergy, or even a rejection reaction, and be well integrated into the body tissues. For example, a metallic implant for bone contact must be stable for the long term, hence the success of the implantation is dependent on the formation of new tissues at the implant surface. The surface of biomaterials governs their compatibility within the body. Biomaterial surface modification represents an important approach to change the surface properties in order to obtain a better integration of the material in surrounding tissues by improving cell adhesion, proliferation, and differentiation, as well as by keeping the bulk properties. Different techniques are focused on improving cell support as well as avoiding efficiently the development of infections, such as by modifying the biomaterial surface with primary amine groups (–NH_2). Previous studies showed that –NH_2 groups could promote cell adhesion and proliferation. Moreover, these chemical functionalities may be used to facilitate the attachment of biomolecules to endow new properties such as antimicrobial activity.

In this context, my project involved development of new coatings rich in primary amines for biomedical applications. Two different strategies were used with plasma technology and protein fibrils. The objectives of this thesis are:

- To identify the most appropriate plasma regime to use to produce coatings rich in primary amines: the usual collisionless α regime with low pressure and high power vs. the collisional γ regime with high pressure and low power.

- To study the atomic composition of the different coatings as well as quantify and compare the density of primary amine groups.
- To produce and characterise whey protein fibrillar coatings including stability and physicochemical composition.
- To enhance whey protein isolate fibrillar coatings with other biomolecules such as phloroglucinol and tannic acids.
- To study the effect of whey protein isolate fibrillar coatings containing additional biomolecules on cells.
- To assess antimicrobial activity of whey protein fibrillar coatings containing additional biomolecules.

To answer these objectives, my thesis was divided into different chapters:

Chapter 2 presents the background and literature review. This gives an overview of biomaterials and the importance of surface modification. Moreover, different techniques to obtain amine-rich coatings such as plasma methods and adsorption of biomolecules were described. Different plasma treatment methods are commonly used with ammonia gas or by polymerisation of precursors such as allylamine, as well as coatings of proteins (for example, collagen) or polymers containing $-NH_2$ groups (for example, polyethyleneimine). Finally, this literature review presents the methods used to characterise such coatings and, in particular, quantify the $-NH_2$ groups present on the surface by using dyes or chemical derivatisation methods.

Chapter 3 deals with the results on the production and characterisation of allylamine plasma polymer coatings. These coatings were produced by using different plasma regimes with high pressure/low power and low pressure/high power to compare their chemical composition. The chemical characterisation of the coatings was analysed by using X-ray photoelectron spectroscopy. Moreover, the quantification of primary amines by chemical derivatisation was studied.

Chapter 4 shows the study of whey protein fibrillar coatings and their physicochemical characterisation. The stability of the fibrils was studied, and different biomolecules were added such as phloroglucinol and tannic acids.

Finally, biological tests were performed to assess the effect of the coatings on bone-forming cells and bacteria.

Chapter 2. Background and literature review

2.1. Introduction

The use of implants or medical devices in the human body may cause problems of integration with surrounding tissues as well as infections due to microbial colonisation. The World Health Organisation estimates that out of every 100 hospitalised patients, 7 in developed and 10 in developing countries will acquire at least one healthcare-associated infection (HCAI) [1]. HCAIs are infections acquired during hospitalisation and represent one of the leading causes of death. The increase in HCAIs is mainly due to the problem of antimicrobial resistance. In fact, microorganisms develop several mutations that render antibiotics inefficient. It is estimated that by 2050, 10 million people will die every year because of antimicrobial resistance [2]. The most common resistant pathogens are certain Gram-negative bacteria such as *Klebsiella pneumonia* and *Escherichia coli,* and Gram-positive bacteria such as *Clostridium difficile* and *Staphylococcus aureus* [3]. Most of these pathogens are resistant to antibiotics that make it difficult to reduce their number. In addition to the impact on the physical and mental health of the patient, the financial loss related to these infections is estimated at €7 billion per year in the European Union due to prolonged medical care of the patients and additional treatments [4]. Another study about the consequences of surgical site infections in five European countries (France, Germany, UK, Spain, and Italy) also investigated the cost associated with these infections and the increase in morbidity, mortality, and prolonged hospitalisation [5]. The direct cost comparison was difficult to make due to the lack of common procedures between each country, but the infections lead to longer hospitalisation with additional expenditure related to staff and medications. These infections also increased patient morbidity, mortality, and health-related quality of life.

To achieve a better integration of biomaterials into the surrounding tissues, one strategy is the modification of the biomaterial surface. In fact, the biological response to biomaterials depends mainly on surface properties. By keeping the bulk properties of the materials, the surface properties may be modified to acquire or change different characteristics (wettability, topography, chemistry, etc) in order to improve the ability of the material to perform with an appropriate host response in its specific application, or biocompatibility (see Section 2.2.2) and resist microbial colonisation.

Primary amine ($-NH_2$) groups are known to promote cell adhesion because of their positive charges that can attract negatively charged biomolecules such as proteins or DNA in aqueous media at physiological pH [6]. The presence of a protein layer may improve cell adhesion afterwards as it is the first step in biomaterial/cell interaction. Some studies showed that amine coatings could promote cell attachment, proliferation, and osteogenic differentiation [7]. For implants, this advantage is important as it will determine if the implant succeeds due to the attachment and proliferation of cells which allow long term implant stability. The adhesion and spreading of cells are an essential prerequisite for the further steps which are proliferation and differentiation of cells. Another advantage of using these chemical groups is the possibility of exploiting them for the immobilisation of molecules such as enzymes [8,9], antibiotics [10], or silver nanoparticles [11,12]. In this way, it is possible to endow antibacterial properties to the coating.

In this chapter, the initial section will be dedicated to biomaterials and their interaction with body tissues. Then, the methods related to the generation of primary amine groups at the surface of materials will be discussed. As shown in Figure 2.1, different general strategies have been identified:

- Application of plasma technology:
  - Plasma surface activation with nitrogen (N_2) or ammonia (NH_3) gas;
  - Plasma polymerisation with a precursor containing $-NH_2$ groups, such as allylamine.
- Chemical modification of the surface by adsorption of molecules:
  - Proteins such as collagen or whey protein isolate (WPI);

- Synthetic polymers that contain $-NH_2$ groups, such as polyethyleneimine (PEI) or polydopamine (PDA).

Finally, the techniques used to characterise the material and especially to quantify the primary amine groups will be presented:

- Physicochemical characterisation of the coatings: contact angle (CA) measurements, X-ray photoelectron spectroscopy (XPS), scanning electron microscopy (SEM), atomic force microscopy (AFM), Fourier-transform infrared spectroscopy (FTIR);
- Amine groups quantification: dyes methods (Coomassie Brilliant Blue, Orange II) or chemical derivatisation (with glutaraldehyde, or compounds in vapor phase).

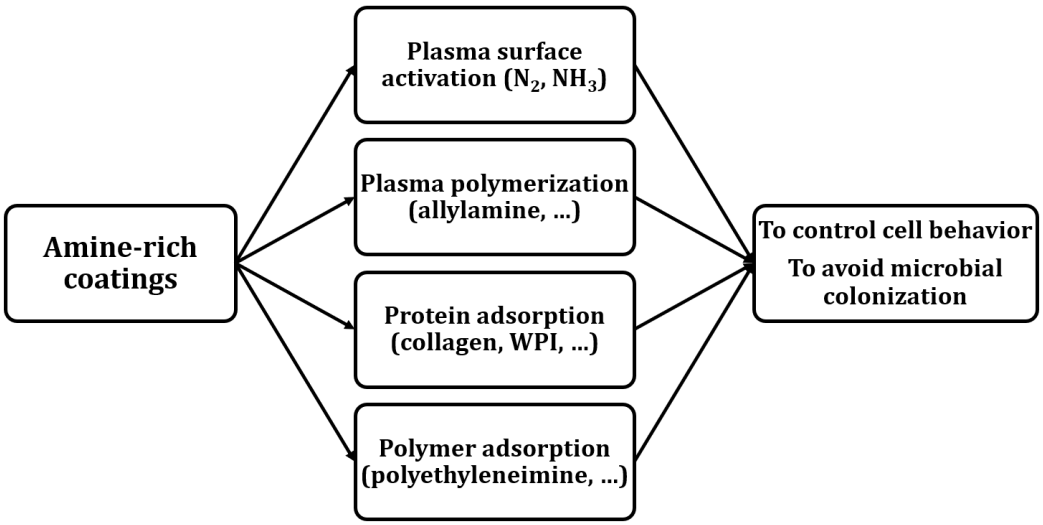

Figure 2.1: Methods used to obtain amine-rich coatings on biomaterials. WPI: whey protein isolate.

2.2. Biomaterials

2.2.1. General definition of biomaterials

A biomaterial is generally defined by the experts in the field as "*[...] a nonviable material used in a medical device intended to interact with biological systems*" [13]. Biomaterials are specific materials that have been used in the past 70 years to improve human health. Different types of biomaterials and medical devices exist

and are commonly used in several fields of application such as cardiovascular (blood vessel prostheses, heart valves, etc), orthopaedic (joint replacements, bone plates, etc), dental (implants), or ophthalmologic (contact lenses), as shown in Figure 2.2. The use of biomaterials may have saved millions of lives, as well as improving the quality of life for millions more [14]. Moreover, with the aging population, this field is growing steadily.

The main challenge in biomaterials field is the biocompatibility which is defined as "*[…] the ability of a material to perform with an appropriate host response in a specific application*" [13]. Ideally, biomaterials should not be toxic, immunogenic, thrombogenic, carcinogenic, or irritant, and side effects should be avoided.

Application	Biomaterials Used	Number/Year – World (or World Market in US$)
Skeletal system		
Joint replacements (hip, knee, shoulder)	Titanium, stainless steel, polyethylene	2,500,000
Bone fixation plates and screws	Metals, poly(lactic acid) (PLA)	1,500,000
Spine disks and fusion hardware		800,000
Bone cement	Poly(methyl methacrylate)	($600M)
Bone defect repair	Calcium phosphates	–
Artificial tendon or ligament	Polyester fibers	–
Dental implant-tooth fixation	Titanium	($4B)
Cardiovascular system		
Blood vessel prosthesis	Dacron, expanded Teflon	200,000
Heart valve	Dacron, carbon, metal, treated natural tissue	400,000
Pacemaker	Titanium, polyurethane	600,000
Implantable defibrillator	Titanium, polyurethane	300,000
Stent	Stainless steel, other metals, PLA	1,500,000
Catheter	Teflon, silicone, polyurethane	1B ($20B)
Organs		
Heart assist device	Polyurethane, titanium, stainless steel	4000
Hemodialysis	Polysulfone, silicone	1,800,000 patients ($70B)
Blood oxygenator	silicone	1,000,000
Skin substitute	Collagen, cadaver skin, nylon, silicone	($1B)
Ophthalmologic		
Contact lens	Acrylate/methacrylate/silicone polymers	150,000,000
Intraocular lens	Acrylate/methacrylate polymers	7,000,000
Corneal bandage lens	hydrogel	–
Glaucoma drain	Silicone, polypropylene	($200M)
Other		
Cochlear prosthesis	Platinum, platinum-iridium, silicone	250,000 total users
Breast implant	Silicone	700,000
Hernia mesh	Silicone, polypropylene, Teflon	200,000 ($4B)
Sutures	PLA, polydioxanone, polypropylene, stainless steel	($2B)
Blood bags	Poly(vinyl chloride)	–
Ear tubes (Tympanostomy)	Silicone, Teflon	1,500,000
Intrauterine device (IUD)	Silicone, copper	1,000,000

Figure 2.2: Example of biomaterials, their applications, and their number per year [14].

2.2.2. Biomaterial interaction with biological tissues

When a biomaterial is implanted in a host body, several physical and chemical interactions occur between the biomaterial surface and the surrounding tissues.

After implantation, the first interaction is the water molecule adsorption to the biomaterial surface which occurs in the first nanoseconds. This interaction is dependent on the surface wettability. Within seconds following the implantation, protein adsorption occurs on the biomaterial followed by a cascade of biological responses, including foreign body reactions [15,16]. The Vroman effect describes the time-dependent process of protein adsorption: the first proteins to adsorb would be the smaller ones due to their rapid transport to the surface, and later, bigger proteins which may have greater affinity with the surface will replace the smaller ones. The types, concentrations, and conformations of these proteins depend on the biomaterial surface and this may be determinant for the next steps which are the adhesion, proliferation, and differentiation of cells in contact with the surface [15,17].

Cell adhesion is essential so that proliferation and differentiation can occur, continuing the tissue healing and regeneration process. Cells can adhere on a biomaterial surface via cell surface ligands, such as integrins which bind on the protein layer [17]. Cell adhesion is influenced by the protein layer as the cells only see the adsorbed proteins rather than the biomaterial surface itself. Cell attachment may also by controlled by the surface topography. Cell differentiation is the last process where a stem cell acquires a specific function as they mature. The different steps are represented in Figure 2.3.

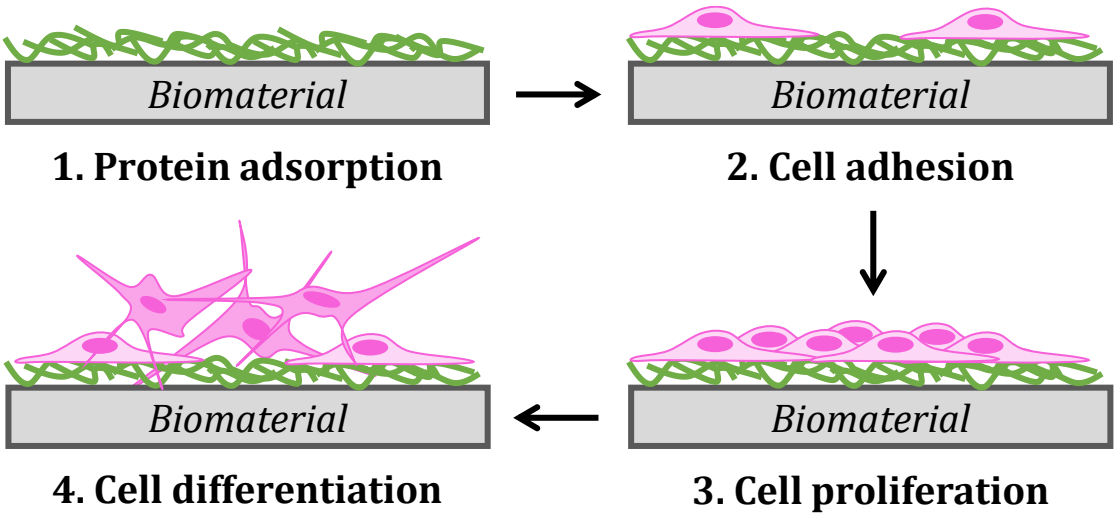

Figure 2.3: Different stages in cell/surface interaction.

To ensure the long-term stability of bone implants such as hip or dental implants, osseointegration is a prerequisite factor [18]. Osseointegration is defined as the direct structural and functional connection between living bone and the surface of a load-bearing artificial implant without the presence of soft tissue in between. The formation of fibrous tissue at the bone-implant interface may lead to the loosening of the implant. Moreover, with the gravity and pressure, the gaps between the bone and the implant increased and produce wear particles which accumulate and lead to a local inflammation and cascade of reactions activated by immune cells [18,19]. The presence of loosened gaps between the bone and the implant can also cause bacteria colonisation and the development of biofilm which is an important challenge due to antimicrobial resistance. Therefore, problems of loosening and infection are two challenges to overcome in the development of biomaterials [18,19].

The interaction of cells with the surface of implants can be modulated by the presence of a coating on top of the biomaterial surface such as a self-assembled monolayer [20] which will affect protein adsorption and in turn cell adhesion. Finally, antibacterial properties may be added to the coating to avoid bacteria development. Different strategies to modify biomaterial surfaces have been identified and will be described in Sections 2.3, 2.4, and 2.5.

2.2.3. Biofilm formation on biomaterials

Microorganisms can be found in planktonic form or more often as biofilms. Indeed, about 99% of bacteria are found in the form of biofilms at various stages of growth [21]. Biofilms are complex and dynamic ecosystems consisting of a community of microorganisms adhered to each other and to a receiving surface. In their natural environment, microorganisms are attached to a surface, organised in structured communities, and embedded in a matrix of extracellular polymeric substances. Bacterial adhesion to a surface is a survival strategy that allows them to settle and colonise an environment [22]. The planktonic state, where bacteria are free and isolated in the environment, could be considered as a transient state. In recent years, the National Institutes of Health (NIH) revealed that 65% of microbial infections and 80% of chronic infections were associated with biofilm formation

[23]. Biofilms can form on catheters or implants (heart valves, hip prostheses, etc...), and attack body tissues such as the teeth, eyes, lungs, ears or urogenital tract [24,25]. The process of biofilm formation takes place in several successive steps as shown in Figure 2.4 [25,26].

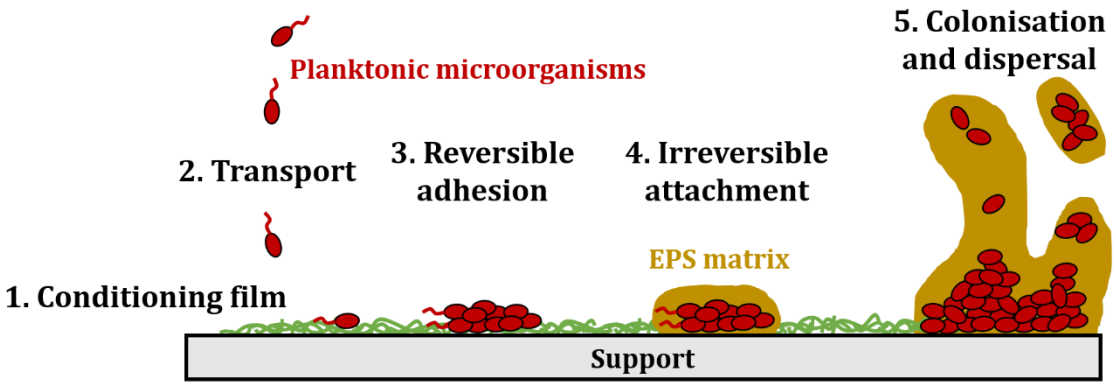

Figure 2.4: The different steps of biofilm formation on a surface.

- Formation of a conditioning film: protein and polysaccharide molecules from the surrounding environment are adsorbed on the surface.
- Transport and reversible adhesion: planktonic microorganisms, moving with their flagella or transported close to the surface by Brownian motion or sedimentation, adhere reversibly to this surface mainly through non-covalent chemical bonds (such as electrostatic, hydrophobic, van der Waals, and Lewis acid/base bonds).
- Irreversible attachment: when these bonds are maintained for a sufficient time, new chemical and physical mechanisms occur that make them permanent and irreversible. Indeed, the attachment of cells to the surface induces a cascade of physiological changes, leading to the production of extracellular polymeric substances (EPS, mainly composed of proteins and polysaccharides), which constitute the protective extracellular matrix and increase the anchoring of microorganisms to the surface. The adhesion then becomes irreversible, resulting in an increase in the mechanical energy required to break the bonds involved.

- Colonisation: the biofilm develops and acquires a complex three-dimensional structure. Microorganisms multiply by cell division, communicate via molecular signals ("quorum sensing") and adapt their metabolism to their sessile state. This stage is strongly influenced by environmental conditions (temperature, humidity, pH, nature of the surface). The mature biofilm develops until it reaches a thickness of a few millimetres.
- Dispersal: after certain influences, such as nutritional deficiencies or physicochemical changes in the environment, individual or groups of microorganisms can return to the planktonic state and colonise other surfaces. A cycle of growth and cellular dispersion is thus established, favouring the dissemination of microorganisms and the proliferation of pathogens.

Different strategies can be adopted to prevent biofilm formation such as antifouling coatings which repel bacteria attachment due to a modification of the surface morphology (for example micro or nanopatterned surfaces) or due to chemical modification (wettability and surface energy) [27]. Coatings may also be produced with bactericidal properties to kill bacteria that attach to the surfaces [27]. Therefore, surface modification is not only important to improve cell behaviour but also to provide antibacterial properties to a material.

2.2.4. Importance of biomaterial surface modification

Biomaterials must be well tolerated by the recipient and be well integrated into the body tissues. The biological response to biomaterials is mainly controlled by the surface of the material which can be modified to tailor this biointeraction. Surface modification is a way to improve cell adhesion, proliferation, and differentiation, which are desirable steps to achieve, for example when a hip or knee prosthesis is implanted. Therefore, it is possible to modify and improve the interaction of the cells onto the surface with the same material by retaining its bulk properties and only by changing its surface. If the surface modification is well achieved, the mechanical properties and functionality of the material will not be altered, but the interaction between the cells and the surface will be improved.

Moreover, surface modification can impact biofilm formation and bacterial survival. Different methods can be used to modify the biomaterial surface such as by chemical grafting, biomolecule immobilisation, or plasma processes. Surface modifications can be classified into three different categories: chemical or physical alteration of the biomaterial surface, addition of a thin film or coating on top of the biomaterial surface, and creation of a texture/pattern on the biomaterial surface [14].

In this thesis, the surface modification was achieved by adding coatings rich in primary amines on top of the surface. Different methods will be used and elaborated in the following parts such as plasma polymerisation which is a quick method to change homogeneously the surface properties of various material geometries by incorporating functional groups that can improve cell behaviour. Protein coatings will be another technique used as it can highly influence cell adhesion, proliferation, and differentiation as described previously.

2.3. Plasma polymer coatings

2.3.1. General information on plasma

Plasma thin film deposition is of considerable importance for many industries in the world, such as the microelectronics and automobile industries. Moreover, it is of considerable interest for biomaterial applications. Plasma, also called the "fourth state of matter", is a macroscopically neutral and conductive ionised gas. It constitutes more than 99% of the visible matter of the universe (stars), but on Earth, it occurs only as a result of lightning or the northern or southern lights. However, there is a multitude of laboratory plasmas.

Plasma is made up of a mixture of electrons, positive or negative ions, neutral molecules, and atoms that move freely in random directions. Two types of plasma exist, namely thermal and non-thermal plasma, depending on the temperature of the electrons, ions, and neutral molecules. In thermal plasma, the temperature of the atoms and heavy particles are equal. In non-thermal plasma, the electrons have higher average energy than heavy particles such as ions, hence $T_e \gg T_i$. The two

main properties of the plasma are electrical neutrality as well as the collective behaviour of the particles (Figure 2.5). To create a plasma discharge, a voltage source is needed to conduct the current through a gas between two electrodes (Figure 2.5). Since electrons are much lighter and faster than ions, the surface of the electrodes will become negatively charged by the electrons, and a negative potential will build up. This negative potential will accelerate ions towards the surfaces and repel electrons. The region around the surface depleted of electrons is called the plasma sheath and does not glow.

To obtain a plasma, several methods can be used with different types of power (continuous DC or alternative AC), at low/high or microwave frequency, radiofrequency (RF), different types of gas and pressures [28,29]. The initiation of a plasma discharge between two electrodes requires an electric field greater than the dielectric strength of the medium. Thus, a voltage higher than the breakdown voltage of the gas V_b is applied, which depends on the pressure p of the medium and the inter-electrode distance d according to Paschen's law [30]:

$$V_b = f(p \times d) \qquad \textit{Equation 1}$$

Depending on the gas used and the parameters of the discharge, it is possible to deposit a variety of thin films at the surface of materials by tuning the pressure and the power. Plasma surface modification is generally a quick method to change homogeneously the surface properties in a one-step process, such as wettability, chemistry, or topography [8]. A disadvantage of this process is the need of a vacuum chamber with a pumping system which may be expensive.

Different plasma techniques exist to prepare amine-rich coatings such as by plasma activation by the injection of inert gases such as ammonia (NH_3) or nitrogen (N_2), or by plasma polymerisation of a monomer containing $-NH_2$ groups such as allylamine. Plasma activation leads to the grafting of functional groups to the surface while plasma polymerisation leads to the deposition of a thin polymeric film onto the surface as described in Section 2.3.2.

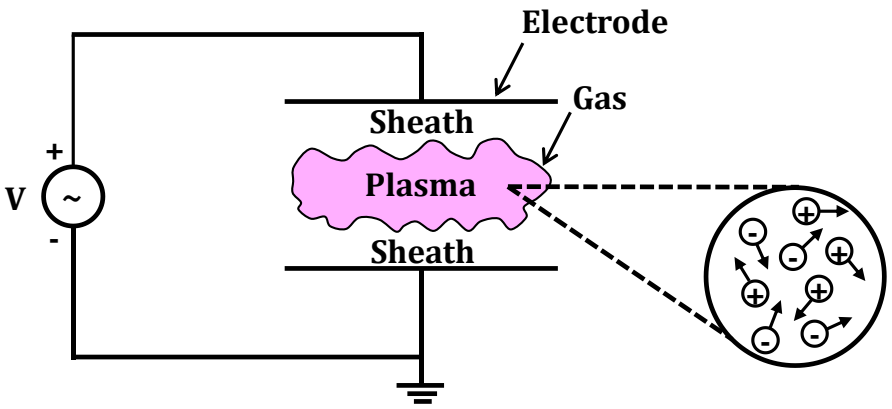

Figure 2.5: Schematic view of a plasma discharge between two electrodes connected to a voltage source. Plasma is a macroscopically neutral and conductive ionised gas constituted of a mixture of particles moving in all directions.

2.3.2. Deposition of polymers by plasma

Plasma polymerisation (PP) is a method to synthesise and deposit polymer-like thin films onto the surface of a material by using non-thermal plasma technology. One interest of PP is to produce thin polymer-like coatings with a high presence of functional groups selected from a monomer [31,32]. Such functional groups may improve cell adhesion, proliferation, and differentiation [7,8], or serve as grafting points for molecule immobilisation to endow new properties to the coatings such as antibacterial activity [10,11,33].

PP is a one-step solvent-free method, and irrespective of material type and geometries, unlike traditional methods using synthetic polymers [34]. However, a regular structure is difficult to achieve with PP due to multiple reactions occurring in the plasma. Indeed, high fragmentation of the precursor molecule and ion bombardment or ablation of the thin film are usually observed which limit the selection of functional groups [34–36]. In a glow discharge, free electrons are produced and gain energy from the electric field. After collisions with neutral molecules, free electrons lose their energy by transferring it towards gas molecules to create chemically reactive species which then lead to PP [37].

Three different steps occur in PP including the initiation stage where atoms and free radicals are produced through the collision of electrons and ions with the gas

monomers, the propagation stage which is the formation of polymeric chains, and the termination stage where the polymer chains are closed [38]. The plasma polymer films are highly branched and crosslinked [37,38].

In PP, the choice of the precursor is an important factor that modulates the coating chemistry. The surface can be modified with different chemical functionalities including primary amines, hydroxyl, or carboxyl [28,39,40]. In this thesis, thin polymeric films made of primary amines will be discussed in Section 2.3.5.

PP is yet not completely understood, and many studies focused on understanding the impact of different factors on PP and the presence of functional groups. These parameters can vary between laboratories depending on plasma reactor design, pressures, flow rates, applied power or frequencies [41].

Numerous studies have been conducted to improve the retention of functionalities such as by reducing or pulsing the RF power which reduces the degree of monomer fragmentation [42–47]. The power is directly coupled to the electrons which gain energy from the electric fields and some of the energy can be distributed to the other species in the reactor. The use of low power decreases the energy delivered per precursor molecule, which is defined by the Yasuda parameter, W/FM, where W is the power input, F is the precursor flow rate, and M is the precursor molecular weight. This parameter has been used since the 1980s to optimise plasma processes [48]. The structure of plasma polymers may be largely affected by the W/FM ratio, with a regular and better-defined structure with a low W/FM ratio [31]. However, low plasma power also led to reduction of the deposition rate and increasing solubility of the coating [49–52]. Moreover, another study showed no correlation between W/FM and the retention of functional groups by varying the pressure from less than 0.01 mbar to 0.2 mbar [53].

More recently, several studies showed the importance of pressure with a key role of polyatomic ions in thin polymeric films deposited by plasma [54]. Indeed, two different pressure regimes have been identified in plasma polymerisation, namely α and γ regimes. The flux and energy of ions in the deposition process are likely to vary significantly in either regime, therefore the distinction between these two

regimes is an important boundary to consider [41,54]. The flux of energy coming to the surface is an important parameter to control. With the impact, the ions can directly deposit or form surface radical sites allowing radical species in the plasma to deposit. The α regime occurs with low pressure, hence the density of particles is lower, and the mean free path is higher. Therefore, the sheaths are largely collision-less and the plasma is homogeneously distributed throughout the reactor [51]. Positive ions can travel through the sheath from the plasma to the substrate without collision and arrive with a kinetic energy equal to the potential difference between the plasma and the substrate. By increasing the pressure to the γ regime, the sheaths become collisional, which decreases the electron temperature. Therefore, the fragmentation of the precursor via electron impact is reduced. Operating the plasma in the α or γ regimes may lead to different polymerisation at the surface of the material. Recently, the ϒ regime has been shown to favour deposition from polyatomic hyperthermal ions, and in a range of monomers, it furbishes coatings with higher degrees of functional group retention [51]. Indeed, a higher pressure coupled with a low power was beneficial for a high retention of functionalities for nitroxide radicals [55,56], epoxy [57], α-bromoisobutyryl [58], or ester functionalities [54]. It is worth mentioning that plasma polymer deposition not only occurs from the ions but also from radical species produced in the plasma which are essential to assemble the film. The ions mainly contribute to the desired chemical functionalities [54].

To date, deposition in the γ regime has not been tested for amine-containing compounds such as allylamine. In this project, the two regimes will be compared in the deposition of primary amine-rich thin film by using allylamine as a precursor.

2.3.3. Plasma amine-rich coatings

Plasma technology has been widely used to produce amine-rich coatings by injecting precursors containing amine groups such as allylamine [7,59–62], heptylamine [63,64], ethylenediamine [65,66], or a mixture of compounds such as ammonia and ethylene [67–70]. These amine-rich coatings have been studied to control cell behaviour demonstrating a positive effect on cell adhesion,

proliferation, and differentiation for different cell types such as osteoblast-like cells [59,64,65] and fibroblasts [60]. Moreover, these coatings could be used to incorporate molecules such as enzymes, or drugs [10,33], as well as particles such as silver nanoparticles [11] to endow the material with new desirable biological properties. The application of such coatings on cell behaviour, molecules' immobilisation, and antimicrobial applications are elaborated in the following sections and summarised in Table 2.1.

Table 2.1: Overview of different applications of amine-rich coatings obtained by plasma and the findings associated.

Application	Precursor	Substrate	Findings	Ref.
Effect on cell behaviour	Mixture of NH_3/C_2H_4	PTFE PET	Human umbilical vein endothelial cells′ adhesion and growth increased More resistant to shear flow	[67]
	Mixture of N_2/H_2	Ti6Al4V	Human osteoblast cells′ adhesion and spreading enhanced	[65]
	Heptylamine	Ti	Osteoblast-like cells′ attachment increased after 24 h Coating with high retention of $-NH_2$ groups enhanced actin cytoskeleton formation	[64]
	Ethylenediamine	Ti6Al4V	Human osteoblast cells′ adhesion and spreading enhanced	[65, 66]
	Allylamine	Ti6Al4V	Human osteoblast cells′ adhesion and spreading enhanced	[65]
		Glass coverslips	Human adipose-derived stem cells′ attachment, spreading, and proliferation enhanced Osteogenic differentiation improved	[7]
		Silicone elastomer	Human skin fibroblasts′ adhesion and spreading increased	[60]
	Cyclopropylamine	Tissue culture polystyrene dishes PCL nanofibers	Initial adhesion of vascular smooth muscle cells (VSMCs) improved for all plasma power settings tested Proliferation and metabolic activity of VSMCs after 7 days higher for coating made at 33 W No increase in inflammatory markers	[71]
Molecules′ immobilisation	Mixture of NH_3/C_2H_4	PET	Grafting of chondroitin sulphate and epidermal growth factor to $-NH_2$ Decrease in cell apoptosis VSMCs growth increased	[72]
	Allylamine	Si	Grafting of trypsin	[73]
	NH_3 *n*-butyl amine Allylamine	Polysulfone films	Immobilisation of glucose isomerase Activity highest for allylamine/Ar plasma coatings close to plasma edge	[74]
	NH_3	Poly (D,L-lactide)	Better anchoring of collagen on plasma-treated substrates and resistance to phosphate-buffered saline (PBS) rinsing Cell affinity of modified substrates improved	[75]

Antimicrobial applications	Allylamine	Silver nanoparticles (AgNPs) coated with polyvinyl sulphonate (PVS)	PVS coated-AgNPs were bound to allylamine coatings Prevent attachment of *S. epidermidis* and biofilm formation	[12]
		Anodic alumina oxide (AAO)	Substrate pores were loaded with vancomycin drug and were reduced by plasma polymer deposition to allow a controlled drug release	[76]
		Low-density polyethylene	Bonding of antibacterial agents by immersion of the coatings in antibacterial solutions	[10]
	1-vinylimidazole	Thin-film composite membranes	Enhanced AgNPs binding onto the plasma-treated substrates which cause a decrease in *E.coli* growth	[11]
	Heptylamine	Si/Glass/Thermanox plastic/Cell culture plate	Release of antifungal drug	[33]

2.3.3.1. Effect on cell behaviour

By using a gas containing amine groups, the material surface may be covered by an amine-rich coating. Different gases have been used to modify the material surfaces by adding chemical functionalities present in the plasma. Previous studies used a mixture of ammonia (NH_3) and ethylene (C_2H_4) in a radiofrequency plasma reactor to treat polytetrafluoroethylene (PTFE) and polyethylene terephthalate (PET) [67]. They demonstrated that human umbilical vein endothelial cells' adhesion was increased as well as their growth on these plasma-treated surfaces compared with uncoated surfaces (Figure 2.6). In addition, the cells were more resistant to induced shear flow [67].

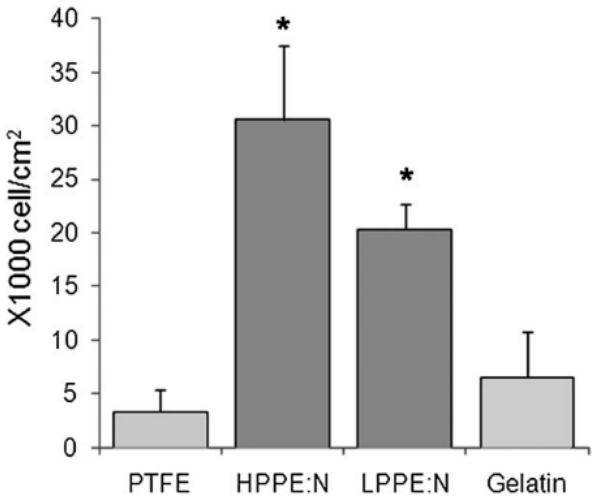

*Figure 2.6: Human umbilical vein endothelial cell adhesion after 4h on PTFE films, bare and coated with gelatin or with plasma polymerised coatings using low- (LPPE:N) and atmospheric-pressure (HPPE:N) plasma discharges. * $p < 0.05$ compared to uncoated surfaces. Copyright (2011) Wiley. Used with permission from* [67].

The other way to change surfaces of material by plasma technology is by polymerisation of a monomer containing the chemical groups needed to functionalise the surface. Plasma polymerisation allows the formation of thin polymeric coatings by using monomers. Different monomers have been used such as heptylamine [63,64], or ethylenediamine [65,66].

Such coatings improved not only the initial adhesion [64] but also the spreading of osteoblasts on titanium (Ti) [64,65]. Ti surfaces obtained with the higher retention of $-NH_2$ groups showed higher osteoblast-like cell attachment after 24h of cell culture which was further confirmed by SEM. In fact, cells were flatter, with longer cellular extensions. This was also demonstrated by actin labelling which showed that modified Ti with the high retention of $-NH_2$ groups enhances actin cytoskeleton formation [64]. Similar results were obtained on Ti alloy, where cell adhesion and spreading were improved on coatings obtained with different precursors (allylamine, ethylenediamine, and a gas mixture of N_2/H_2) [65].

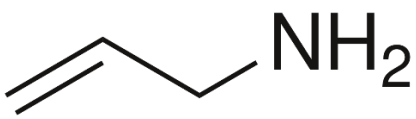

Figure 2.7: Molecular structure of allylamine, the most common precursor for primary amine-rich coatings.

One of the main precursors rich in $-NH_2$ groups used is allylamine. Liu *et al.* obtained an allylamine coating in a plasma RF reactor [7]. The allylamine coating obtained displayed hydrophilicity which can promote protein adsorption and cell adhesion. The authors showed that such coatings improve the attachment, spreading, and proliferation of human adipose-derived stem cells [7]. Moreover, their osteogenic differentiation was significantly improved compared with other coatings, without $-NH_2$ groups, due to a higher mineralisation level, as shown in Figure 2.7 [7]. This may be due to the changes in surface chemistry which affect protein conformation, such as fibronectin, and then the type of binding integrins. Integrins are important to mediate cell adhesion. The influence of $-NH_2$ groups on cells may be also due to their positive charge in an aqueous medium at physiological pH (7.4), which attracts negatively charged biomolecules such as proteins or cells [6]. This can also explain the enhancement of osteogenic differentiation. Liu *et al.* described the possibility of a microenvironment with a higher pH value which can promote osteogenic differentiation. Moreover, another study of plasma functionalisation with allylamine showed that these coatings enhanced the focal adhesion of osteoblastic cells [59]. A work from Ren *et al.*, using

allylamine to modify silicone elastomer by microwave plasma, showed that the biocompatibility of the material was improved. In fact, human skin fibroblasts adhered and spread well on the modified surface [60].

Recently, Nemcakova *et al.* studied the behaviour of vascular smooth muscle cells (VSMCs) on amine-rich coatings with different plasma parameters and substrates [71]. The initial adhesion of VSMCs on all amine coated-polystyrene (PS) and polycaprolactone nanofibers was improved for the different plasma powers tested. However, the proliferation and metabolic activity of VSMCs, after 7 days in culture, were higher with the coating made at a power of 33 W due to better properties such as stability, $-NH_2$ content, and wettability. The immunogenicity of such coatings was also investigated with the evaluation of inflammatory markers (TNF-α and IL-1β) and showed no increase in their expression [71].

The mechanism of cell adhesion to nitrogen-rich coatings has been investigated by Girard-Lauriault *et al.* [77,78]. They demonstrated that a critical value of nitrogen concentration was necessary to induce cell adhesion for atmospheric-pressure plasma coating, which depends on the cell type [78]. Moreover, the role of amine groups to positively influence cell behaviour has been confirmed [77]. Results showed the existence of a critical value of concentration of amine groups [77]. When the concentration of $-NH_2$ groups was higher than the critical value, the adhesion of monocytes induced a transient expression of TNF-α and IL-1β which decreased within 24h to control values. However, PPARγ, a marker of monocytes' adhesion and retention, had a more sustained expression for the same incubation period. The authors suggested that the transient expression of inflammatory markers (TNF-α and IL-1β) may induce monocyte cell adhesion via the activation of PPARγ since previous studies showed that PPARγ can be induced by TNF-α and IL-1β [77].

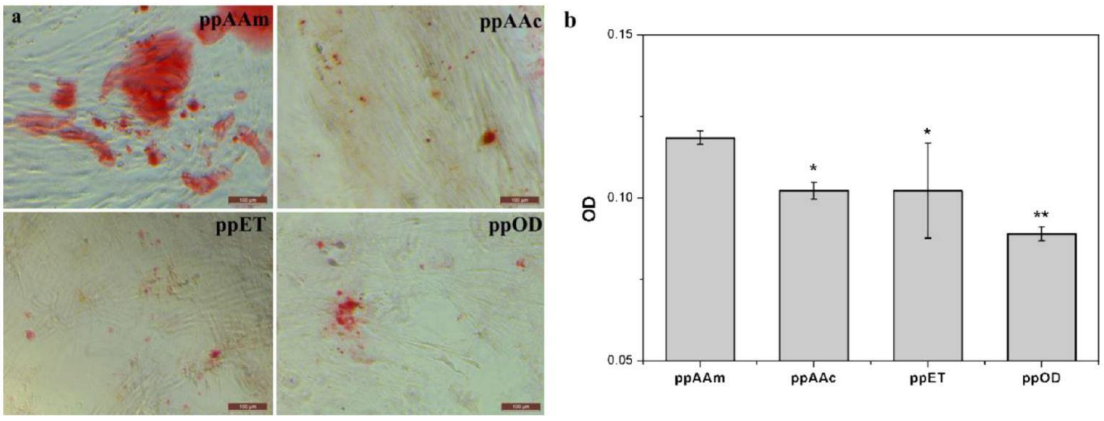

*Figure 2.8: (a) Alizarin Red S staining for mineral deposition formed by hASCs cultured on different samples in medium with osteogenic supplement at day 14. (b) The quantitative result of retention of Alizarin Red. Data were expressed as means ± SD (n = 4 for each sample). Single asterisk * and double asterisks ** denote a statistical significance of p < 0.05 and p < 0.01, respectively, compared with data obtained on the ppAAm sample. Reprinted with permission from* [7]*. Copyright (2014) American Chemical Society.*

Finally, cell behaviour can be also controlled by grafting molecules to amine groups. A previous study investigated the use of these functionalities to graft chondroitin sulphate (CS) and epidermal growth factor (EGF) to promote healing around stents [72]. The $-NH_2$ coatings were obtained by plasma with a mixture of NH_3 and C_2H_4. Cell experiment results showed a decrease in cell apoptosis after 6 and 24h on plasma coated with CS + EGF-grafted PET compared with untreated PET. Moreover, the coatings significantly increased vascular smooth muscle cells (VSMC) growth [72]. The use of $-NH_2$ groups to immobilise molecules will be further discussed in the following Section 2.3.3.2.

2.3.3.2. Molecules' immobilisation

As mentioned earlier, amine-rich coatings can also be used to immobilise molecules such as bioactive molecules such as CS and EGF [72]. These coatings can also be used to immobilise other molecules such as enzymes or drugs. A previous study involved the preparation of amine-rich coatings by allylamine plasma and covalent attachment of an enzyme, trypsin, via $-NH_2$ groups [73]. Similar work was performed with ammonia; *n*-butylamine and allylamine plasma and glucose isomerase were successfully immobilised on the modified samples [74]. Ammonia

plasma has been also used to modify poly (D, L-lactide) and coat collagen on it to improve cell affinity and the resistance of the coatings [75]. Collagen coated on plasma-treated samples seems to be more resistant to phosphate-buffered saline (PBS) rinsing due to interactions between collagen and plasma-treated surfaces. Finally, different molecules, such as silver nanoparticles [11] or drugs [10,33,76], have been incorporated in these coatings to make them antibacterial, which will be discussed in the next Section 2.3.3.3.

2.3.3.3. Antimicrobial applications

Microorganisms′ growth has also been inhibited by using amine coatings on the surface of the material. In fact, some studies used amine groups to functionalise material surfaces with silver nanoparticles (AgNPs) due to a strong affinity [11,12]. These AgNPs, which are known for their antimicrobial properties, were found to be responsible for the decrease in *E. coli* growth [11]. Allylamine thin films deposited by plasma have also been used to control the release of drugs such as vancomycin from porous material by reducing the pore diameters at the surface of the material [76]. A previous study demonstrated the ability of allylamine coatings to graft antibacterial agents onto low-density polyethylene samples [10]. The surfaces were first pre-treated by air plasma, then treated by allylamine coatings. Finally, these coatings were immersed into antibacterial solutions (benzalkonium chloride, bronopol, chlorhexidine, and triclosan) for 24h, leading to the bonding of the antibacterial agents to the surface, which was confirmed by XPS and FTIR. The antibacterial tests demonstrated higher antibacterial activity for samples treated with allylamine due to a higher quantity of antibacterial agent grafted.

A following work by the same authors showed the effect of the monomer used on antibacterial agent grafting [79]. Three monomers (allylamine, N-allylmethylamine, and N,N-dimethylallylamine) were tested and they demonstrated that less antibacterial agent was grafted onto the allylamine coating compared with the two others. Recently, heptylamine coating has been used as a matrix for the release of fluconazole, an antifungal drug. Results showed a

significant reduction in *C. albicans* colonies after 48h due to a controlled release of the drug [33].

2.4. Protein coatings

Proteins are widely available and certain proteins such as fibronectin (FN) or collagen are present in the human body. Collagen and FN are well known to have binding sites for cells and have been extremely widely employed as biomaterial [80,81]. However, they are expensive proteins, and therefore, whey protein could constitute an alternative approach due to its low cost. WPI preparations, such as BiPro from Davisco Inc. used in previous studies [82], typically cost tens of US dollars per kg, while collagen preparations used to coat biomaterial surfaces, such as those from Sigma Aldrich and BD Biosciences [83,84], would cost hundreds of US dollars per g. Due to a high surface/volume ratio, fibrillar structures are interesting candidates to coat materials since this increases the adherence at the surface. Moreover, compared with globular proteins which may change their conformation after adsorption on the material's surface, fibrillar proteins are unlikely to do so [85,86]. Fibrillar proteins are generally larger than globular proteins which means that they are likely to have more adhesion points to substrates. In addition to their high stability, properties can be added to the coating such as antibacterial properties, by binding other molecules to the fibrillar structures [87,88]. Fibrillar structures could even form aligned superstructure scaffolds for cells [89]. Functional lysozyme fibrillar coatings improved attachment of immortalised fibroblasts and epithelial cell lines and can act as biomimetic cell culture platforms [90–92]. Fibrils are obtained from fibrous proteins such as collagen or whey protein isolate (WPI).

The application of protein coatings such as FN, collagen, and amyloid fibrillar coatings are discussed in the following Sections 2.4.1 and 2.4.2 and summarised in Table 2.2.

Table 2.2: Overview of different applications of amine-rich coatings obtained with proteins and the findings associated.

Protein	Substrate	Findings	Ref.
Fibronectin (FN)	Poly (lactic acid) Silicon oxide	Osteoblast-like cells′ adhesion and spreading enhanced after 3 days Cell proliferation and mitochondrial activity improved after 7 days	[93]
	Si	Human osteoprogenitor cells′ attachment enhanced and formation of actin filaments Formation of dense stress fibres attached to FN coatings	[94]
	PTFE	FN combined with phosphorylcholine Endothelial cells′ adhesion and spreading enhanced Higher cell viability after 24 h	[95]
Collagen	Ti6Al4V	Osteoblast cells′ initial adhesion enhanced	[96]
		Osteoblast cells′ spreading, proliferation and differentiation improved	[97]
		Collagen coupled with phloroglucinol (PG) Fibroblast- and osteoblast-like cells adhere and spread well Reduction in inflammatory response Osteogenic differentiation promoted with a high PG concentration Osteoclast activation reduced with a low PG concentration	[98]
	Ti	Early osseointegration enhanced in vivo	[99]
	Porous Ti oxide	Collagen coating coupled with AgNPs Osteoblast cells′ adhesion improved Adhesion and proliferation of *E.coli* were reduced	[100]
Amyloid fibrils from whey protein isolate (WPI)	Hydrogel (no substrate)	Osteoblast and fibroblast cells′ growth enhanced Calcium deposition of osteoblasts increased Osteogenic differentiation of human adipose-derived stem cells increased	[101]
		WPI coupled with aragonite Osteoblast cells′ proliferation supported for 3 weeks	[102]
	Turkey Frankfurter (food application)	Nisin, grape seed extract, malic aid, and ethylenediamine tetraacetic acid incorporated in WPI coatings Effective antimicrobial activity against different pathogens	[103]
	Films (no substrate)	Oregano, rosemary, and garlic essential oils incorporated in WPI films Film containing oregano and garlic essential oil most effective against *S. aureus, S. enteritidis, L. monocytogenes, E. coli,* and *L. plantarum*	[104]

	Glass	Resistance of WPI fibrillar coatings to autoclave sterilisation Human bone marrow stromal cells′ spreading, and differentiation enhanced	[82]
	Ti6Al4V	Resistance of WPI fibrillar coatings to autoclave sterilisation Incorporation of heparin and tinzaparin into WPI fibrillar coatings successful Support human bone marrow stromal cell differentiation (increase in TNAP activity) Hydrophilicity increased	[105]
Amyloid fibrils from lysozyme	Mica	Fibroblast and epithelial cells′ spreading increased Increased of focal adhesion and associated stress fibres	[91]
Silk fibroin (SF)	Ti	Gentamycin and silver nanoparticles incorporated to SF coatings Antibacterial activity against *S.aureus* Osteoblast cells′ adhesion, growth, and osteogenic activities enhanced	[106]
	PEEK	SF combined with bone-forming peptide Initial attachment and proliferation supported Osteoblast cell proliferation, spreading, and osteogenic differentiation enhanced for SF with bone-forming peptide coating	[107]
	Electrospun nanofibers	SF modified with graphene oxide which resulted in a Decrease in *E. coli* and *S. aureus* survival rates Osteoblast cells′ growth enhanced	[108]
	Electrospun nanofibers	SF combined with heparin Cell growth and proliferation improved	[109]

2.4.1. Globular protein coatings

Fibronectin (FN) is a well-known globular protein present in two different forms in the human body: an insoluble form in the extracellular matrix and a soluble form in the body fluids such as plasma. This protein can interact with different macromolecules such as collagen or heparin, and promote cell attachment [81,110–112]. It is also involved in cell migration during embryonic development as well as in wound healing [113]. FN has been widely studied, especially with a view to modifying biomaterials' surfaces to improve their biocompatibility [114]. Depending on its conformation, FN interacts with cells via integrins and promotes cell attachment and proliferation [115]. A study investigated FN adsorption on poly (lactic acid) and silicon oxide substrates [93]. It was found that osteoblast-like cell adhesion was enhanced by the presence of FN on both surfaces as well as cell spreading after 3h of culture. Moreover, cell proliferation and mitochondrial activity after 7 days of culture were improved in the presence of FN [93]. The effect of FN adsorption on cell attachment has also been investigated on other substrates such as silicon [94]. The attachment of human osteoprogenitor cells with the formation of actin filaments was enhanced due to the presence of FN. Moreover, the formation of dense stress fibres attached to the FN coatings was noticed, as indicated in Figure 2.8. A FN coating has also been combined with other biomolecules such as phosphorylcholine, to enhance endothelialisation as well as to avoid thrombus formation [95]. The authors found that the adhesion of endothelial cells on FN coatings was enhanced compared with uncoated polytetrafluoroethylene (PTFE). Moreover, cell spreading was improved on FN coatings. Finally, the study of the cell metabolic activity after 24h showed higher cell viability on FN coatings compared with uncoated PTFE.

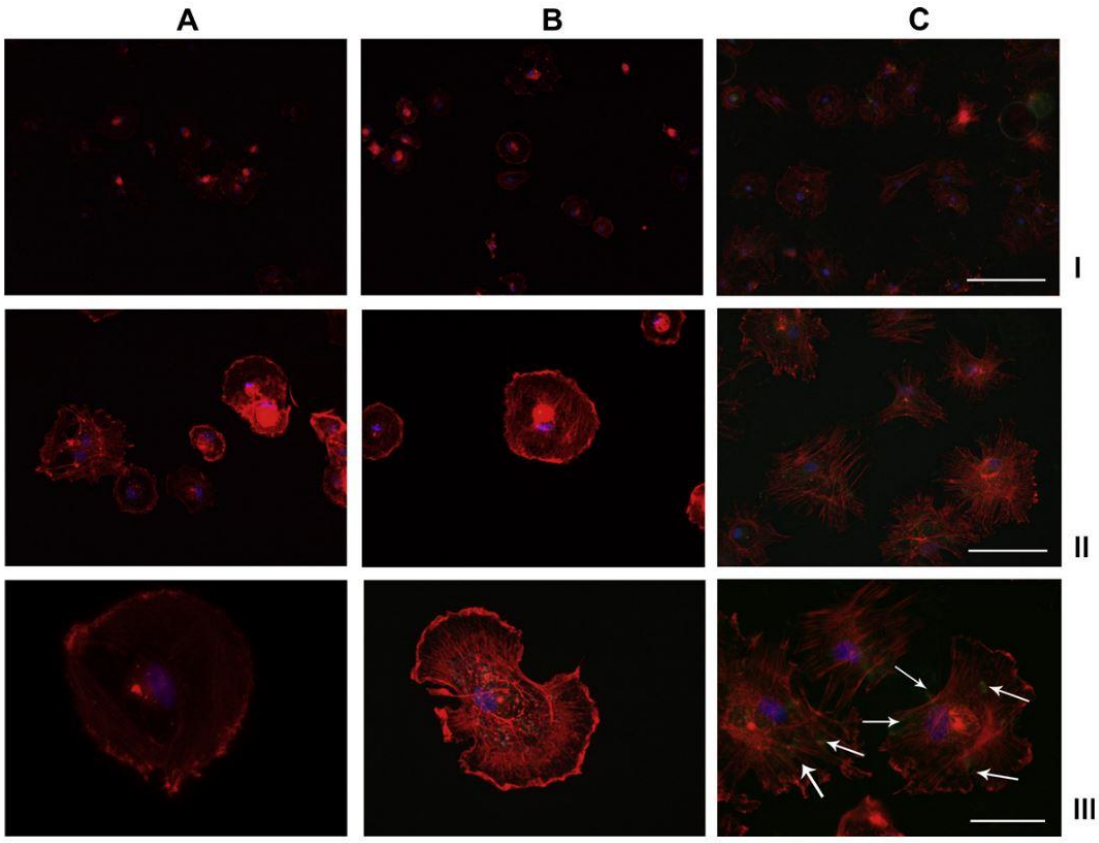

Figure 2.9: Human osteoprogenitor cell actin filament staining on (A) standard cover slips, (B) silicon and (C) FN-covered silicon after 3 h in cell culture. Red colour stains actin and blue stains cell nuclei. On Figure 2.8C, white arrows indicate the green staining of the dense stress fibres attached to the FN coating. Scale bars are of 200 (I), 100 (II) and 50 (III) µm, respectively. Reprinted with permission from [94]*. Copyright (2011), with permission from Elsevier.*

2.4.2. Fibrillar protein coatings

2.4.2.1. Collagen fibrillar coatings

Many studies focus on the use of collagen coatings for biomedical applications. In fact, collagens represent a major part of the extracellular matrix [116]. They contribute to the mechanical properties and biological functions of various types of tissues, such as skin, bone, or blood vessels. Collagen is found in multicellular animals and represents about 25% of all body proteins, making it the most abundant protein [117]. There are approximately 28 collagen types, but types I, II, and III are the most predominant. Collagens provide structural support to tissue,

and they mediate adhesion, migration, and proliferation of cells. Collagen type I is a popular biomaterial for tissue engineering and regenerative medicine due to its abundance in the human body and its functions as a scaffold material, as well as its relatively low cost compared with other proteins [80,117,118]. Collagen consists of a triple helix (tropocollagen molecule), formed by three polypeptide chains that can self-assemble in different networks such as fibrils or fibres [116].

Collagen type I is important for osteoblast response and some studies showed that collagen type I coatings on Ti6Al4V alloy could enhance cell adhesion, osteoblast proliferation, and differentiation [96,97]. Collagen type I grafted on titanium substrates promoted early osseointegration in vivo [99]. A study from Hsueh *et al.* demonstrated that the adhesion and proliferation of *E.coli* were reduced as well as the cell adhesion of osteoblast cells improved by using collagen coatings containing silver nanoparticles [100]. Recently, a study from our group demonstrated the effect of collagen coatings enriched with phloroglucinol (PG) on fibroblast- and osteoblast-like cells [98]. Results showed that such coatings significantly reduce the gene expression of inflammatory markers. Moreover, the expression of an osteoclast activation marker was reduced at a low PG concentration and the expression of osteogenic differentiation marker was promoted at a high PG concentration.

Despite their numerous advantages, collagen fibrils do not withstand sterilisation by autoclaving which is a method widely used in biomedical field. Other type of fibrils can be produced and autoclaved such as amyloid fibrils from whey protein, and this will be discussed in the next Section 2.4.2.2.

2.4.2.2. Amyloid fibrillar coatings

Amyloids are β-sheet structures of protein and peptide aggregates that form fibrils at the nanoscale. These fibrils are obtained from diverse proteins or peptides, and especially from proteins coming from the food industry such as whey protein isolate (WPI) or lysozyme from hen egg white.

WPI comes from whey, which is a by-product from the dairy industry that contains more than 95% protein, of which 75% is β-lactoglobulin, whereas whey protein

concentrate contains less protein than WPI (more than 80%) [101]. WPI can form fibrils under acidic conditions (<pH 3.5) and a long heating time due to the degradation of β-lactoglobulin into peptides. These peptides self-assemble into fibrils of a few nanometres in thickness and a length between 1 to 10 μm [119]. The morphology of these fibrils is pH-dependent; it has been shown that long semi-flexible fibres are formed at pH 2 and worm-like structures at pH 3.5 [120–122]. Previous studies showed that WPI could improve cell proliferation and osteogenic differentiation. Moreover, it demonstrates some antibacterial properties [101,102,123]. Quantification of WPI fibrils in solution can be performed with the Thioflavin T fluorescence assay [124].

Furthermore, these WPI solutions may be enriched by different compounds such as antimicrobial molecules. Material surfaces could be covered by a thin film of WPI and previous works studied the antimicrobial properties of these coatings especially for food packaging [103,104]. Recent work demonstrated the ability of WPI fibril coatings to withstand autoclave sterilisation as well as support the spread and differentiation of human bone marrow stromal cells [82]. WPI fibrillar coatings have also been deposited on Ti6Al4V alloy widely used in bone contact implants, and combined with heparin and tinzaparin, known for their ability to improve blood compatibility and promote cell adhesion, proliferation, and differentiation [105]. The study showed that WPI fibrils were successfully adsorbed at the surface of Ti6Al4V alloy. Moreover, heparin was successfully loaded into the fibrillar coatings as demonstrated by XPS analyses. The effect of such coatings on human bone marrow stromal cells was positive with an increase in TNAP activity which improves osteogenic differentiation. WPI has been extensively studied for food applications and it constitutes a new research area in the biomaterial field which needs to be explore.

Amyloid fibrils can also be obtained from hen egg white lysozyme at high temperature and low pH. Reynolds *et al.* produced fibrils from lysozyme at high temperature and low pH [91]. They demonstrated that this fibrillar coating could enhance cell spreading due to an increase in the number of focal adhesions compared with lysozyme control [91]. Recently, fibrils have also been obtained

from legume proteins instead of animal proteins such as whey or egg proteins. This could constitute another approach to coat materials for cell support [125].

2.4.2.3. Other fibrillar coatings

Numerous other fibrous proteins may be used to modify material surfaces. One which has been widely studied is silk fibroin (SF) protein. Silk fibres are composed of two SF filaments which are formed by self-assembly of nanofibrils (3–5 nm in diameter) into larger fibrils (20–200 nm in diameter) [126]. SF possesses interesting biocompatibility but due to low antibacterial activity, it is often used in combination with other nanomaterials. For instance, SF coatings have been used as a matrix to incorporate gentamycin and silver nanoparticles in a previous study [106]. The antibacterial activity of these coatings has been successfully demonstrated by a significant reduction in bacterial growth and adhesion, and biofilm formation. Furthermore, the attachment and proliferation of osteoblast-like cells were improved. In another study, polyetheretherketone (PEEK) was coated with SF and bone-forming peptide to increase the osteogenesis of PEEK implants [107]. Results showed good cytocompatibility with an increase in cell proliferation, spreading, and osteogenic differentiation. SF nanofibers have also been obtained by electrospinning and modified with graphene oxide which resulted in a decrease in *E. coli* and *S. aureus* survival rates, as well as an increase in the growth of osteoblast-like cells [108]. Cestari *et al.* have also produced SF nanofibers by electrospinning [109]. In their work, heparin was successfully immobilised at the surface of SF nanofibers due to the formation of hydrogen bonds. Higher cell growth and proliferation were observed on the SF fibres with heparin [109].

2.5. Synthetic polymer coatings

Dopamine, a biomolecule with catechol and amine functionalities, can self-polymerise into polydopamine (PDA). Inspired by the adhesive foot proteins secreted by mussels, PDA has been used as a coating on various types of materials [127]. Due to the presence of chemical functionalities (catechol and amine groups), this coating can be further used as a platform to bind other compounds. For

example, Cong *et al.* used this coating to bind and reduce silver ions to form a nanocomposite coating made of silver nanoparticles (AgNPs), which displays interesting antibacterial properties [128]. Cotton fabrics have also been successfully modified with polydopamine to incorporate AgNPs to render them antibacterial [129]. Another work investigated the use of PDA to deposit AgNPs and polyethylene glycol (PEG) to create an antimicrobial and antifouling surface, respectively, due to the presence of AgNPs and PEG [130]. The combination of both properties, antibacterial and antifouling, was only possible through the PDA coating acting as a binding platform for AgNPs and PEG. Another way to produce antibacterial PDA coatings is by preparing the coating by a shaking-assisted method which leads to the formation of a roughened PDA coating [131]. These coatings have exhibited strong antibacterial activity compared with smooth PDA coatings, which was close to 100% against *E. coli*, *S. aureus,* and *P. aeruginosa*. This antibacterial activity remained strong after 10 days of storage of the coatings in deionised water. Moreover, bacterial morphologies have been studied by scanning electron microscopy (SEM). The results showed major changes in their structure with a loss of the intact rod-like shape for *E. coli* and of the spherical shape for *S. aureus*, which may indicate damage of cell membrane.

Polyethyleneimine (PEI) is a cationic polymer containing the highest number of amine groups and it is mostly used as a precursor layer for polyelectrolyte multilayer films for dental and orthopedic implants or tissue engineering [132]. Previous studies showed that multilayer thin films of PEI/heparin on NiTi alloy demonstrate better biocompatibility compared with NiTi alloy itself [132,133]. In addition, PEI demonstrated some antibacterial properties against *S. aureus* and *P. aeruginosa* after 24h and its non-cytotoxicity against fibroblasts after 7 days [134]. However, other studies have shown that PEI may be cytotoxic; some authors say that this cytotoxicity is molecular weight-dependent, with lower molecular weight preparations demonstrating lower cytotoxicity [135,136]. The effect of PEI immobilisation on poly (lactic acid) by adsorption or covalent binding has also been investigated using high and low molecular weight PEI. Results showed that cell adhesion was enhanced in the presence of PEI compared with uncoated poly (lactic acid). The proliferation and differentiation of an osteoblast cell line have

been also improved, in particular by low molecular weight PEI [137]. Recently, another study evaluated adhesive properties and cytotoxicity towards human mesenchymal stromal cells (hMSCs) of PEI coatings [138]. PEI coatings improved cell adhesion after 1h of incubation compared with uncoated culture plates. Cells also exhibited high metabolic activity in the presence of PEI with 10% fetal bovine serum.

2.6. Addition of biomolecules into the coatings

2.6.1. Phloroglucinol (PG)

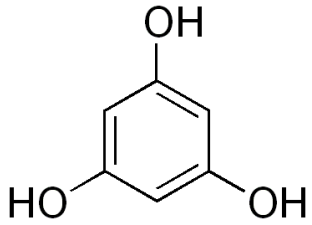

Figure 2.10: Molecular structure of phloroglucinol (PG).

Phloroglucinol (PG) is the building block of phlorotannins which are a group of marine-derived polyphenols occurring in brown seaweeds. The molecular structure of PG is shown in Figure 2.9. Previous studies showed the anti-inflammatory properties that PG can have, by reducing the production of inflammatory factors [139]. Furthermore, oxidative stress has been also decreased [140] which may be interesting in bone regeneration, since oxidative stress may hinder osteogenic differentiation [141–144] and stimulate bone resorption [145]. A previous study demonstrated the ability of phlorotannins to promote hydrogel mineralisation [146]. Finally, phlorotannins possess antimicrobial properties, especially against bacteria such as *Staphylococcus aureus (S.aureus)*, methicillin-resistant *S.aureus* (MRSA), and some fungi [146–148]. PG has also been conjugated with chitosan to produce antioxidant and antibacterial biopolymer [149]. The complex PG/chitosan showed higher antioxidant activity compared to unmodified chitosan. Moreover, the antibacterial activity was significantly increased against MRSA and foodborne pathogens compared to unmodified chitosan.

Another study by Liskova et *al.* investigated the addition of PG into injectable hydrogels containing chitosan by analysing its antioxidant and antibacterial activities as well as its ability to support cell adhesion and proliferation of osteoblast-like cells [150]. The study showed that the addition of PG not only increased the antioxidant activity of the hydrogels but also reduced bacterial growth (*E.coli*) after 1h, 3h, and 6h. Moreover, these PG/chitosan hydrogels had no negative impact on cell adhesion and growth. More recently, our research group showed the possibility to incorporate PG into coatings made of collagen fibrils on top of Ti6Al4V alloy [98]. Osteoblast- and fibroblast-like cells both spread and adhered well on PG/collagen fibrillar coatings. Moreover, the inflammatory response was significantly reduced, and the osteogenic differentiation was increased by the coating containing a high PG concentration.

As previously described, PG is a promising low-cost biomolecule with antibacterial, antioxidant and anti-inflammatory properties, as well as positive impacts on cell adhesion, proliferation, and differentiation. Therefore, PG was chosen to be incorporated into WPI fibrillar coatings.

2.6.2. Tannic acids (TAs)

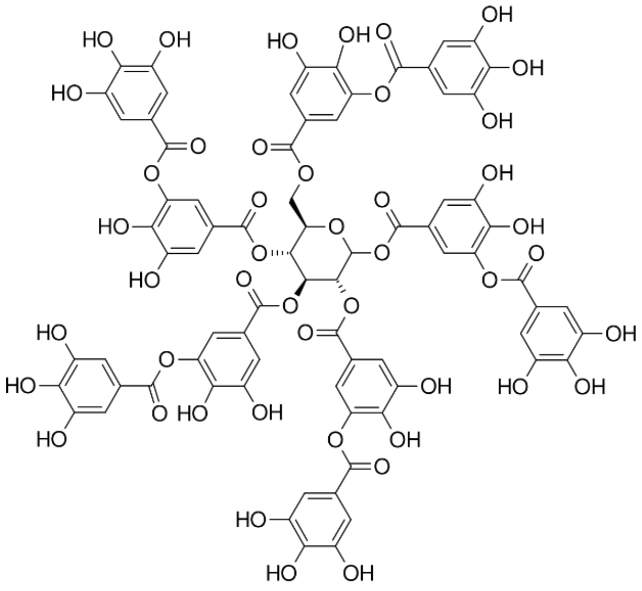

Figure 2.11: Example of the molecular structure of a tannic acid (TA).

Tannic acids (TAs) are a specific form of tannins, which are polyphenolic biomolecules found in a wide range of plants (Figure 2.10). Several studies have investigated the use of TAs as crosslinkers in protein-based biomaterials. Moreover, different TAs have been previously used in gellan gum polysaccharide hydrogels, such as pentagalloyl glucose (PGG), or gallotannin-rich extract from mango kernel, which are 2 types of gallotannins (hydrolysable tannins) [151]. These hydrogels decreased cell growth and did not show any antibacterial activity. However, the study showed that some gallotannins promoted hydrogel mineralisation. Gallotannins have also been grafted to Ti6Al4V alloy for bone implant application. TAs may possess anticancer properties as investigated by Chai *et al.* [152]. Their study showed some promising results on the use of TAs as drug for breast cancer.

More recently, TAs were successfully loaded into WPI hydrogels to target cancer cells and the release of TAs was studied depending on pH [153]. Two types of TAs were added, namely a polygalloyl glucose-rich extract (ALSOK 2), and a polygalloyl quinic acid-rich extract (ALSOK 4). Hydrogels enriched with these TAs were successfully obtained and their swelling properties were studied for different pH (5, 7, and 9). Mayorova *et al.* showed that the release of ALSOK 2 from the WPI hydrogel was higher compared to ALSOK 4. The cytotoxicity of these WPI hydrogels increased against cancer cells when the concentration of TAs inside the hydrogels increased [153]. Moreover, tannins are well known in leathermaking as they are used as crosslinkers to prevent disintegration of collagen fibres of the leather [154].

Therefore, TAs are another promising low-cost type of biomolecule to use in biomaterial applications due to their numerous advantageous properties (anticancer, pro-mineralisation, antibacterial) and their ability to bind to proteins. Hence, different types of TAs will be incorporated into WPI fibrillar coatings.

2.7. Characterisation of amine-rich coatings

2.7.1. Physicochemical characterisation

2.7.1.1. Water contact angle measurements

Contact angle (CA) measurement is a simple method to analyse the interaction between a liquid and a solid in order to define the wetting properties of the material. A contact angle is defined geometrically as the angle formed by a liquid at the three-phase boundary where a liquid, gas and solid intersect [155]. A low CA indicates that the material is hydrophilic, whereas a high CA indicates a hydrophobic material. It is defined by the mechanical equilibrium of the droplet under the action of the three interfacial tensions, namely solid-gas (γ_{SG}), solid-liquid (γ_{SL}), and liquid-gas (γ_{LG}), as represented in Figure 2.11. This equilibrium relation is defined by Young's equation:

$$\gamma_{LG} \cos \theta_Y = \gamma_{SG} - \gamma_{SL} \qquad \textit{Equation 2}$$

Where θ_Y is the Young contact angle, γ_{LG} the surface tension of liquid and gas, γ_{SG} the surface tension of solid and gas, and γ_{SL} the surface tension of solid and liquid.

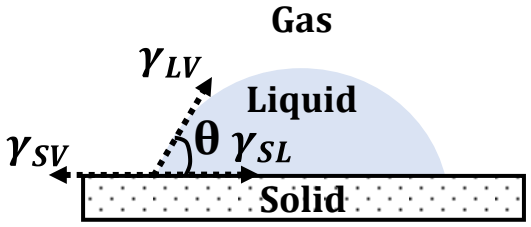

Figure 2.12: Contact angle θ formed by a droplet on a solid surface.

WCA measurements can be used to detect the presence of a coating by comparison to the uncoated material. In fact, for amine-rich coatings, due to the introduction of hydrophilic nitrogen functionalities, the WCA decreases compared with the uncoated samples, as shown in a previous study [61]. Furthermore, surface wettability may influence cell behaviour [156].

2.7.1.2. X-ray photoelectron spectroscopy (XPS)

X-ray Photoelectron Spectroscopy (XPS), also known as Electron Spectroscopy for Chemical Analysis (ESCA), is a surface sensitive technique used to provide information about the elemental composition and chemical state of the first few atomic layers of a material [157–159]. A schematic diagram of XPS is represented in Figure 2.12. With a survey spectrum, it is possible to detect all the elements present on the top surface of the material. With a high-resolution spectrum, the peak of the elements found in the survey can be separated into components corresponding to different chemical bonds [160,161]. However, the nitrogen high-resolution spectrum is difficult to analyse due to the close binding energy of each component (amine, imine, amide,…) and may require techniques such as labelling to distinguish between components (refer to Section 2.7.2) [61].

In brief, the technique works by irradiation of a sample with X-rays and measurement of the kinetic energy of emitted photoelectrons. While the X-rays will penetrate several microns into the material, any electrons that are generated this deeply will lose energy via multiple inelastic collisions before they can escape the surface. Only electrons generated close to the sample surface retain sufficient energy to escape from the sample. These electrons contribute to characteristic photoelectron peaks (if they do not lose any energy from inelastic collisions) or the XPS background (if they lose some energy via a small number of inelastic collisions). The XPS surface sensitivity is defined by the Beer-Lambert law (Equation 3) and it is estimated that 95% of the electrons will be emitted from a depth of 10 nm or less (known as the “information” or “sampling” depth) [158].

$$I = I_0 exp\left(-\frac{d}{\lambda}\right) \qquad \textit{Equation 3}$$

Where I is the intensity of electrons emitted from a depth d, I_0 is the total number of electrons generated from the sample, and λ is the attenuation length of the electron which depends on the electron energy and the material through which it is traveling.

Due to this surface sensitivity, and the ability to determine elemental composition and chemical state, XPS is widely used in the analysis of thin films and coatings [158].

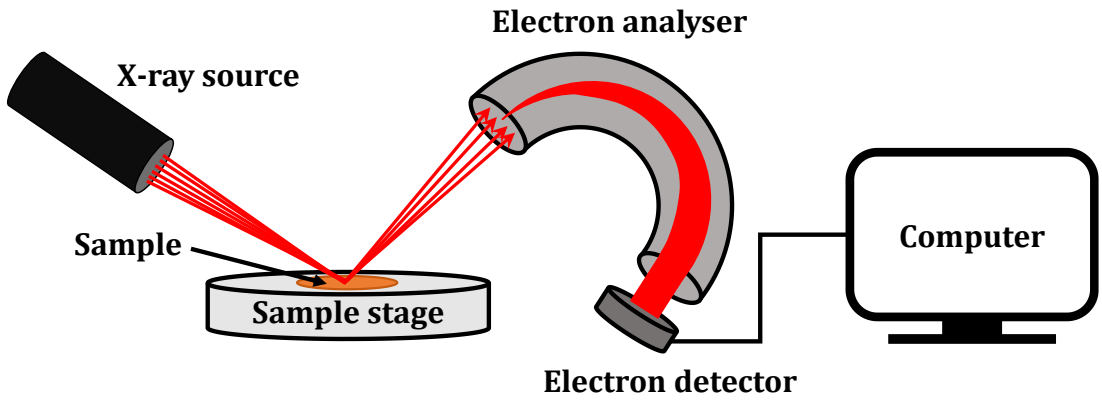

Figure 2.13: Schematic diagram of an X-ray photoelectron spectroscopy.

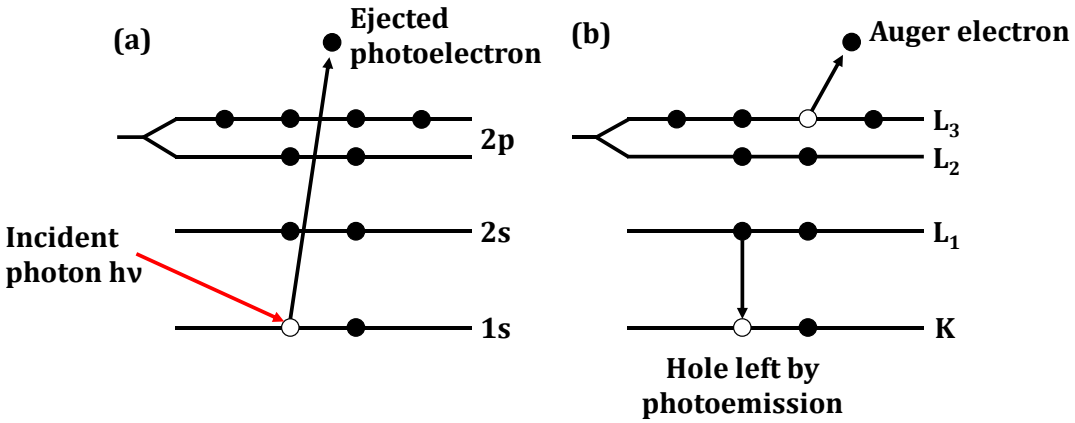

Figure 2.14: Schematic of the (a) photoelectron, and (b) Auger electron emissions after X-ray irradiation.

Due to the irradiation of a sample by a beam of X-rays from an X-ray source (commonly a Al-Kα or Mg-Kα source, but other X-rays can be used), photoelectrons are emitted from the material as represented in Figure 2.13a [157,158]. These electrons are detected by the spectrometer and their kinetic energies measured. Each energy is characteristic of an element (and orbital from which the electron is emitted) present within the surface of the material. The data obtained is presented as a graph plotting the number of electrons emitted (usually

expressed as counts per second, CPS) versus their binding or kinetic energy, with the convention of binding energy decreasing from left to right (Figure 2.14). For elements of particular interest, high resolution spectra may be acquired over a narrower range around the peak of interest.

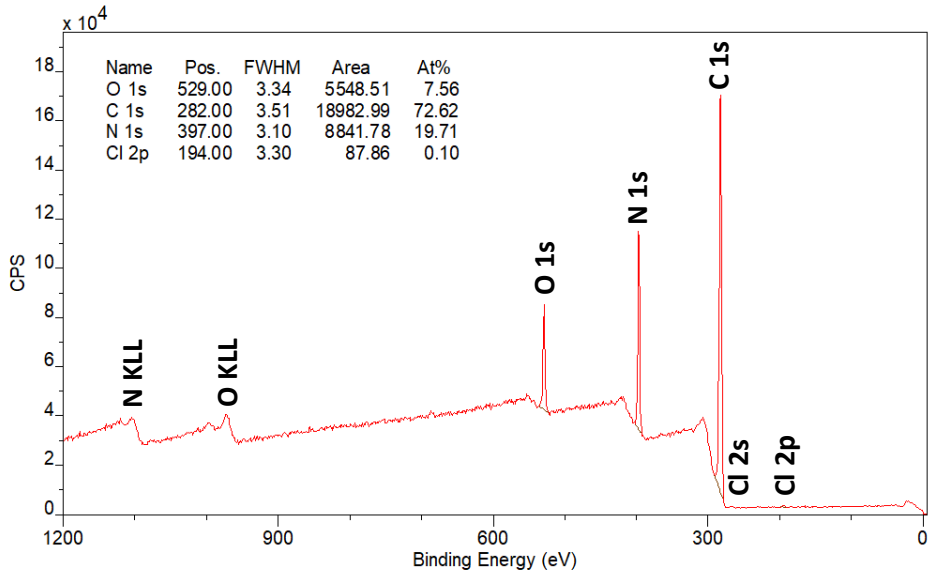

Figure 2.15: Representative wide survey spectrum of an allylamine plasma polymer coating.

2.7.1.2.1. Emission of photoelectrons

Photons with a sufficient incident energy cause the electrons to be ejected from the material via the photoelectric effect according to Equation 4 [158]:

$$E_{BE} = h\nu - E_{KE} - \phi \qquad \textit{Equation 4}$$

where E_{BE} is the electron binding energy in the material, $h\nu$ is the incident photon energy, E_{KE} is the kinetic energy associated, and ϕ is the work function of the spectrometer (constant value). Within an XPS system, the X-ray energy ($h\nu$) and work function are known values, and the system detects the kinetic energy of emitted electrons, allowing the photoelectron binding energy to be calculated.

The main interesting features of an XPS spectrum are the photoelectron peaks which come from the detection of photoelectrons which have escaped the surface without energy loss through inelastic collisions. These peaks have a specific

position which corresponds to a specific element and orbital [162], and allows the identification of elements in the surface [158]. For example, "C1s" describes electrons emitted from the 1s orbital of a carbon atom. Analysis of the detected photoemission peaks allows the quantification of elements present in the material's surface. For example, in Figure 2.14 which represents a XPS spectrum of allylamine plasma polymer coating, three elements have been identified, namely carbon at 285 eV, nitrogen at 399 eV, and oxygen at 532 eV. Electrons that have lost energy via inelastic collisions but have still escaped the surface contribute to the background upon which the photoelectron peaks sit. The shape of the background can also provide useful information, such as indicating if there is substrate influence due to a thin film coating.

2.7.1.2.2. Emission of Auger electrons

Auger electrons which are low energy electrons may also be emitted. Because of the loss of an electron in the ground state, an electron from a higher orbital will fill the electron-hole and the energy released can result in the emission of an Auger electron (Figure 2.13b) [158]. Auger electrons will be detected and can be used in XPS for qualitative analysis. Auger peaks are generally identified by the nomenclature K, L, M for atomic orbitals. For example, the main oxygen Auger peak is notated as KLL, which indicates that the first ejected electron came from a K orbital, the electron that filled the core hole came from an L orbital, and the final Auger electron ejected also came from an L orbital.

2.7.1.2.3. Chemical environment

In addition to the elemental composition, XPS is a technique that can identify the chemical environment of the atoms present in the material's surface, such as nearest neighbours and oxidation state of the element. Indeed, the binding energy of electrons depends on the chemical environment of the atoms especially the electronegativity of the nearest neighbour atom [158]. For the carbon, C-C bonds are referenced to 284.8 eV. The largest shift of carbon environment is observed for C-F bonds since fluorine is the most electronegative element. The main binding energies of C1s chemical states are summarised in Table 2.3.

Table 2.3: Binding energies of C1s chemical states [158,163,164].

Functional group	Chemical state	Binding energy (eV)
Hydrocarbon	C-R	~ 284.8
Amine (primary, secondary, tertiary)	C-NR	~ 286.0
Hydroxyl/Ether	C-O	~ 286.5
Imine	C=N	~ 286.5
Carbonyl	C=O	~ 288.0
Amide	N-C=O	~ 288.0
Carboxyl/Ester	O-C=O	~ 289.0
Fluoromethyl	C-F	~ 289.0
Difluoromethyl	$C-F_2$	~ 292.0
Trifluoromethyl	$C-F_3$	~ 293.0

Regarding nitrogen, the binding energies are in the range 399-400 eV which include amine (primary, secondary, tertiary), or amide [157]. As the binding energies are close, it is difficult to differentiate the different chemical environments and it may require techniques such as labelling to distinguish between components (refer to Section 2.7.2) [61].

2.7.1.2.4. Data analysis

The first step in XPS data analysis is the assignment of all the peaks present in the survey spectrum corresponding to a specific element and orbital. A variety of backgrounds can be used to determine the peak area for quantitative analysis or peak fitting for chemical state analysis. The most common approaches to define the background are the linear method, the Shirley method, and the Tougaard method [157]. In the case of polymers that have a large band-gaps, the linear background can be used since the step in the background over the energy range is relatively small. After background subtraction, atomic concentrations can be calculated by measuring the area under a peak. When quantifying atomic concentrations, Relative Sensitivity Factors (RSFs) are used to scale the measured peak areas in order to be representative of the amount of material present in the sample surface. One elemental peak is taken as the standard to which other peaks are referred, usually F1s. Different libraries of RSFs exist depending on the XPS

instrument and software. RSFs can also be calculated experimentally by analysing pristine materials such as polymers whose chemical structure is known. Finally, the XPS peak shapes are influenced by a combination of the physics involved in the ionisation process and the contribution from the spectrometer. The type of line shape mainly used for peak fitting is a convolution of a Gaussian and a Lorentzian function.

2.7.1.2.5. Angle-resolved XPS

Angle-resolved XPS helps to increase surface sensitivity by varying the emission angle at which electrons are detected from the surface. Most commonly, the electron analyser is positioned so that most of the detected electrons have originated from the sample surface with a trajectory in line with the surface normal. By tilting the sample, it is possible to modify the surface sensitivity. When the sample is untitled ($\alpha = 0°$), the escape depth and the sampling depth are the same as shown in Figure 2.15a. However, when the sample is tilted (for example, $\alpha = 70°$), the sampling depth becomes smaller than the escape depth due to the path they must travel to reach the detector is increased (Figure 2.15b). The escape depth remains the same as it only depends on the electron energies and the material.

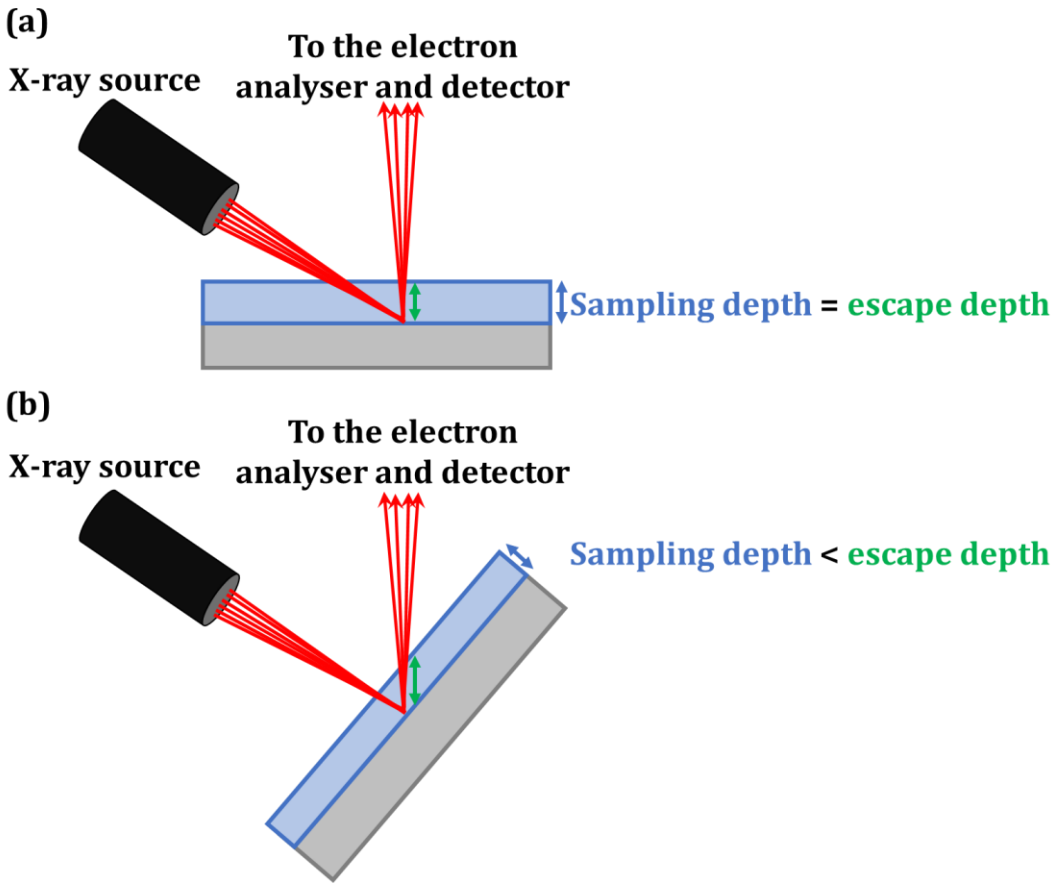

Figure 2.16: Schematic diagram of the differences in escape depth for (a) untitled and (b) titled samples for angle-resolved XPS.

2.7.1.3. Scanning electron microscopy (SEM)

Scanning electron microscopy (SEM) produces detailed and magnified images of an object by scanning its surface with a focused beam on electrons to create a high-resolution image. The electrons from the beam interact with the atoms of the material through either elastic or inelastic scattering. Elastic scattering is when incident electrons are deviated with no loss of energy, whereas inelastic scattering is when energy is lost, often through the ionisation of the atoms of the material. The interaction of the electrons and material's atoms produce different types of signals containing information about the surface topography and composition of the material. The most common imaging mode is the detection of secondary electrons. A schematic diagram of a SEM is represented in Figure 2.16.

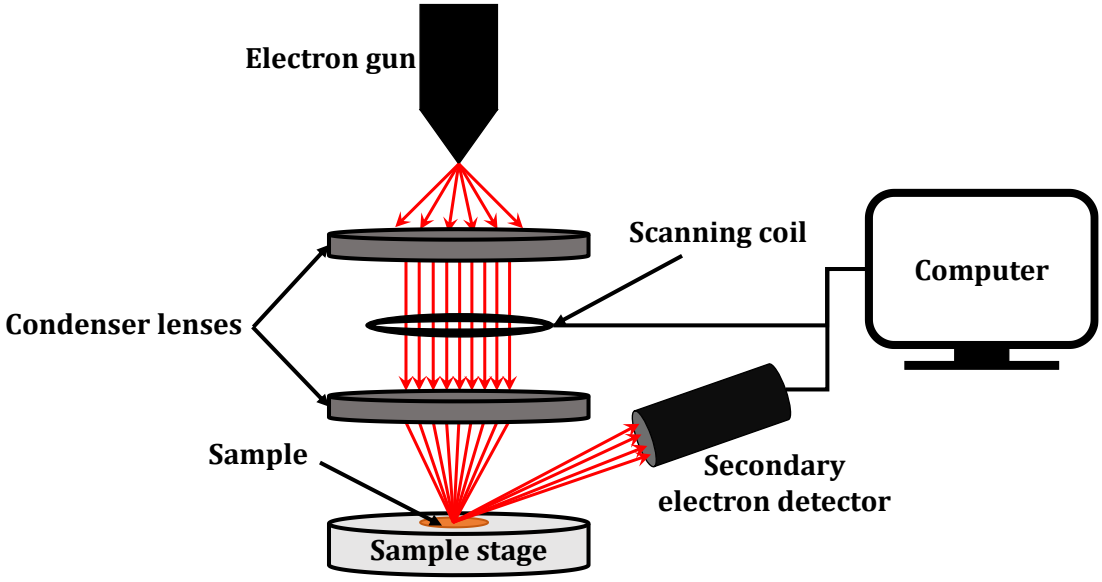

Figure 2.17: Schematic diagram of a scanning electron microscope.

This method can be used to image the coatings, which may be important to show the possible defects, leading to a non-homogeneous layer. Moreover, fibrils from collagen [165] or WPI [82] are easily detected on the substrates (Figure 2.17). Finally, this method is also used to analyse the cell adhesion and spreading on the material [82] or the damage of bacteria after contact with the coating [131].

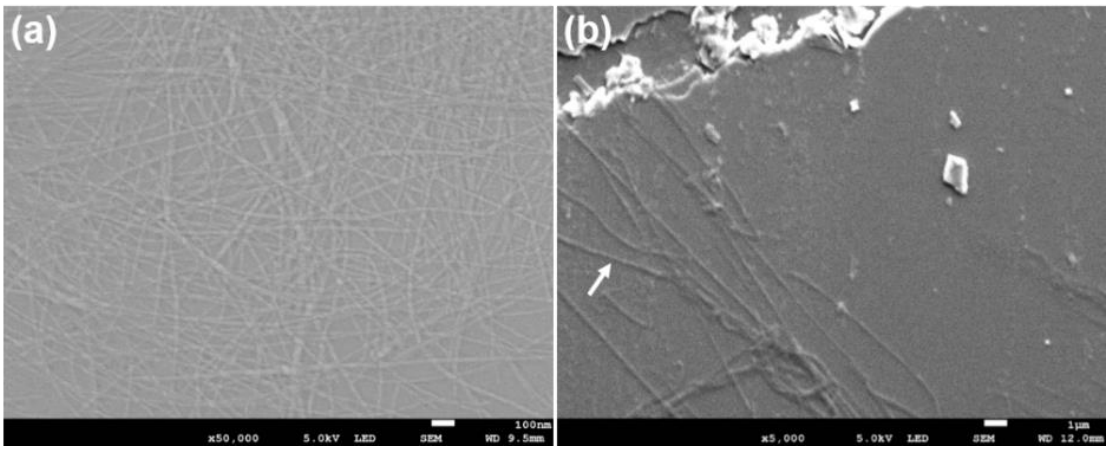

Figure 2.18: SEM images of (a) WPI fibrils and (b) collagen fibrils on glass substrates. Arrow indicates a collagen fibril. Scale bar: (a) 100 nm and (b) 1 µm.

2.7.1.4. Atomic force microscopy (AFM)

Atomic force microscopy (AFM) is a high-resolution type of scanning probe microscopy where a sharp tip coupled to a cantilever scans the surface of a material to obtain high-resolution nanoscale images. When the tip is brought close to a sample surface, forces between the tip and the sample lead to a deflection of the cantilever. A schematic diagram of an AFM is represented in Figure 2.18.

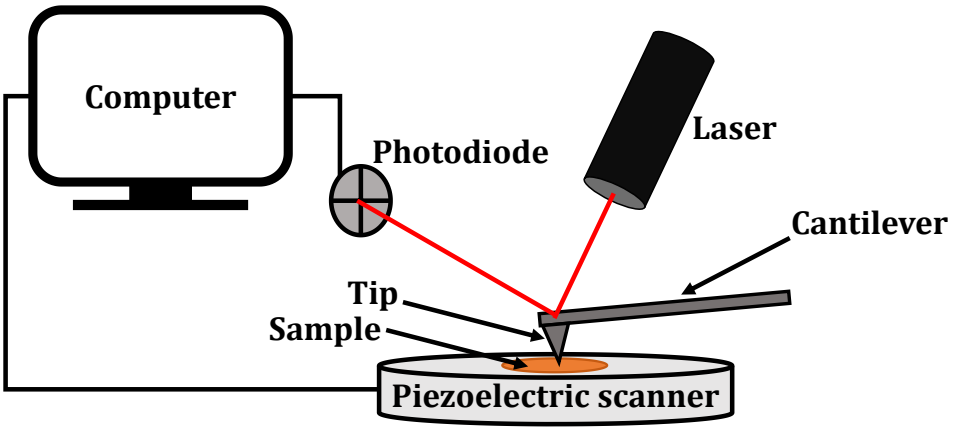

Figure 2.19: Schematic diagram of an atomic force microscope.

Different modes of imaging exist which are contact, non-contact, or tapping modes, as shown in Figure 2.19. In contact mode, the tip is in constant physical contact with the sample surface and scans the surface. Due to the surface topography, a cantilever deflection is detected and analysed. In non-contact mode, the tip is vibrated about its resonance frequency near the sample surface and brought close to the surface to sense van der Waals interactions. Finally, in tapping mode, the tip is oscillated near to its resonance frequency and the amplitude of this oscillation is measured. The tip is brought close to the surface, so it intermittently taps along the surface. Regardless of mode, the motion of the cantilever is monitored via a laser that is reflected off the back of the cantilever onto a photodetector. A feedback circuit is used, with a default cantilever deflection or amplitude value entered by the system operator. If the measured signal (e.g. deflection or amplitude) changes from the setpoint value, the sample is raised or lowered to compensate, allowing a topographical map of the sample surface to be built up. Further data, such as deflection, amplitude or phase data can be captured at the

same time, and a range of wider scanning probe techniques use these AFM modes as a based to collect information about different material properties.

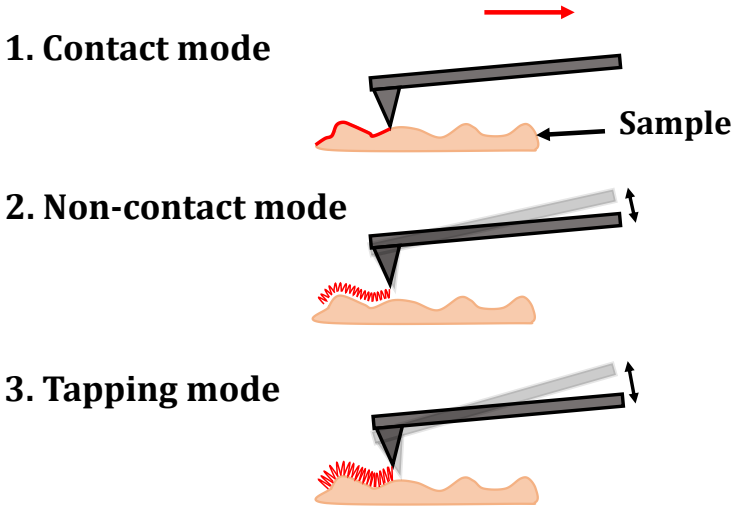

Figure 2.20: The three different imaging modes of AFM namely contact, non-contact, and tapping modes.

AFM can be used to study the morphology of the coatings, as Michelmore *et al.* performed for allylamine plasma coatings by varying the treatment time [166]. Fibrils from collagen or WPI can also be detected by this technique (Figure 2.20) [83,91]. Moreover, the surface roughness can be estimated, which is an important parameter since it affects cell behaviour, especially cell morphology and cell proliferation [156], as well as bacterial growth [167].

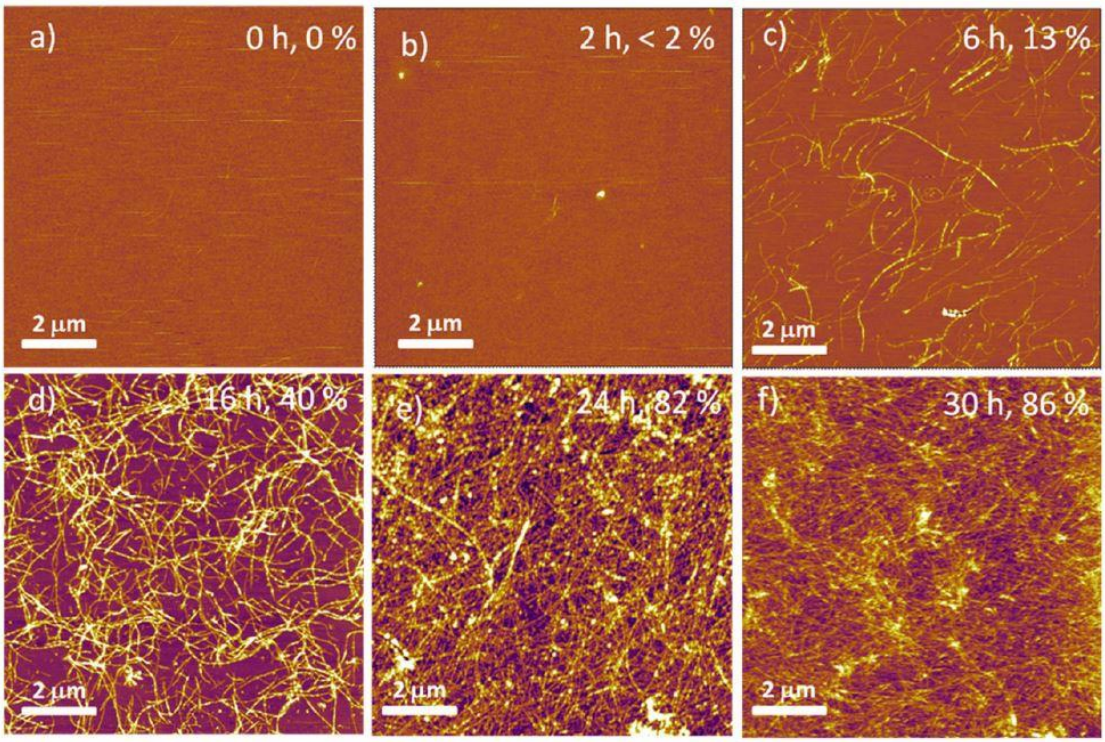

Figure 2.21: AFM images of (a) 2 wt.% lysozyme solution, and (b–f) amyloid fibril network from lysozyme solution by incubating fibrillar suspensions onto mica substrates for 10 min. Fibrillar suspensions formed at 90°C for (b) 2 h, (c) 6 h, (d) 16 h, (e) 24 h, and (f) 30 h (% coverage also listed on images). Z-scale = 10 nm. Reprinted with permission from [91]. *Copyright (2014) American Chemical Society.*

2.7.1.5. Fourier-transform infrared spectroscopy

Fourier-transform infrared spectroscopy (FTIR) is a method used to study the structural properties of materials, and especially the chemical bonds. This technique is based on the interaction between infrared light and vibrational states of the matter. Atoms in molecules are able to vibrate in different modes. When the frequency of a specific vibration mode is equal to the frequency of the incident infrared radiation, the molecule absorbs the radiation. The associated energy is converted into different types of motions. The vibrational motion is usually accompanied by other rotational motions. These combinations lead to the absorption bands commonly observed in the middle infrared region (4000–400 cm^{-1}). This technique is useful to detect protein coatings with specific absorption bands (amide A, amide I, amide II, …) [106,168]. This technique has been used by Sima *et al.* to detect possible structural changes of the FN by identifying the

characteristic peaks [94]. FTIR spectroscopy is also used to identify chemical bonds present in plasma polymer coatings, and it usually shows the fragmentation and re-organisation of the broken monomer used as well as the formation of new bonds as described by Abbas *et al.* [169].

2.7.2. Quantification of primary amine groups

2.7.2.1. Dyes

Different dyes can be used to quantifiy -NH_2. A comparative study between Orange II and Coomassie Brilliant Blue dyes showed that Orange II dye seems to be the most appropriate in the case of primary amine grafted on PET [170]. In another study, the Orange II dye was used on PET membrane treated by allylamine plasma. A positive correlation was found between the results of the colorimetric staining and XPS and FTIR analyses. Coomassie Brilliant Blue is commonly used following the amino density estimation by colorimetric assay (ADECA) method based on the reversible formation of a complex of CBB with the N^+ groups [171]. After staining and washing, the dye in solution is quantified, leading to an evaluation of the amine groups. The reversibility of the process provides an advantage to this method. However, this method seems to be less reliable than the Orange II quantification method due to steric hindrance that limits the interaction between the dye and amine groups [170].

2.7.2.2. Chemical derivatisation

Chemical derivatisation is widely used by grafting glutaraldehyde with an enzyme detectable by fluorescence spectroscopy or microscopy [73]. Regarding plasma deposition, in the vapor phase, amine groups may be identified via the grafting of compounds such as 4-trifluoromethyl-benzaldehyde (TFBA) as shown in Figure 2.21 [9] or pentafluorobenzaldehyde [160]. It can be chemically grafted via imine bonds to –NH_2 groups. Then, XPS analyses are performed to detect the presence of fluorine in the coating. Different equations can be found in the literature to calculate the amount of primary amine groups as shown in Table 2.4. TFBA has been widely used to quantify primary amines of plasma polymer coatings [68,172–176].

Girard-Lauriault *et al.* used this technique to quantify primary amine groups on nitrogen-rich plasma coatings [174]. They studied the reaction kinetics, the depth profile of the functional group or derivatised surfaces, the possible side reactions, and different samples. Different conditions of derivatisation were tested, under vacuum and at atmospheric pressure, and different samples. Regarding the kinetics of the reaction, some differences were noticed depending on the samples and the experimental conditions. They recommended starting any derivatisation work with a kinetic study to determine the optimum parameters [174]. The derivatisation time should also be longer than the time to reach saturation since samples may be slightly different. Since plasma polymer films may have an irregular structure which can be tortuous, a small fraction of functional groups is likely to be inaccessible by the derivatisation molecule [174].

Different commercially available polymers were also derivatised to assess possible side reactions [174]. Linear polyethyleneimine, which contains secondary amines only, reacted with TFBA although it should not react. Moreover, branched polyethyleneimine was derivatised more than it should have been. This was likely due to the possible reaction of secondary amines separated by two carbons that can form a five-membered heterocycle by reacting with an aldehyde [174]. However, in plasma polymer films, this structure is unlikely. Therefore, for plasma polymer films, TFBA should only bind primary amines, but it is worth mentioning that possible side reactions can occur with conventional polymers [174]. Hence, positive controls are difficult to find but amino parylene may be a suitable commercially available standard as it previously showed total derivatisation of all primary amines to TFBA [177]. Another study investigated the depth profile of derivatised plasma coatings with TFBA [173]. They found a strong variation in the amount of fluorine within the coating likely due to the low permeation of TFBA molecules inside the coating (large size of the molecule) which can lead to an underestimation of primary amines. A smaller molecule, 2-trifluoromethyl-propionaldehyde, may be another suitable candidate for primary amine quantification. However, this molecule is highly toxic [173]. Due to the high sensitivity of TFBA to air, the reaction needs to occur in a controlled environment

(glovebox), or under vacuum. Therefore, all these elements need to be considered before performing this experiment.

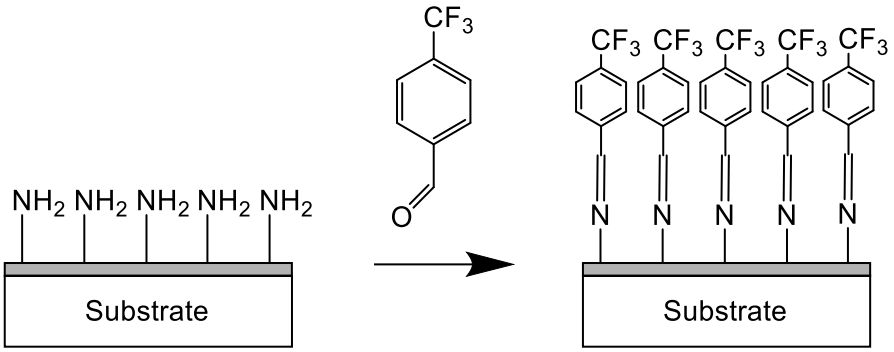

Figure 2.22: TFBA derivatisation of primary amines. TFBA molecules are chemically grafted to the primary amines which are present in the coating. Then, fluorine can be quantified by XPS which allows the quantification of primary amines.

Table 2.4: The different equations used to calculate the concentration of primary amines.

	Equation	**Ref.**
$\frac{[NH_2]}{[N]} = \frac{[F]/_3}{[N]} \times 100$	where $[NH_2]$, $[F]$, and $[N]$ represent respectively the relative concentration of primary amines, fluorine, and nitrogen at the sample surface.	[28,68, 70,163]
$\frac{[NH_2]_u}{[C]_u} = \frac{[F]_d[N]_u}{3[N]_d[C]_u} \times 100$	where $[NH_2]$, $[F]$, and $[N]$ represent respectively the relative concentration of primary amines, fluorine, and nitrogen at the sample surface. Subscripts u and d refer to XPS before and after TFBA derivatisation, respectively.	[68]
$\frac{[NH_2]}{[C]} = \frac{[F]/_3}{[C] - 8[F]/_3} \times 100$	where $[NH_2]$, $[F]$, and $[C]$ represent respectively the relative concentration of primary amines, fluorine, and carbon at the sample surface.	[163,178,179]

2.8. Conclusions

Multiple methods have been developed to create amine-rich coatings such as plasma techniques and more importantly plasma polymerisation, which is a

method widely used for its numerous advantages (quick deposition, homogeneous coating, deposition on multiple samples in a one-step process). However, this method requires an equipment which may be expensive due to the pumping system.

Moreover, these amine coatings may be obtained from biomolecules such as proteins. The ability of proteins to form fibrils (collagen fibrils or amyloid fibrils) makes them interesting due to their high surface/volume ratio, which increases the fibril adhesion. They can be used as a matrix to incorporate other molecules with additional, desirable characteristics such as antimicrobial properties. Collagen fibril coatings have been deeply investigated but this method can also be expensive due to the high cost of collagen. However, much less work has been performed on amyloid fibrils and especially fibrils from whey protein (a by-product from the dairy industry), which is an inexpensive protein possessing interesting properties.

Synthetic polymers such as polyethyleneimine or polydopamine have been used as coatings to control cell behaviour, and they might have antibacterial properties. This effect needs to be investigated in more detail since the results have been controversial. Their possible cytotoxicity has to be more studied since it must be avoided for biomedical applications. To summarise, these strategies still need to be explored in order to obtain amine functional coatings for biomaterial applications such as implants, which could prevent bacterial infection as well as enhancing cell adhesion, proliferation, and differentiation.

On the basis of this literature review, different methods to generate primary amine-rich coatings were used in this research project. Firstly, allylamine plasma polymer was studied by using different conditions of power and pressure to investigate their impact on the amount of primary amine groups. Moreover, the use of whey protein to make fibrillar coatings was investigated to produce protein coatings rich in primary amines that can be sterilised by autoclaving. These two methods will be further developed in the next chapters.

Chapter 3. Materials and methods

3.1. Introduction

This chapter presents all the experimental methods used in this thesis, including those used to produce plasma coatings and protein coatings. Moreover, the method used for cell tests and antibacterial tests will be described. Finally, all the characterisation methods performed will be explained, including X-ray photoelectron spectroscopy (XPS), scanning electron microscopy (SEM), water contact angle (WCA) measurements, atomic force microscopy (AFM), and the quantification of primary amine groups by chemical derivatisation.

3.2. Experimental methods

3.2.1. Plasma coatings

3.2.1.1. Material

Allylamine (purity ≥ 99%) was purchased from Sigma Aldrich, UK. Glass coverslips (10 mm diameter) were obtained from Scientific Laboratory Supplies, UK. Silicon wafer was acquired from Inseto, UK, and cut into samples of approximately 1 cm x 1 cm. Substrates were cleaned in an ultrasonic bath of isopropanol followed by washing in Milli-Q water, and a final cleaning in an ultrasonic bath of acetone.

3.2.1.2. Plasma deposition equipment

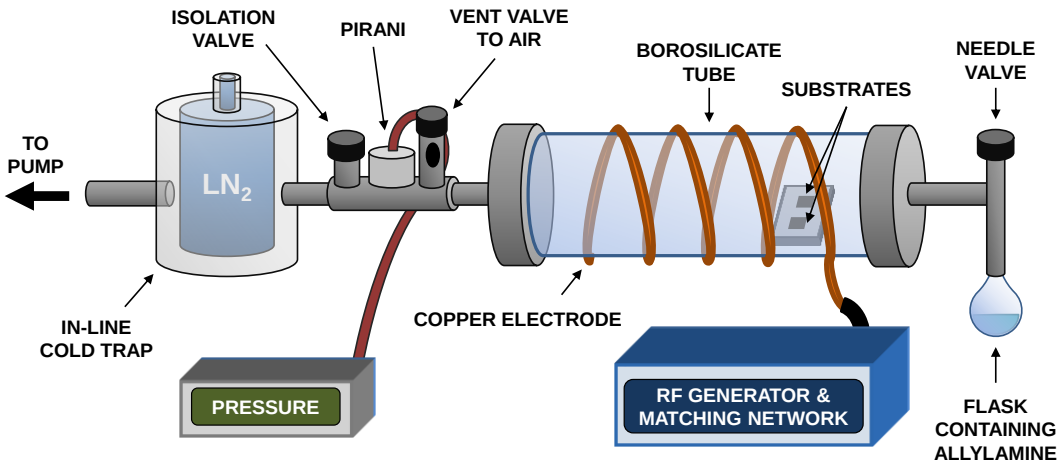

Figure 3.1: Diagram of the plasma reactor used for the deposition of allylamine plasma polymer coatings. From the right to the left: flask containing allylamine monomer connected to a glass barrel surrounded by a copper electrode. Inside the borosilicate tube, substrates are placed on a glass slide on the right near the precursor injection. The copper electrode is connected to the RF generator coupled with a matching network. All the other parts of the reactor are grounded. An in-line cold trap filled with liquid nitrogen (LN_2) is used to trap all the monomer vapour residues. The system is connected to a pumping system and a pressure gauge.

All allylamine plasma polymer (AApp) coatings were deposited in a glass barrelled plasma polymerisation reactor as shown in Figure 3.1. The glass barrel of the reactor was a QVF process pipe (De Dietrich, UK) – dimensions 500 mm length, 100 mm diameter, clamped between two custom-made steel end plates which serve as ground electrodes. The vacuum chamber was evacuated by a pumping system consisting of an Edwards RV3 rotary vane vacuum pump (Edwards Vacuum, UK) and an in-line cold trap (Kurt J Lesker, UK) filled with liquid nitrogen to prevent allylamine vapour reaching the pumping system. The pressure was measured by a Pirani gauge and controller (Leybold, UK) and the base pressure was less than 5×10^{-1} Pa. A 10 mm wide copper braid (Tranect, UK) wound around the glass barrel three times acted as the load electrode and was connected to Coaxial Power Systems RFGC 100-13 RF generator coupled with an automatic matching network. Allylamine was degassed using LN_2 and kept in a water bath at

room temperature to maintain a constant temperature during the plasma deposition.

3.2.1.3. Preparation of allylamine plasma polymer coatings

Allylamine plasma coatings were made by varying different parameters, namely the pressure (2 Pa, 20 Pa) and the power (5.5 W, 30 W), as described in Table 3.1. The deposition time was fixed at 20 min since it allows a thick enough coating to mask the substrate signal for XPS analysis (>15 nm). The substrates were placed on a glass slide in the glow region of the plasma.

Table 3.1: Allylamine plasma coating denomination depending on the plasma parameters used (pressure and power).

Sample name	Pressure	Power
AApp1	2 Pa	30 W
AApp2	20 Pa	5.5 W

3.2.2. Protein coatings

3.2.2.1. Material

Glass coverslips (10 mm diameter) were purchased from Scientific Laboratory Supplies. WPI was provided by BiPro, Davisco Foods International Inc. (Eden Prairie, MN, USA). Phloroglucinol (PG) was obtained from Sigma Aldrich, UK and tannic acids (ALSOK 2 (1040 kD, 20% PGG), ALSOK 4 (850 kD), and Brewtan F (1450 kD, 5% PGG)) from Omnichem NV, Belgium. Ti6Al4V discs (10 mm diameter and 2 mm thick) were obtained from Dr. Roman A. Surmenev (National Research Tomsk Polytechnic University, Russia). These Ti alloy discs were additively manufactured in an A2 ARCAM EBM machine (ARCAM EBM, Mölnlycke, Sweden). Electron beam melting (EBM®), is a technology where the components are manufactured layer by layer in vacuum from a metallic precursor powder melted by an intense electron beam.

3.2.2.2. Preparation of whey protein isolate (WPI) fibrillar suspensions

WPI fibril suspensions were prepared as previously described by Keppler *et al.* [121]. A stock solution of WPI in water was prepared at a concentration of 2.5% w/v with stirring until complete dissolution. pH was set to 2.0 by adding 2 M HCl solution dropwise. 40 mL of WPI solution was heated in a 100 mL Duran glass bottle at 90°C for 5h with a stirring speed of 350 rpm to induce fibril formation resulting in a fibrillar suspension. Finally, the WPI fibrillar suspension was cooled down at 4°C in a water bath to stop the reaction and subsequently stored at 4°C.

PG was also incorporated in WPI fibrillar suspensions. After cooling down the WPI fibrillar suspension in cool water (4°C), PG was added to obtain suspensions enriched with PG at two different concentrations: 0.1%, and 0.5% w/v. Another way to make WPI fibril coatings enriched with PG was by adsorption of PG on top of WPI fibrillar coatings as described in Section 3.2.2.3 and in Figure 3.2.

Other WPI fibrillar suspensions were prepared by adding three different TAs (ALSOK 2, ALSOK 4, and Brewtan F) as shown in Figure 3.3. WPI fibrillar suspensions were made with TAs added before fibril formation with a concentration of 1% w/v, and others were made with TAs added after fibril formation, in the same way as for PG, with a concentration of 1% w/v.

3.2.2.3. Preparation of WPI fibrillar coatings

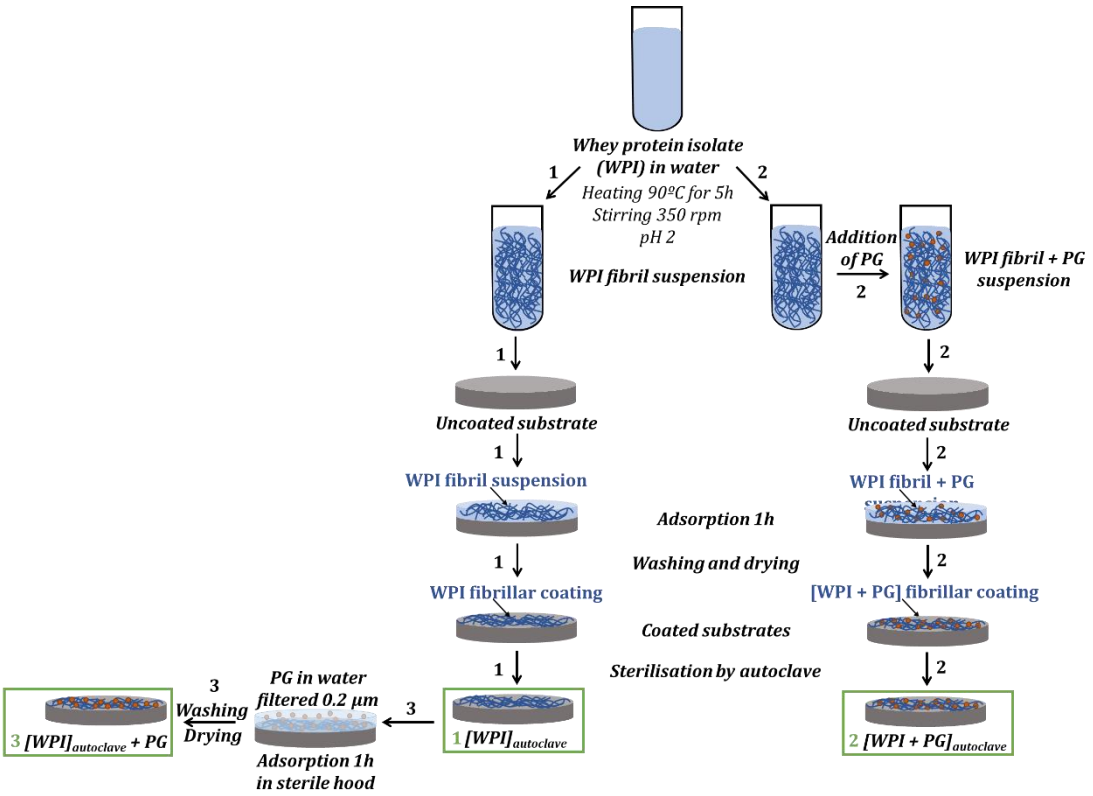

Figure 3.2: Diagram of the WPI coating process with PG. Three different ways of making coatings are represented here namely 1 which is WPI coating only, 2 which is WPI + PG coating which was autoclaved, and 3 which is WPI + PG coating with PG added after the sterilisation of WPI coating only.

Glass slides or Ti6Al4V alloys were first cleaned with ethanol and water. Then, WPI fibril suspension was placed onto the substrates for 1h to allow fibril adsorption as shown in Figure 3.2. After rinsing three times with Milli-Q to remove non-adhered fibrils, and drying at room temperature, the substrates were coated with a thin layer of WPI fibrils. Finally, these coatings were sterilised by autoclaving (121°C, 1 atm, 15 min). In Figure 3.2, this procedure is represented by the process 1. The same procedure was followed to make WPI coatings enriched with PG as described by the processes 2 and 3 in Figure 3.2. For process 2, WPI fibrillar suspensions containing PG were used to coat the substrates, then the same steps as described earlier were followed. For process 3, PG solution in Milli-Q water (0.2 µm filtered) was added on top of an autoclaved WPI fibrillar coating in sterile conditions. PG adsorption was for 1h, and coatings were then washed 3x with

Milli-Q water and dried at room temperature. Two different concentrations of PG were tested, 0.1% and 0.5% (w/v) in Milli-Q water. PG/WPI coatings are named as indicated in Table 3.2.

Table 3.2: WPI coatings denomination with and without PG.

Coating denomination	Description
$[WPI]_{autoclave}$	WPI fibrillar coating autoclaved
$[WPI + PG\ 0.1\%]_{autoclave}$	WPI + PG 0.1% mixed coating autoclaved
$[WPI + PG\ 0.5\%]_{autoclave}$	WPI + PG 0.5% mixed coating autoclaved
$[WPI]_{autoclave}$ + PG 0.1%	WPI fibrillar coating autoclaved + PG 0.1% added after
$[WPI]_{autoclave}$ + PG 0.5%	WPI fibrillar coating autoclaved + PG 0.5% added after

WPI coatings were also made with TAs. The procedure is represented in Figure 3.3. The procedure 1 is the WPI coating as previously described. The procedure 2 is WPI + TAs coating with TAs added before fibril formation. Finally, the procedure 3 is WPI + TAs coating with TAs added after fibril formation, similarly to the previous procedure 2 with PG. Three different TAs were used namely ALSOK 2 (AL2), ALSOK 4 (AL4), and Brewtan F (BRW). The concentration of TAs was set to 1% w/v. TAs/WPI coatings are named as indicated in Table 3.3.

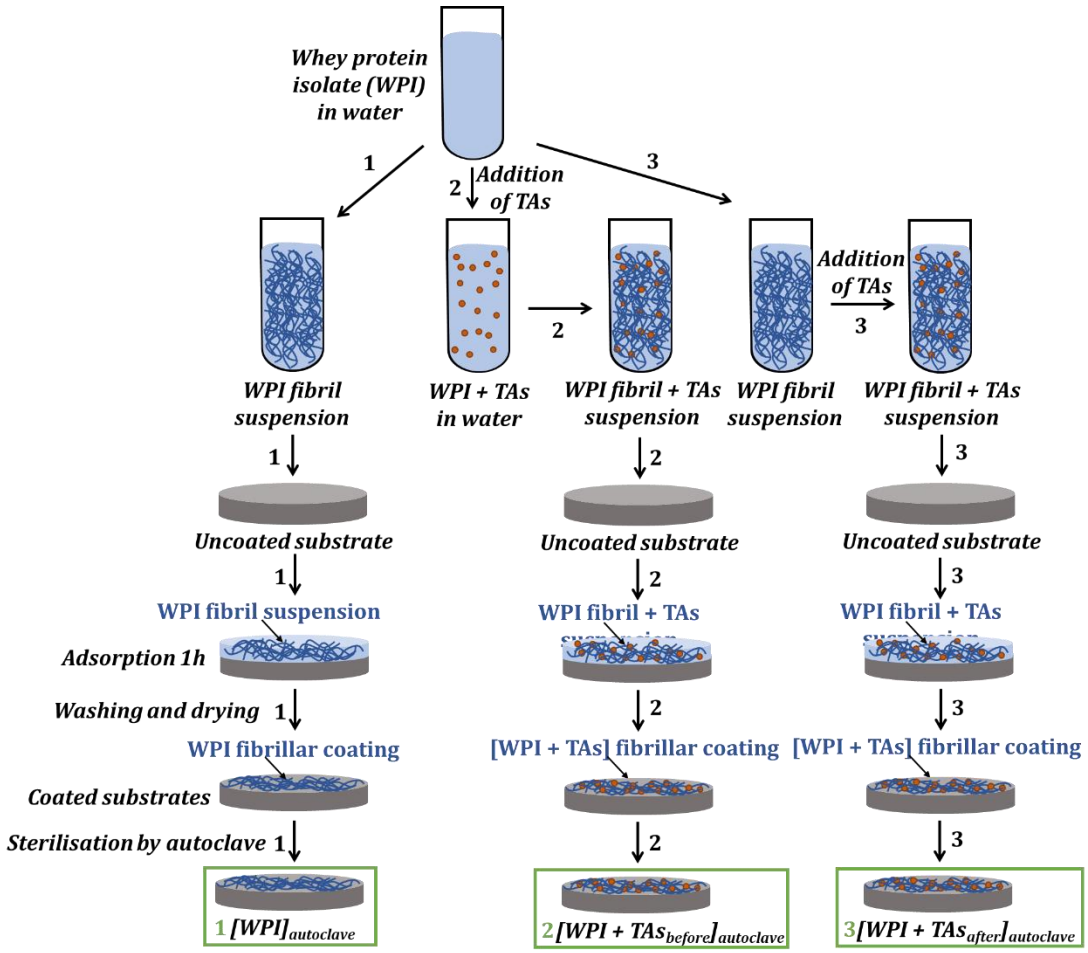

Figure 3.3: Diagram of the WPI coating process with TAs. Three different procedures of making coatings are represented here namely 1 which is WPI coating only, 2 which is WPI + TAs coating with TAs added before fibril formation, and 3 which is WPI + TAs coating with TAs added after fibril formation.

Table 3.3: WPI coating denominations with and without TAs. The concentration of TAs was fixed to 1% w/v.

Coating denomination	TA	TA added before/after fibril formation
$[WPI]_{autoclave}$	-	-
$[WPI + AL2_{before}]_{autoclave}$	ALSOK 2	Before
$[WPI + AL4_{before}]_{autoclave}$	ALSOK 4	Before
$[WPI+BRW_{before}]_{autoclave}$	Brewtan F	Before
$[WPI + AL2_{after}]_{autoclave}$	ALSOK 2	After
$[WPI + AL4_{after}]_{autoclave}$	ALSOK 4	After
$[WPI+BRW_{after}]_{autoclave}$	Brewtan F	After

3.2.2.4. Coating stability study

WPI coatings stability was studied by immersing the coatings in PBS for different times (1h, 5h, and 24h). After immersion, the samples were washed three times with Milli-Q water and imaged by SEM (refer to Section 3.3.2 for the SEM procedure).

3.2.2.5. *In vitro* studies of WPI/PG coatings

The in vitro tests were performed by Anna Mieszkowska from Jagiellonian University in Krakow (Poland) under the supervision of Dr. Katarzyna Gurzawska-Comis fron the University of Birmingham (UK) whom I would like to acknowledge them for their collaboration. Samples were made at Lancaster University and sent to Poland for the tests.

3.2.2.5.1. Bacterial strains and culture conditions

Bacterial strains used in this study were obtained from the Periodontal Research Group culture collection (School of Dentistry, University of Birmingham, UK). *Streptococcus mitis* ATCC 49456 and *Aggregatibacter actinomycetemcomitans* ATCC 43718 were grown for 24h at 37°C, 5% CO_2 on horse blood agar plates (Oxoid, Basingstoke, UK). *Fusobacterium nucleatum* ssp*. polymorphum* ATCC 10593 was grown at 37°C in an anaerobic chamber (80% N_2, 10% CO_2 and 10% H_2; Don Whitley DG250 Anaerobic Workstation, Don Whitley Scientific, Bingley, UK) on Schaedler Anaerobe agar plates (Sigma-Aldrich/Merck, Darmstadt, Germany) for 48h. *Porphyromonas gingivalis* ATCC 33277 was grown on horse blood agar plates (anaerobically, 37°C) for at least 96h.

Liquid cultures of *S. mitis* and *A. actinomycetemcomitans* were grown in Brain Heart Infusion broth (Oxoid, Basingstoke, UK), *F. nucleatum* and *P. gingivalis* in Schaedler Anaerobe broth (Oxoid, Basingstoke, UK).

3.2.2.5.2. Biofilm formation

Multi-species biofilms were prepared as previously described [180,181]. Briefly, overnight cultures were standardised to 1 x 10^7 colony-forming units/ml in artificial saliva (AS) prepared as follows: porcine stomach mucins 0.25% w/v,

potassium chloride 0.02% w/v, calcium chloride dihydrate 0.02% w/v, yeast extract 0.2% w/v, proteose peptone 0.5% w/v (all obtained from Sigma-Aldrich/Merck, Darmstadt, Germany), sodium chloride 0.35% w/v (Thermo Fisher Scientific, Loughborough, UK), and Lab-Lemco powder 0.1% w/v (Oxoid, Basingstoke, UK) in ultrapure water (Milli-Q, Merck Millipore, Burlington, MA, USA); urea was added after autoclaving to a final concentration of 0.05% v/v (Sigma-Aldrich).

To initiate biofilm growth, standardised *S. mitis* culture was added to a 24-well plate containing 13 mm Thermanox™ coverslips (Thermo Fisher Scientific, Loughborough, UK) and incubated at 5% CO_2, 37°C. After 24h, biofilm supernatant was removed, standardised *F. nucleatum* culture was added and biofilms were further incubated for 24h under anaerobic conditions at 37°C. The supernatant was removed, *A. actinomycetemcomitans* and *P. gingivalis* were added and biofilms were incubated anaerobically for 4 days at 37°C, with AS replaced every 24 hours.

3.2.2.5.3. Biofilm structure

Biofilms for SEM imaging were prepared as described by Muchova *et al.* [182]. Firstly, fixation of biofilms was performed using 2.5% glutaraldehyde (Agar Scientific, Stansted, United Kingdom) in 0.1M sodium cacodylate buffer (pH 7.4, BioWorld, Dublin, Ireland) for 10 min at room temperature. Biofilms were then dehydrated using increasing concentrations of ethanol (20 – 100%). Subsequently, a drying agent hexamethyldisilizane (HMDS; SigmaAldrich/Merck, Darmstadt, Germany) was applied. After an overnight HMDS evaporation, biofilm samples were mounted onto aluminium specimen stubs (Agar Scientific, Stansted, United Kingdom), sputter-coated with gold and images were taken with a scanning electron microscope (Zeiss EVO MA10).

3.2.2.5.4. Culture and seeding of human bone marrow-derived mesenchymal stem cells (BM-MSCs)

The study was performed using commercially available human bone marrow-derived mesenchymal stem cells (BM-MSCs; catalog no. PCS-500-012) obtained from American Type Culture Collection (ATCC; Manassas, VA, USA). Cells were

cultured in α-minimum essential medium (Lonza, Verviers, Belgium) containing 10% fetal bovine serum (Invitrogen, Paisley, UK), 100 U/mL penicillin (Sigma-Aldrich, Gillingham, UK), 100 µg/mL streptomycin (Sigma-Aldrich, Gillingham, UK) and incubated at 37°C in a humidified atmosphere of 95% air and 5% CO_2 until confluence. BM-MSCs from passage 3–5 were used in the present study. For all *in vitro* assays, BM-MSCs were seeded directly on titanium uncoated (Ti) and titanium coated ($[WPI]_{autoclave}$, $[WPI+PG\ 0.1\%]_{autoclave}$, $[WPI+PG\ 0.5\%]_{autoclave}$, $[WPI]_{autoclave}$ + PG 0.1%, $[WPI]_{autoclave}$ + PG 0.5%) discs placed in the wells of 48-well tissue culture polystyrene (TCPS) plate (Life technologies, Paisley, UK) at a concentration of 3×10^4 cells/disc and cultured for 72h. For osteogenic differentiation, to assess ALP activity, medium was replaced with fresh standard medium supplemented with 10 nM dexamethasone, 25 µg/ml ascorbic acid, and 10 mM β-glycerophosphate (Sigma-Aldrich, Gillingham, UK) after 72h of cell cultivation.

3.2.2.5.5. Cell morphology

SEM analyses were performed to study the morphology of BM-MSCs grown on the surface of tested titanium discs. Briefly, after 72h of cell cultivation, samples were washed three times with PBS for 10 min to remove the non-adherent cells. The cells were then fixed using 2% glutaraldehyde in 0.1M sodium cacodylate buffer, pH 7.4, for 2h at room temperature. After removal of the glutaraldehyde solution, the samples were sequentially dehydrated in ascending concentrations of ethanol. Finally, hexamethyldisilane (HMDS – Sigma-Aldrich, Gillingham, UK) was added onto each sample and left to dry overnight at room temperature. Imaging was performed using a scanning electron microscope (Zeiss, Göttingen, Germany).

3.2.2.5.6. Biofilm challenge

After 72h of cell cultivation in standard medium, each of the titanium discs with BM-MSCs was carefully removed from the wells of 48-well TCPS plate with sterile forceps and placed in the wells of 24-well TCPS plate (Life technologies, Paisley, UK). BM-MSCs on titanium were washed twice with fresh medium and then challenged for 2h in antibiotic-free medium at 37°C in 5% CO_2 with one biofilm-coated glass coverslip per well. Glass coverslips were placed on the ring support

with the biofilm towards the titanium surface according to the co-culture set-up as previously described [183]. The distance between BM-MSC layer and biofilm-coated coverslip was necessary to allow fluid flow. After 2h the biofilm-coated glass coverslips were removed from all wells, and titanium discs with BM-MSCs were washed twice with fresh medium and cultured for 48h in standard medium with antibiotics for further *in vitro* assays (metabolic activity and gene expression analysis). For the ALP activity assay, standard medium was replaced with osteogenic medium.

3.2.2.5.7. Metabolic activity

The metabolic activity of BM-MSCs was determined by the MTT assay at 48h after biofilm stimulation. Metabolic activity was assessed in both unstimulated and biofilm-stimulated BM-MSCs in parallel. Briefly, the cell culture medium was replaced by fresh medium containing methylthiazolyldiphenyl-tetrazolium bromide (MTT) (Sigma-Aldrich, Gillingham, UK) with a final concentration of 0.5 mg/ml. After 3h of incubation at 37°C in a humidified CO_2 incubator, medium containing MTT was removed, and isopropanol with 0.04 N HCl was added to dissolve formazan crystals. The absorbance was measured at 570 nm. All experiments were performed 4 times in duplicate (n=8).

3.2.2.5.8. Gene expression analyses

To determine gene expression, total RNA was isolated after 48h from both unstimulated, and biofilm-stimulated BM-MSCs using TRI reagent (Sigma-Aldrich, Gillingham, UK) and the RNeasy Mini Kit (Qiagen, Crawley, UK). The protocol was followed according to the manufacturer's specification. Purity and quantity of RNA was measured using NanoDrop (Thermo Fisher Scientific). The RNA was reverse-transcribed to cDNA using one-step high-capacity cDNA RT kit (Applied Biosystems, Warrington, UK) according to the manufacturer's instructions. Real-time PCR was performed on the CFX96 Touch Real-Time PCR Detection System (BioRad, Feldkirchen, Germany) using Roche SYBR Green PCR Master Mix (Roche Diagnostics GmbH, Mannheim, Germany). Real-time PCR reactions were carried out in 10 µL volumes in a 96-well plate (Roche Diagnostics GmbH, Mannheim, Germany) containing 1 µL of cDNA and 9 µL reaction mixture, according to the

manufacturer's instructions. All samples were amplified in duplicates. PCR conditions consisted of an initial denaturation step of 95°C for 5 min, followed by 40 cycles of 95°C for 10 s, 60°C for 15 s, and 72°C for 20 s. The primer sequences (Sigma-Aldrich, Gillingham, UK) for the specific target genes are presented in Table 3.4. GAPDH was used as reference gene in each experiment. Relative quantification of messenger RNA levels of the target genes was analyzed using the comparative CT (threshold cycle values) method ($2^{-\Delta\Delta Ct}$), as previously described by Livak *et al.* [184]. Relative expression levels were calculated for each sample after normalisation against the reference gene. All experiments were performed 4 times in duplicate (n=8).

Table 3.4: Primer sequences for Real-Time PCR.

Gene name	Gene abbreviation	Primer	Sequence 5' to 3'
glyceraldehyde-3-phosphate dehydrogenase	*GAPDH*	forward	GAAGGTGAAGGTCGGAGTC
		reverse	GAGATGGTGATGGGATTTC
RUNX family transcription factor 2	*RUNX2*	forward	TCTTAGAACAAATTCTGCCCTTT
		reverse	TGCTTTGGTCTTGAAATCACA
collagen 1 type 1 alpha	*COL1A1*	forward	GGTCAAGATGGTCGCCCC
		reverse	GGAACACCTCGCTCTCCAG
alkaline phosphatase	*ALP*	forward	CCTCGTTGACACCTGGAAGAG
		reverse	TTCCGTGCGGTTCCAGA
osteopontin	*OPN (SPP1)*	forward	CGAGGTGATAGTGTGGTTTATGG
		reverse	GCACCATTCAACTCCTCGCTTTC
bone gamma-carboxyglutamate protein (osteocalcin)	*BGLAP*	forward	CTACCTGTATCAATGGCTGGG
		reverse	GGATTGAGCTCACACACCT
interleukin 1 alpha	*IL1A*	forward	CGCCAATGACTCAGAGGAAGA
		reverse	AGGGCGTCATTCAGGATGAA
interleukin 1 beta	*IL1B*	forward	TTCGAGGCACAAGGCACAA
		reverse	AAGTCATCCTCATTGCCACTGT
interleukin 8	*IL8*	forward	ATGACTTCCAAGCTGGCCGTGGCT
		reverse	TCTCAGCCCTCTTCAAAAACTTCT

3.2.2.5.9. Alkaline phosphatase (ALP) activity

For evaluation of the osteogenic differentiation, early marker alkaline phosphatase (ALP) was analysed after 7 days. The ALP enzyme activity was determined in cell lysates using an alkaline phosphatase assay kit (Abcam, Cambridge, UK) that is based on p-nitrophenyl phosphate as a phosphatase substrate which turns yellow when dephosphorylated by ALP. The absorbance was measured at 405 nm. The ALP activity was determined in agreement with manufacturer instructions and normalized by the total protein content determined by BCA protein assay kit (Thermo Fisher Scientific, Waltham, USA). The ALP activity is expressed as mU/mg protein. All experiments were performed 3 times in duplicate (n=6).

3.2.2.5.10. Statistical analyses

Data are presented as the mean values ± standard error of the mean. Statistical differences in the *in vitro* studies were calculated by one-way ANOVA, followed by a multiple comparison Bonferroni test using SPSS version 22 (IBM, Armonk, NY, USA). A p value < 0.05 was regarded as significant.

3.2.2.6. Antibacterial tests

Bacteria were maintained in 15 % (v/v) glycerol freezer stocks at -80°C. They were streaked out onto Luria-Bertani (LB) agar to obtain single colonies.

For susceptibility tests, bacterial strains were grown overnight on LB agar at 37°C. Bacteria suspensions were prepared in Milli-Q water to an optical density of 0.05 (OD_{600} = 0.05). 200 µL of bacteria suspension was spread on LB agar or Diagnostic Sensitivity Test (DST) agar. Coated glass with WPI (control) and WPI containing PG were placed on the bacterial inoculum as shown in Figure 3.4. The plates were incubated overnight at 37°C. After 18h, the zones of inhibition (ZOI) were measured.

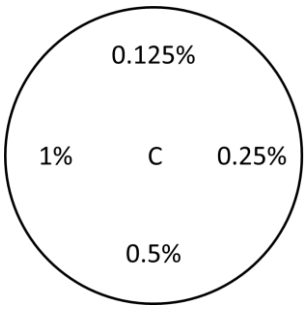

Figure 3.4: Schematic diagram of the placement of the coatings in the agar plate for the antibacterial tests. C is the control sample which corresponds to WPI coatings. WPI/PG coatings were placed around the control. Different concentrations of PG were tested: 0.125, 0.25, 0.5, and 1%.

3.2.2.7. Bacterial attachment study

For this assay, *S. epidermidis (RP62A)* was plated out onto CAP plate and incubated at 37°C for 24h. 3 mL of nutrient broth was inoculated with a single colony and incubated at 37°C for 24h. The bacteria suspension was diluted to 3 x 10^7 CFU mL^{-1}. The samples were inoculated in 1 mL of bacterial suspension at 37°C for 24h. The samples were then washed with PBS (1 mL, x3) and dried. Finally, samples were stained with crystal violet for 1 min, washed with water, stained with Lugol's iodine for 1 min, washed with water, decolorise with acetone for 1-2 s, and washed immediately with water. Finally, the samples were counterstained with neutral red for 1-2 min and washed with water. Samples were observed under a light microscope and images were obtained (x100 oil immersion objective).

3.2.2.8. *In vitro* studies of WPI/TAs coatings

These tests were performed by Dr. Ute Hempel from Technische Universität Dresden (Germany) whom I would like to acknowledge for her collaboration. Samples were made at Lancaster University and sent to Germany for the in vitro tests.

3.2.2.8.1. Isolation and culture of human bone marrow stromal cells (hBMSCs)

Human bone marrow stromal cells (hBMSCs) were isolated from bone marrow aspirated obtained from 4 donors (donor 1: female, 32 yrs ; donor 2: male, 21 yrs. ; donor 3: male, 22 yrs. ; donor 4: female, 39 yrs.) at the Bone Marrow Transplantation Center, University Hospital Dresden (Germany). The donors were

duly informed about the procedures and gave their full consent. The study was approved by the local ethics commission (ethic vote No. EK466112016).

For the in vitro tests, the seeding density was 5,555 hBMSC/cm^2 in cell culture medium (Dulbecco's minimal essential medium, DMEM, Merck-Millipore, Darmstadt, Germany), with 10% heat-inactivated fetal calf serum and antibiotics (Sigma Aldrich). Cells were seeded on the surface of each sample. At day 4 after plating, cell culture medium was replaced by osteogenic differentiation medium (DMEM with 10% heat-inactivated fetal calf serum and antibiotics supplemented with 10 mM α-glycerophosphate, and 300 µM ascorbate. The medium was changed twice per week.

3.2.2.8.2. Metabolic activity

At day 2 after plating, the metabolic activity of hBMSCs was determined by the MTS assay (Cell Titer96 AQ_{ueous} One Solution Proliferation Assay; Promega, Germany). The cell culture medium was replaced by fresh medium containing 10% of MTS dye solution. After 2h of incubation at 37°C in a humidified CO_2 incubator, 80 µL of medium was transferred into a 96-well plate and the absorbance of the formed formazan dye was measured photometrically at 490 nm.

3.2.2.8.3. Tissue non-specific alkaline phosphatase (TNAP) enzyme activity

At day 11 after plating, hBMSCs were analysed for TNAP enzyme activity. TNAP enzyme activity was determined from cell lysates (TNAP lysis buffer: 1.5 M Tris-HCl, pH 10 containing 1 mM $ZnCl_2$, 1 mM $MgCl_2$ and 1% Triton X-100; Sigma-Aldrich, Germany) with p-nitrophenylphosphate (Sigma-Aldrich, Germany) as a substrate, as previously described [185]. TNAP activity was calculated from a linear calibration curve ($r > 0.99$) prepared with p-nitrophenolate. Protein concentration of the lysate was determined with RotiQuant protein assay (Roth GmbH, Karlsruhe, Germany) and was calculated from a linear calibration curve ($r > 0.99$) obtained with bovine serum albumin (Serva, Heidelberg, Germany).

3.2.2.8.4. Calcium deposition

After 22 days of seeding, calcium deposition was quantified with the calcium kit (Greiner Diagnostics, Bahlingen, Germany) as previously described [185]. Cell layers were washed with PBS, dried, and incubated with 0.5 M HCl at 4°C for 24h. Calcium content in the lysates was quantified photometrically with cresolphthalein complexone at 570 nm from a linear calibration curve ($r > 0.99$) prepared with calcium chloride.

3.2.2.8.5. Statistical analyses

Cell experiments were performed with cells from four different donors ($n = 4$), each in duplicate. The results were presented as mean ± standard error of the mean (SEOM). Statistical significance was analysed with GraphPad Prism 8.4 software (Statcon, Witzenhausen, Germany) by ANOVA analysis with Bonferroni's post-test.

3.3. Characterisation techniques

3.3.1. X-ray photoelectron spectroscopy

XPS was performed to analyse the surface chemical composition of the coatings using an Axis Supra spectrometer (Kratos Analytical Ld, Manchester, UK) with a monochromatic Al Kα source (1.487 keV). Samples were mounted using carbon tape on a sample holder. An internal flood gun was used for neutralising charging effects. Wide scans were recorded at a pass energy of 160 eV, a step size of 1 eV, and a sweep time of 120 s. Core line spectra were recorded at a pass energy of 20 eV, a step size of 0.1 eV, and sweep times of 120 s for C1s, and 60 s for other components (N1s, F1s, O1s). Samples were measured at an emission angle of 0° (relative to the surface normal), power of 225 W (15 kV x 15 mA) and an analysis area of 700 x 300 µm. For each coating condition, three different locations were analysed. For angle resolved XPS, the spectra were taken at five take-off angles (relative to the surface normal) of 0, 40, 55, 63, and 75°. Spectra were analysed with CasaXPS software (version 2.3.22, Casa Software Ltd, Devon, UK). All binding energies were referenced to the C-C component of the C1s spectrum at 284.8 eV to

compensate the surface charging effects. The curve fitting procedure of the components was performed using Gaussian-Lorentzian function and a linear background. The Kratos experimental sensitivity factors were used in the atomic composition calculations.

3.3.2. Scanning electron microscopy

In this work, WPI fibrillar coatings were imaged using a Jeol JSM-7800F Field Emission Scanning Electron Microscope (FEG-SEM) using the lower secondary electron detector. Before imaging, the samples were mounted on standard aluminium pin stubs using double sided conductive carbon adhesive dots and sputter coated with approximately 5 nm of gold (at 20 mA for 60 s, 1 x 10^{-2} mBar, under argon) using a Quorum Technologies Ltd, Q150RES.

3.3.3. Water contact angle measurements

CA measurements were performed with a homemade system composed of a light source, a support, and a camera connected to a computer as shown in Figure 3.5. A 5 µL droplet was deposited on the sample with a calibrated pipette. The images were analysed with ImageJ software with the drop analysis plugin [186]. For each coating, one measurement was performed on three different samples. Statistical analyses were performed

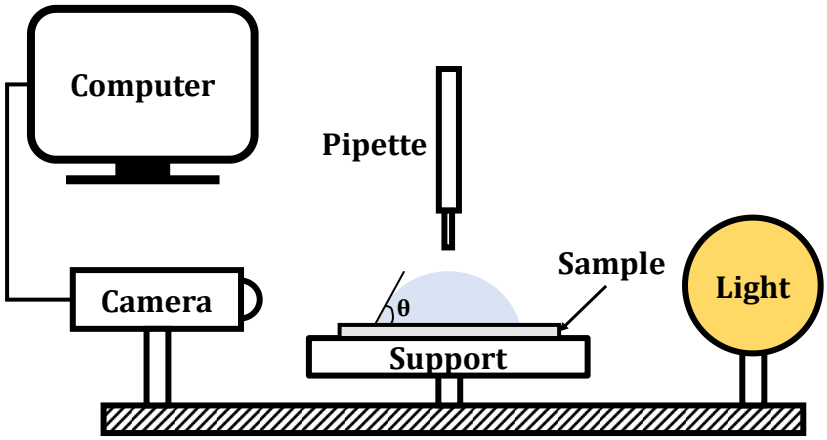

Figure 3.5: Schematic diagram of the contact angle set up.

3.3.4. Atomic force microscopy

The topography and roughness of the coatings were characterised by AFM in tapping mode using a Bruker MultiMode 8 AFM with silicon tips (SCOUT 70 RAI, Nunano, UK). The tips (radius of curvature < 10 nm) had a typical force constant of 2 N/m and a resonant frequency of 70 kHz. Samples were mounted on a sample holder using carbon tape. The images were obtained at a resolution of 256 samples per line and at a frequency of 1.5 Hz. The images were analysed with Bruker's NanoScope Analysis software and flattened at the first order. Surface coverage was calculated using the ImageJ software package. AFM images (10 x 10 μm) were converted to black and white 8-bit images, and the threshold was set to maximise the contrast between the fibrils and the glass substrate. The surface coverage of the fibrils was measured using the area fraction measurement in ImageJ. Surface coverage values were calculated from 2 or 3 images.

3.3.5. Quantification of primary amine groups by chemical derivatisation

This experiment was facilitated by the collaboration with Ben Wood and Dr. Lefteris Danos from the Chemistry Department at Lancaster University who I would like to acknowledge for their help and time in using their glovebox.

3.3.5.1. Material

4-(trifluoromethyl)benzaldehyde (TFBA, purity 98%) was obtained from Fisher Scientific, UK. Amino parylene coating (aminomethyl-[2-2]paracyclophane, Parylene 'diX-AM') deposited on Si wafer was purchased from Kisco Conformal Coating LLC, Japan with a thickness estimated to be around 100 nm (manufacturer specification). Silicon wafer was obtained from Inseto, UK, and polymers (polypropylene (PP), polystyrene (PS), polyethylene terephthalate (PET), and nylon 6 (N6)) from Goodfellow, UK. All substrates were cut into samples of approximately 1 x 1 cm.

3.3.5.2. Methodology

The quantification of primary amine groups was performed by chemical derivatisation of TFBA combined with XPS analyses. The reaction was carried out by exposing the control samples and AApp coatings to TFBA vapour in a glovebox filled with nitrogen due to the high sensitivity of TFBA to the air. Silicon wafer, PP, PS, PET, and N6 were used as negative controls, and amino parylene coating (diX-AM) on silicon as a positive control. Control samples and AApp coatings were placed in the glovebox. The glovebox was pumped down and filled with N_2 three times to minimise oxygen and moisture. The samples were positioned on the top of glass beads in a container filled with 150 µL of TFBA as shown in Figure 3.6a. The glass beads were used to avoid direct contact between the samples and the TFBA. The samples were left in the closed container for 24h. The TFBA vapour directly reacts with primary amine groups by grafting to them via an imine bond as shown in Figure 3.6b. After 24h in the closed container, the samples were directly analysed by XPS.

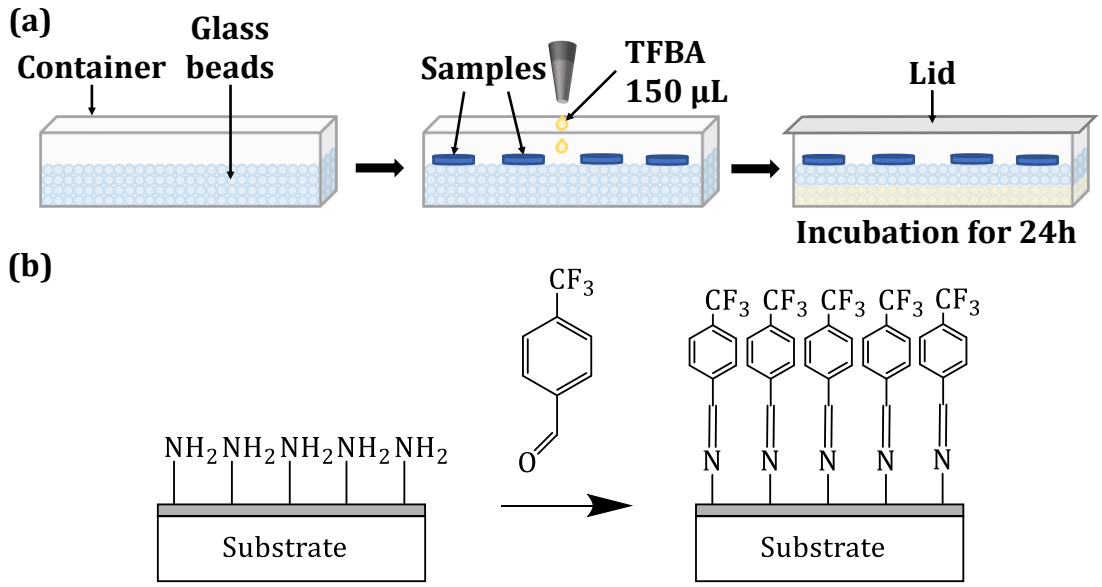

Figure 3.6: (a) Diagram of the TFBA derivatisation experiment. All takes place in a glovebox filled with nitrogen. Samples are placed on top of glass beads in a closed container filled with 150 µL of TFBA. (b) TFBA vapour reacts with the coatings by directly grafting to the primary amines -NH_2 from a coated substrate.

Primary amines -NH_2 were quantified by using atomic composition obtained by XPS, and Equation 5 and Equation 6 derived from the following reaction [187]:

$$C_x(NH_2)_y + y(CF_3)C_6H_5CHO \rightarrow C_{x+8y}N_yF_{3y}\ (+H)$$

With x and y values defined by: $y = {}^{[F]}/_{3}$ and $x = [C] - 8y$

Therefore

$$\frac{[NH_2]}{[C]} = \frac{{}^{[F]}/_{3}}{[C]-({}^{8}/_{3})[F]} \times 100 \qquad \textit{Equation 5}$$

And

$$\frac{[NH_2]}{[N]} = \frac{{}^{[F]}/_{3}}{[N]} \times 100 \qquad \textit{Equation 6}$$

where $[NH_2]$, $[F]$, $[N]$ and $[C]$ represent respectively the relative concentrations of primary amines, fluorine, nitrogen and carbon at the sample surface. These concentrations were obtained from the wide XPS scan spectra.

For AApp coatings, three samples for each condition with three different locations were analysed.

Chapter 4. Allylamine plasma polymer coatings rich in primary amines

4.1. Overview

This chapter presents the production and characterisation of allylamine plasma polymer (AApp) coatings. AApp coatings were made by plasma polymerisation as described in Section 3.2.1. Allylamine was chosen as it is the simplest unsaturated amine and the most commonly used precursor for the production of aminated coatings. AApp coatings obtained from different plasma conditions were compared: the more usual α regime with low pressure and high power (AApp1 – 2 Pa and 30 W) vs. the ϒ regime with high pressure and low power (AApp2 – 20 Pa and 5.5 W). The atomic and functional group composition of these AApp coatings was investigated by X-ray photoelectron spectroscopy (XPS). The -NH_2 groups were further quantified by using a chemical derivatisation technique with 4-(trifluoromethyl)benzaldehyde (TFBA) as previously defined in Section 3.3.5. Finally, AApp coatings made at the University of Liverpool (UoLiv) were also analysed by XPS before and after TFBA derivatisation allowing a comparison between AApp coatings produced in two different plasma reactors.

4.2. Methodology

As described in Section 3.2.1.3, AApp coatings were made in two separate conditions – 2 Pa and 30 W for AApp1 (α regime) and 20 Pa and 5.5 W for AApp2 (ϒ regime), with the aim of investigating whether transitioning from the α regime to the ϒ regime could enhance functional group retention, here primary amines, as

previously shown for other functionalities such as for nitroxide radicals [55,56], epoxy [57], α-bromoisobutyryl [58], or ester functionalities [54].

AApp coatings were made in a glass barrel reactor as previously shown in Section 3.2.1.2. Samples were coated onto sections of clean Si wafer, chosen as a substrate due to its suitability for XPS (low surface roughness, unambiguous chemical composition, etc). Samples were stored in sealed 24-well plates prior to analyses or TFBA derivatisation.

A number of AApp samples produced at the University of Liverpool (UoLiv) were also studied during this work, and data from those samples is presented here as well, allowing a comparison between AApp coatings produced in two separate reactors. UoLiv samples were produced in an QVF glass cruciform vessel with two separate conditions: 2.7 Pa and 20 W (α regime), and 80 Pa and 5 W (ϒ regime). The schematic diagram of the reactor is shown in Appendix B.1. The UoLiv reactor also features a number of plasma diagnostic systems including a mass spectrometer – for in-situ measurements of neutral and positive ions species as well as ion energy distribution functions, and a quartz crystal microbalance – to investigate the deposition rate. The measurements using these systems are correlated with deposited coatings. AApp coatings and measurements at UoLiv were made by Dr Mike Barnes, Dr. Stephane Simon and Prof. James Bradley, with samples being passed to Lancaster University for XPS measurements and TFBA derivatisation.

4.3. Results and discussion

4.3.1. Physicochemical characterisation of the coatings

4.3.1.1. Water contact angle measurements

The wettability of AApp coatings was studied by static water contact angle (WCA) measurements. This method is an easy and quick way to identify the presence of the coating before further analyses. As shown in Figure 4.1, the WCA was significantly higher in presence of the AApp coatings compared to the uncoated Si substrate. Indeed, WCA for Si was estimated to be 34.3 ± 1.5° whereas WCA for

AApp1 and AApp2 were 48.1 ± 1.2° and 42.7 ± 1.9°, respectively. The droplet angle did not change appreciably during the contact angle measurements. Moreover, no sign of the droplet removing was observed during the experiment. No significant difference was observed between AApp1 and AApp2 coatings. The chemical composition of the coatings will be further analysed by XPS in the next part.

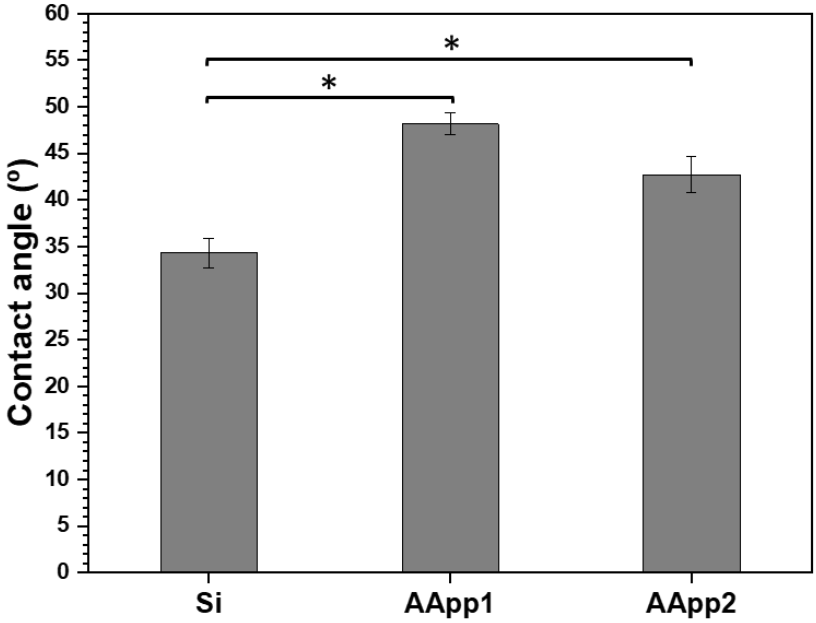

*Figure 4.1: CA measurements of uncoated Si and AApp coatings on Si. The results are shown as mean (n = 3) and bars represent the standard error of the mean. * represents statistical analyses between uncoated Si and AApp coatings (p < 0.05). No statistical difference was observed between AApp1 and AApp2.*

4.3.1.2. XPS analyses

AApp coatings deposited on Si wafer were characterised by XPS. Wide scan spectra, as well as high-resolution spectra for C1s, N1s, and O1s, were recorded for both samples.

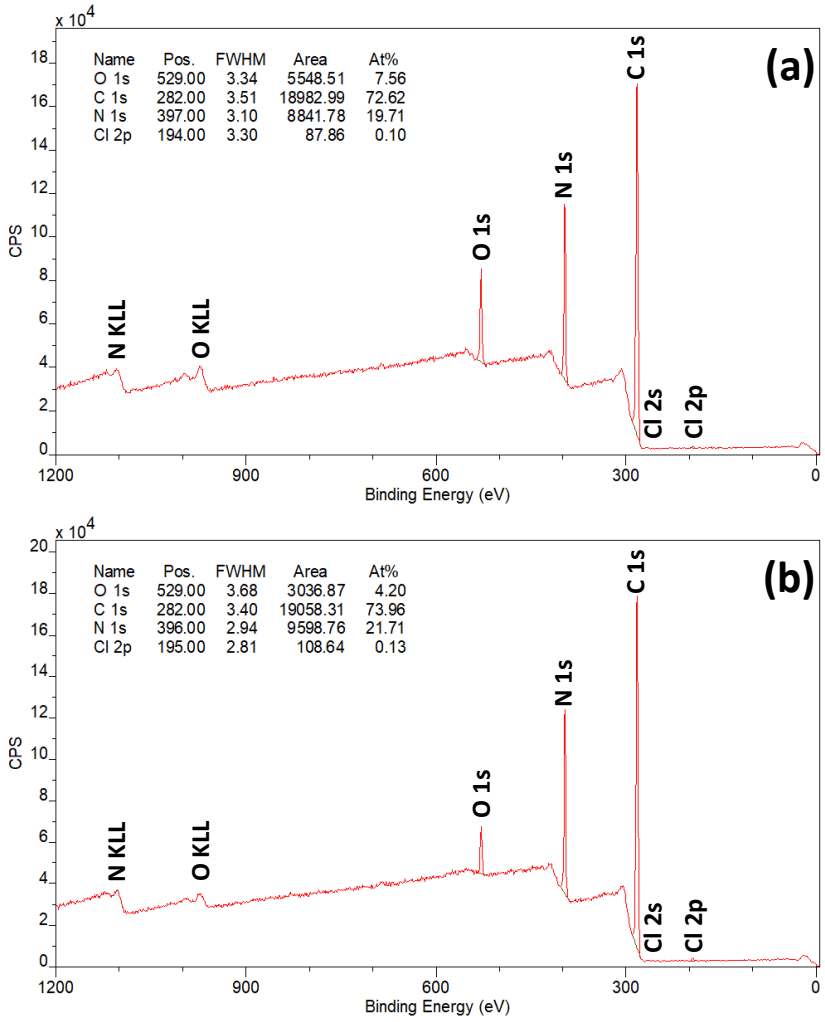

Figure 4.2: Representative XPS wide scan spectra of (a) AApp1 and (b) AApp2 deposited on Si wafer. Both coatings are mainly composed of C, N, and O as shown by the emission peaks. Traces of Cl are also detected which may come from contamination from the glovebox where the samples are stored.

Typical wide scan spectra obtained for AApp coatings are shown in Figure 4.2. XPS data from wide scan spectra are summarised in Table 4.1. AApp coatings were mainly composed of carbon and nitrogen, as expected from the allylamine molecular structure. Small quantities of oxygen were detected due to residual oxygen species within the plasma and post-polymerisation oxidation with atmospheric oxygen. No silicon from the substrate was detected which indicates that the coatings were thicker than the XPS sampling depth (> 10 nm), and free of gaps in the coatings which would give rise to a substrate signal.

AApp1 was consisted of 72.6 ± 0.2 %% of C, 20.3 ± 0.3 % of N, 7.0 ± 0.2 % of O, and 0.1% of Cl. AApp2 had similar content with 74.2 ± 0.3 % of C, 21.3 ± 0.4 % of N, and 4.3 ± 0.2 % of O (Table 4.1). The presence of oxygen was likely due to the post polymerisation oxidation of the coatings before loading in the XPS chamber. The higher amount of oxygen for AApp1 was attributed to the low monomer pressure in comparison to the system base pressure (c. 10 x base pressure), as opposed to AApp2 (c. 100 x base pressure). Background air ingress into the reactor is therefore more likely to have an effect on AApp1. Small quantities of Cl (0.1%) were also identified for both coating types which is possibly due to contamination from chlorine compounds from the glove box where samples were stored prior to XPS analysis.

Table 4.1: Summary of the main components of AApp coatings. Data are presented as mean ± STD (n = 3 with three locations on each sample).

	C1s	**N1s**	**O1s**
AApp1 2 Pa – 30 W	72.6 ± 0.2 %	20.3 ± 0.3 %	7.0 ± 0.2 %
AApp2 20 Pa – 5.5 W	74.2 ± 0.3 %	21.3 ± 0.4 %	4.3 ± 0.2 %

The stoichiometry of the coatings was close to the original stoichiometry of the allylamine molecule (C_3H_7N) with $C_{3.6}H_xN$ for AApp1 and $C_{3.5}H_xN$ for AApp2. However, this does not, in itself, indicate the presence of primary amines.

Figure 4.3 shows the high-resolution XPS spectra of C1s for AApp1 (Figure 4.3a) and AApp2 (Figure 4.3b) as well as the overlaid high-resolution spectra of C1s (Figure 4.3c). On the C1s core line, the carbon environments likely to be present were identified as C-C/C-H, C-N, C-O/C=N, C=O/CNO, and O-C=O. As expected from the wide scan spectra, more carbon-oxygen functionalities were detected with a larger high binding energy foot in AApp1 compared to AApp2, which can be identified with the shoulder arising around 288-289 eV and the value associated with C=O, N-C=O, or O-C=O environments. Moreover, a clear shoulder was identified in AApp2 around 286-287 eV likely to be a combination of C-N and C-

O/C=N peaks. The introduction of these environments clearly indicated the fragmentation of the allylamine molecule and the crosslinking of different fragments. If no fragmentation or crosslinking was observed, the peaks would sit closer to the C-C peak at 285 eV, as in this case, no C=N or C-O environments would be present. Despite these differences, no significant change in the peak shapes was observed meaning that the regimes might not be different. The α and γ regimes could be identified with the analyses of the ion energy distribution and mass spectrometer data. However, the design of this plasma reactor does not allow these analyses. XPS indicated that AApp coatings had similar chemical compositions compared to coatings produced in previous works [7,188–190].

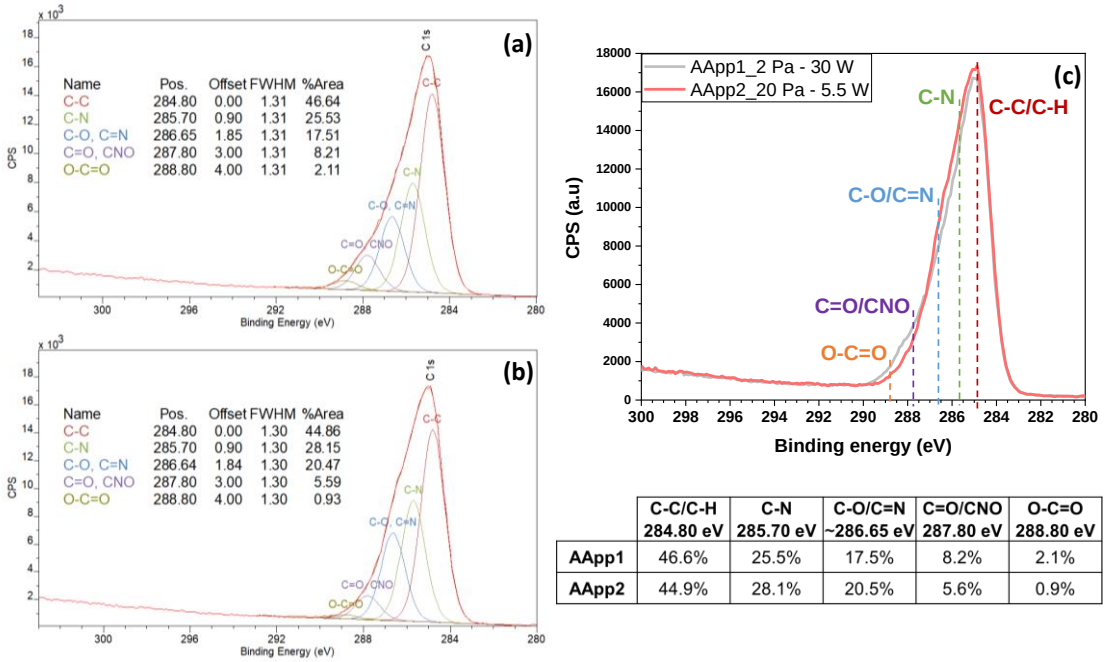

	C-C/C-H 284.80 eV	C-N 285.70 eV	C-O/C=N ~286.65 eV	C=O/CNO 287.80 eV	O-C=O 288.80 eV
AApp1	46.6%	25.5%	17.5%	8.2%	2.1%
AApp2	44.9%	28.1%	20.5%	5.6%	0.9%

Figure 4.3: High-resolution XPS spectra of C1s with fits for (a) AApp1 and (b) AApp2. An overlaid C1s high-resolution spectrum is represented in (c) for both coatings. C1s peaks are fitted with different carbon-nitrogen and carbon-oxygen environments. Small differences are observed as shown in the table.

The determination of nitrogen-containing functional groups present in AApp is more difficult due to the overlap in chemical shifts from amine functionalities. N1s spectra displayed similar peak shapes for both coatings (Figure 4.4) with the peak centred around 399.3 eV, which corresponds to C-N bonds [157]. Since amine functionalities (primary, secondary, and tertiary) have close binding energies, the

fit into different chemical groups was not feasible. Therefore, another method was necessary for the quantification of functional groups, especially primary amines - NH_2.

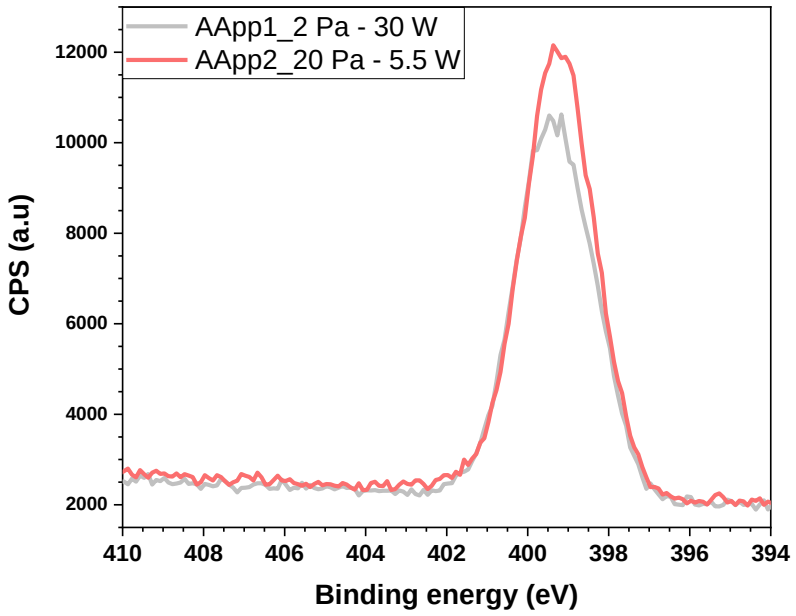

Figure 4.4: Overlaid high-resolution XPS spectrum of N1s for AApp1 and AApp2 coatings. Both spectra have similar peak shapes due to close binding energies of amine functionalities.

4.3.2. Quantification of primary amine groups by chemical derivatisation

TFBA derivatisation was used to quantify primary amine retention in allylamine plasma coatings. Indeed, due to a variety of reactions happening in the plasma, the final chemistry of the plasma coating is difficult to control, and several functional groups may appear in addition to the original monomer. As shown previously, the XPS technique showed similar atomic compositions between AApp coatings, but this technique cannot clearly define the difference between amine groups (primary, secondary, and tertiary) in the nitrogen spectrum, due to small binding energy offsets. The quantification of -NH_2 will help to confirm whether it is possible to use specific plasma parameters, which are high pressure and low power, to deposit high concentrations of primary amines on a surface. TFBA can specifically bind to -NH_2 which allows the incorporation of fluorine atoms that can

be quantified by XPS. Chemical derivatisation of positive control (amino parylene diX-AM) and negative controls (silicon, polypropylene, polystyrene, polyethylene terephthalate, and polyamide) was also investigated.

4.3.2.1. TFBA derivatisation of amino parylene coatings

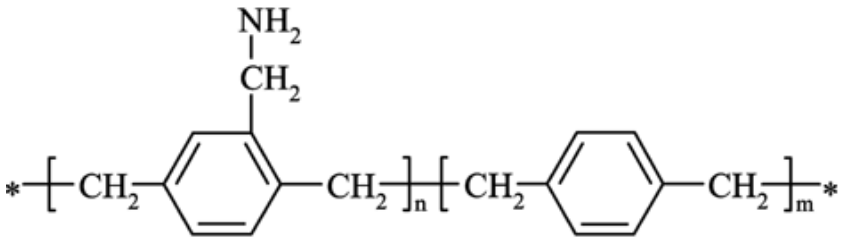

Figure 4.5: Molecular structure of amino parylene (diX-AM) coated on Si wafer.

The nitrogen component of amino parylene (diX-AM) is composed only of primary amines as displayed in the molecular structure in Figure 4.5. The derivatisation will occur between these primary amines and the TFBA molecule as previously described in Section 3.3.5. Amino parylene was chosen as a commercially available standard as it previously showed total derivatisation of all primary amines to TFBA [177]. Moreover, in a previous study, different commercially available polymers were tested, and the results showed that a reliable standard polymer was difficult to find [174]. The successful derivatisation was investigated by XPS with the introduction of fluorine from the TFBA molecule (Figure 4.6). Since diX-AM has a known primary amine group, it was used to find the optimum parameters for TFBA derivatisation, especially the time of derivatisation. This parameter was then kept constant for subsequent labelling with negative controls and AApp coatings.

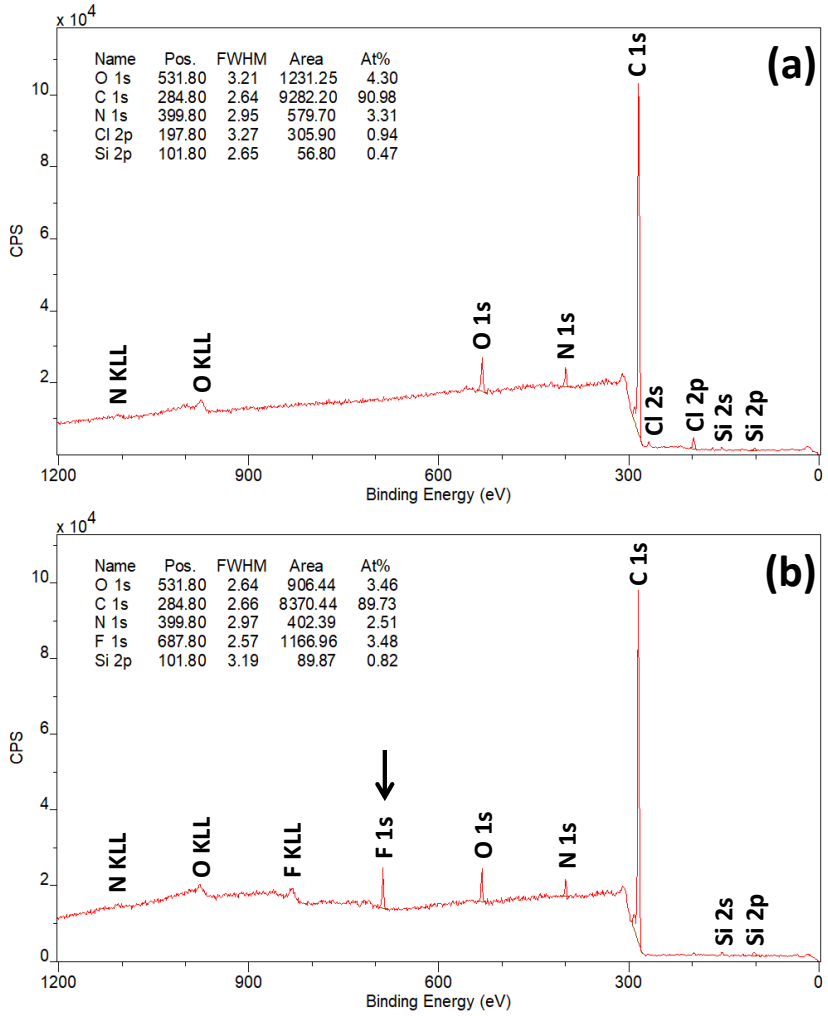

Figure 4.6: Representative wide spectra of amino parylene (diX-AM) coatings (a) before and (b) after 24h derivatisation. Before and after derivatisation, diX-AM coatings are mainly composed of C, N, and O. After derivatisation, fluorine is detected, as indicated by the arrow, due to the TFBA labelling. Some traces of Si are detected due to possible scratches on the samples. Traces of Cl are also detected which may come from contamination from the glovebox where the samples are stored.

Figure 4.7 shows a summary of the atomic composition of diX-AM coatings before and after TFBA derivatisation for different derivatisation times (1, 4, and 24h). Before derivatisation, the diX-AM coating was mainly composed of carbon (90.1 ± 1.1 %), oxygen (4.3 ± 0.1 %), and nitrogen (3.4 ± 0.2 %). A small amount of silicon (1.2 ± 0.8 %) was detected due to possible scratches which revealed the silicon wafer underneath as the coating is expected to be about 100 nm thick (manufacturer specifications). Oxygen may come from the oxidation of the coating

post-polymerisation or the Si wafer. Chlorine traces (< 1%) were possibly due to contamination from chlorine compounds stored in the glovebox. The expected N/C from the molecular structure was 5.9% with m = n (as defined by the manufacturer). From the XPS data, N/C was estimated to be 3.8% which is less than the expected value. However, this may be due to the oxidation of the coating since about 4% of oxygen was detected.

After 1h of derivatisation reaction, the presence of fluorine can clearly be identified in the XPS spectra, making up 1.5 ± 0.1 % of the surface atomic composition. The other atomic percentages were similar to the original coating with 88.3 ± 2.6 % of carbon, 4.3 ± 1.0 % of oxygen, and 3.3 ± 0.1 % of nitrogen. For the same reasons mentioned before, some traces of silicon and chlorine were detected. With 4h of TFBA derivatisation, the fluorine content increased to 2.6 ± 0.1 %. However, the rest of the composition showed a possible problem with this sample. Indeed, high oxygen and silicon levels were measured, 12.4 ± 0.4 % and 8.8 ± 0.6 %, respectively. This could be explained by the coating being damaged which exposes the silicon wafer. A likely explanation for the damaged coating is that the samples were sitting on glass beads and so can easily move, flip, and be damaged by friction with the beads or tweezers during setup of the experiment. Therefore, this data point may be unreliable. Finally, after 24h of reaction, the fluorine level increased to 3.3 ± 0.3 %. Carbon and oxygen contents were close to previous samples with 87.0 ± 3.7 % and 4.4 ± 1.0 %, respectively. Nitrogen level slightly decreased to 2.5 ± 0.2 % and silicon increased to 2.8 ± 2.9 %, which may be due to the silicon wafer being more visible due to scratch marks.

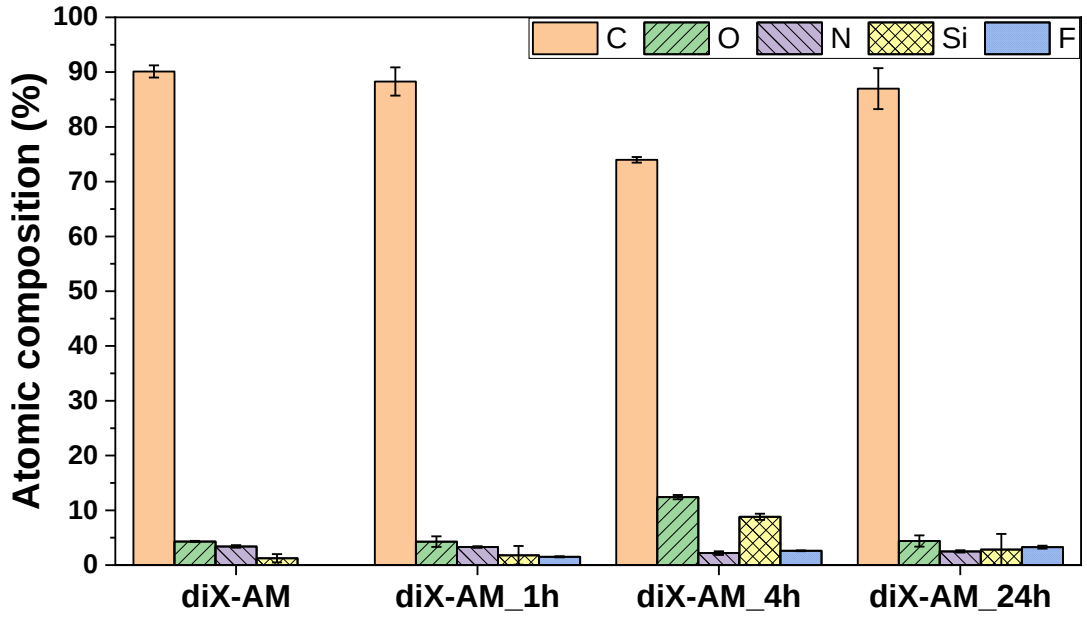

Figure 4.7: Atomic composition obtained by XPS of diX-AM coatings before and after derivatisation for different times (1, 4, 24h). Three locations on each sample were analysed.

The increase of fluorine content when derivatisation time increases clearly demonstrated the time dependence of the reaction. High-resolution spectra of carbon were obtained to identify the chemical environments involved and are represented in Figure 4.8 and Figure 4.9a. The carbon peak was composed of an aromatic carbon bond, C-C/C-H, C-N, C-O, and shake-up features for the underivatized sample as shown in Table 4.2. After chemical derivatisation a new chemical bond was noticed, corresponding to C-F_3 from the TFBA which indicates the successful labelling. The percentage of C-F_3 increased when the derivatisation time increased which is in accordance with the data obtained with the wide spectra. Moreover, this also can be observed on the F1s high-resolution spectrum where the fluorine content increased over time (Figure 4.9b). However, in both cases, the percentage of fluorine and C-F_3 did not reach a plateau which may indicate that the derivatisation is not total.

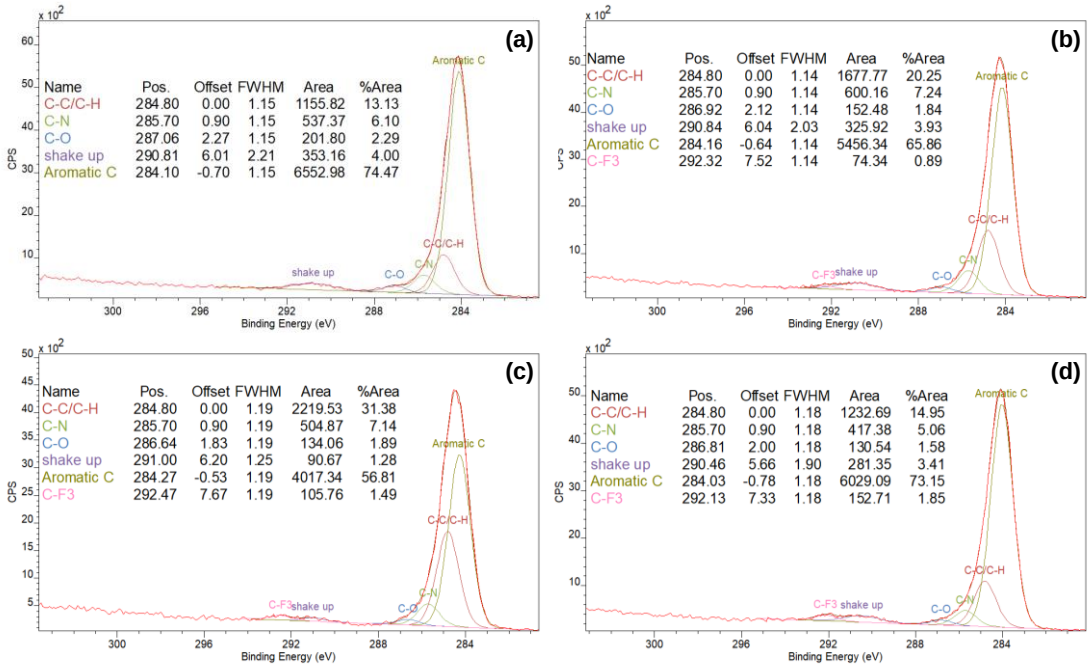

Figure 4.8: C1s fits for diX-AM (a) before derivatisation, (b) after 1h, (c) 4h, and (d) 24h of TFBA derivatisation.

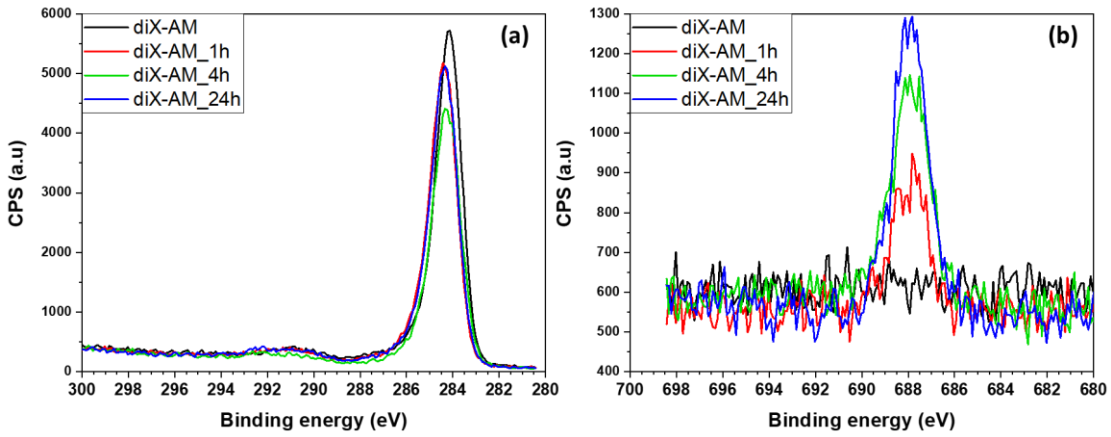

Figure 4.9: (a) C1s and (b) F1s high resolution spectra of diX-AM coatings before and after derivatisation for different times (1, 4, 24h).

Table 4.2: Components of carbon from the C1s high-resolution spectra of diX-AM coatings before and after derivatisation for different times (1, 4, and 24h).

TFBA time (h)	Aromatic carbon ~284.15 eV	C-C/C-H 284.80 eV	C-N 285.70 eV	C-O ~286.85 eV	Shake-up ~290.78 eV	C-F_3 ~292.31 eV
0	74.5%	13.1%	6.1%	2.3%	4.0%	0%

1	65.9%	20.2%	7.2%	1.8%	3.9%	0.9%
4	56.8%	31.4%	7.1%	1.9%	1.3%	1.5%
24	73.1%	14.9%	5.1%	1.6%	3.4%	1.8%

The main hypotheses were that a longer derivatisation time was needed, or that TFBA did not penetrate through the coating and -NH_2 groups under the outermost layer were not labelled.

To answer these questions, longer derivatisation times (48 and 72h) were tried to check if fluorine content reached a plateau, and angle-resolved XPS was performed to check the outermost layer of the samples and if the fluorine content varies according to the depth of analysis.

Figure 4.10 shows a summary of the atomic composition of diX-AM coatings before and after TFBA derivatisation for different derivatisation times (24, 48, and 72h). Before derivatisation, the diX-AM coating was mainly composed of carbon (90.1%), oxygen (4.3%), and nitrogen (3.4%), as well as a small amount of silicon (1.2%) as described earlier.

After 24h of derivatisation reaction, the presence of fluorine can clearly be identified with about 3.0 ± 0.4 %. However, a lower level of carbon (68.8 ± 2.3 %), and higher levels of oxygen and silicon were measured with 16.5 ± 1.2 % and 9.8 ± 1.0 %, respectively. This could be explained by the coating being damaged which exposes the silicon wafer as previously described for the 4h-derivatised sample. Therefore, this data point may be unreliable. After 48h and 72h, similar atomic compositions were observed with about 85.4 ± 2.4 % and 83.8 ± 4.4 % of C, 6.6 ± 1.3 % and 7.6 ± 1.9 % of O, and 2.8 ± 0.3 % and 2.8 ± 0.8 % of N, respectively. The fluorine increased up to 4.2 ± 0.4 % for the 48h-derivatised sample, and to 3.7 ± 0.8 % for the 72h-derivatised sample. As shown in Figure 4.11, F/C ratio reached a plateau after 24h of derivatisation meaning the derivatisation was completed.

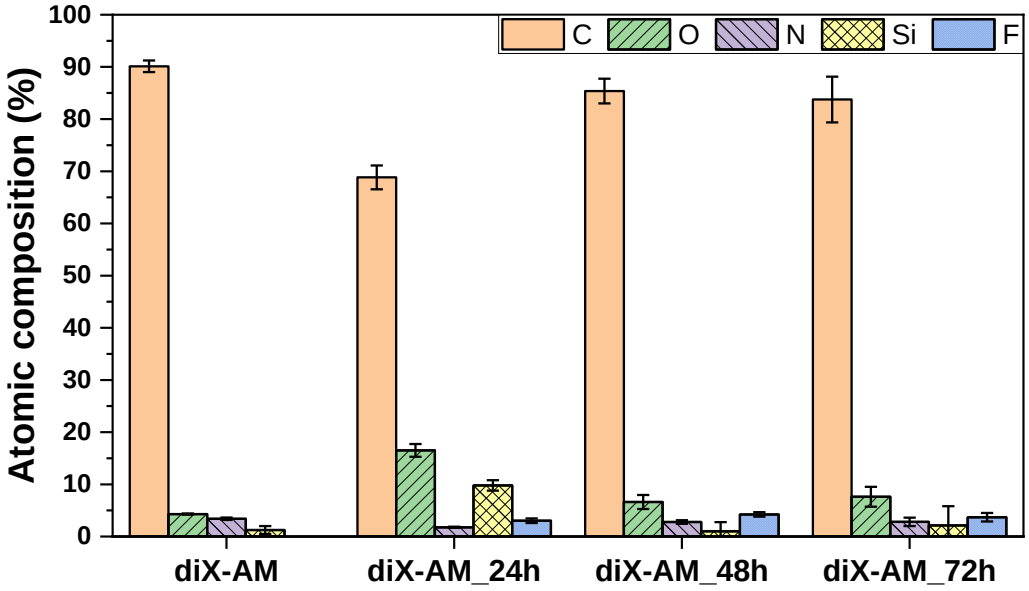

Figure 4.10: Atomic composition obtained by XPS of diX-AM coatings before and after derivatisation for different times (24, 48, 72h). Three locations on each sample were analysed.

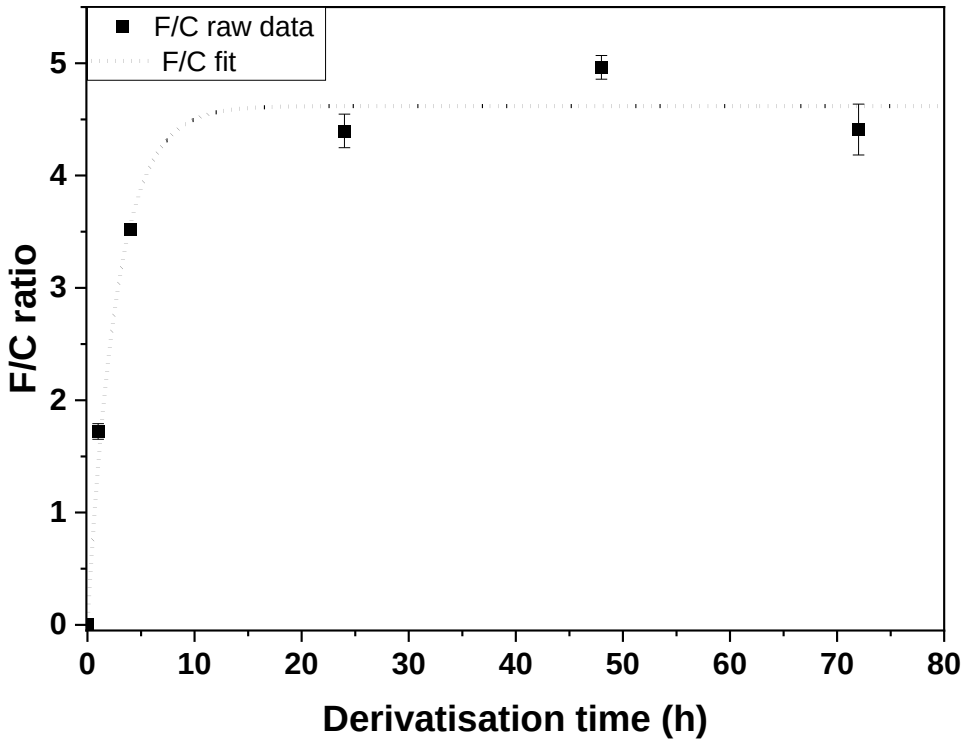

Figure 4.11: F/C ratio of amino parylene coating after different derivatisation times (0, 1, 4, 24, 48, and 72h). Three locations on each sample were analysed.

Moreover, to check the penetration of TFBA into the coating, angle-resolved XPS was performed for amino parylene coatings after 24, 48, and 72h of TFBA derivatisation (Figure 4.12). As described in Section 2.7.1.2.4, angle-resolved XPS helps to increase surface sensitivity. Indeed, when the sample is tilted, the sampling depth decreases and if TFBA does not penetrate through the coating and stay at the surface, more fluorine would be detected at a high angle. Therefore, the analyses were performed at different angles (0, 40, 55, 63, and 75°, with respect to the XPS take-off angle, which is itself normal to the sample surface) to check the outermost layer of the coatings and see if F/C ratio decrease through the depth of analysis. As shown in Figure 4.12, F/C ratios did not significantly change depending on the angle of analysis which indicates that TFBA may penetrate through the coatings.

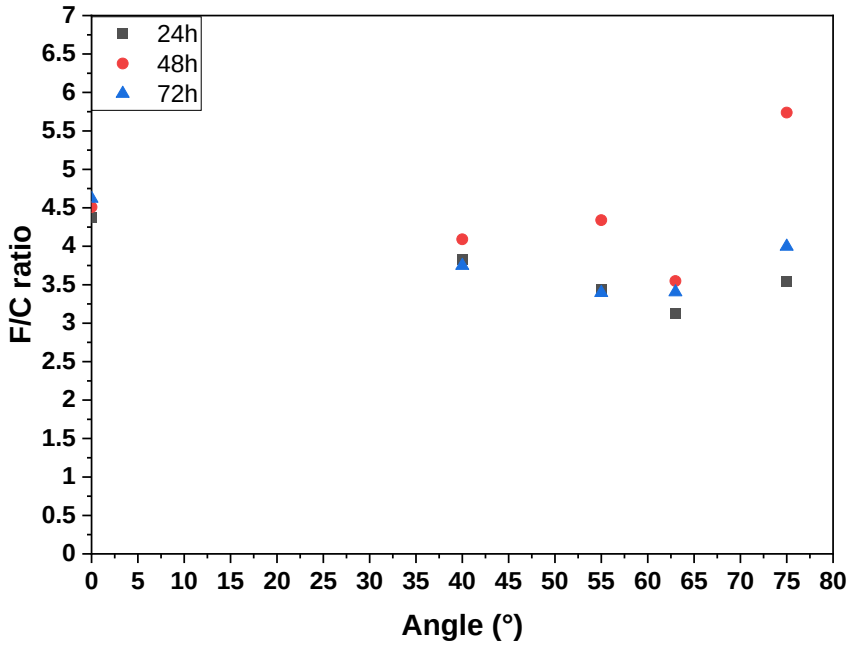

Figure 4.12: F/C ratios as a function of derivatisation times (24, 48, and 72h) and the angle of analysis (0, 40, 55, 63, and 75°).

Primary amine content was calculated with the Equations 5 and 6 as previously described in Section 3.3.5:

$$\frac{[NH_2]}{[C]} = \frac{[F]/_3}{[C]-(8/_3)[F]} \times 100 \qquad \textit{Equation 5}$$

$$\frac{[NH_2]}{[N]} = \frac{[F]/_3}{[N]} \times 100 \qquad \textit{Equation 6}$$

$\frac{[NH_2]}{[N]}$ and $\frac{[NH_2]}{[C]}$ were estimated to be 43.6% and 1.4%, respectively, whereas the expected $\frac{[NH_2]}{[C]}$ was estimated to be 3.8% before derivatisation. Therefore, the derivatisation is not total, but this could be explained by the oxidation of the coatings which was also shown by the presence of oxygen in the XPS wide spectra. For the following experiments, derivatisation time was fixed to 24h since it seems to have plateaued by this point.

4.3.2.2. TFBA derivatisation of negative controls: silicon wafer and polymers

Silicon wafer was chosen as a control since it was the substrate used for allylamine coating and should not bind TFBA. XPS wide scan and high-resolution spectra were recorded. Figure 4.13 shows the XPS wide spectra of silicon wafer before and after TFBA derivatisation. The atomic composition before derivatisation was 61.9 ± 3.8% of Si, 27.2 ± 2.1% of O, and 10.9 ± 5.9% of C. After derivatisation, the atomic composition was similar with 60.2 ± 2.2% of Si, 27.2 ± 1.2 of O, and 12.2 ± 3.5% of C. Moreover, after derivatisation, a small amount of fluorine was detected around 688 eV with 0.3 ± 0.2%. However, this amount is very low and does not indicate that TFBA binds to Si.

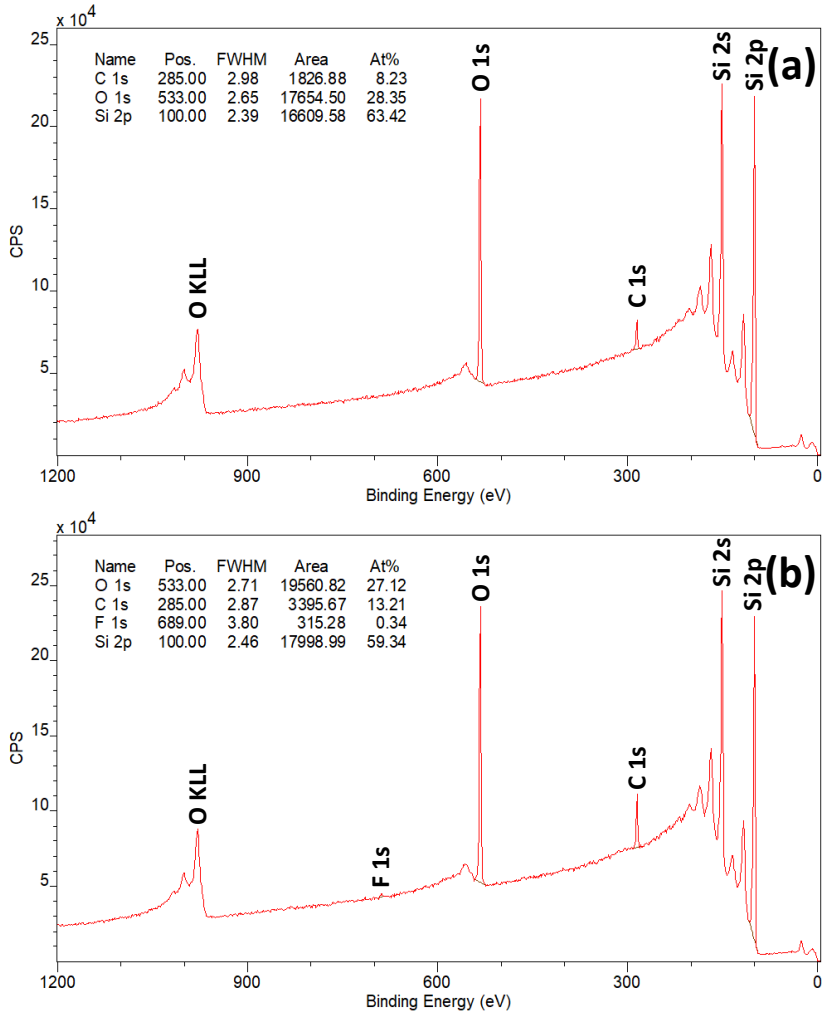

Figure 4.13: XPS wide scan spectra of silicon wafer (a) before and (b) after 24h of TFBA derivatisation.

Moreover, different polymers (PP, PS, PET, N6) which do not contain primary amines were tested. PP, PS, and PET contain only carbon or carbon and oxygen, while N6 contains CNO. In the case of Nylon 6, the nitrogen is secondary amine, and should not bind TFBA. XPS analyses were performed to demonstrate the specific binding of TFBA to primary amines. All the XPS wide scans can be found in Appendix A. The atomic compositions are summarised in Table 4.3. Small quantities of F were detected for polystyrene (PS) – 0.6 ± 0.1%, and nylon 6 (N6) – 0.9 ± 0.2%. However, some traces of F were already present in N6 before derivatisation which may come from contamination during the manufacturing process. Other contaminations were also detected with Si, Cl, and Ca especially for

the N6 sample. As the %F was small for these polymers, it was hypothesised that TFBA only binds to primary amines as already suggested in the literature [177].

Table 4.3: XPS data summary of the main atomic composition ± STD (%) of different polymers (PP, PS, PET, and N6) before and after derivatisation. After derivatisation, Si, Cl, and Ca may come from contamination from the glovebox or during sample handling. Three locations on each samples were analysed.

	Before derivatisation				**After derivatisation**						
	C	**O**	**N**	**F**	**C**	**O**	**N**	**F**	**Si**	**Cl**	**Ca**
PP	99.9 ± 0.2 %	0.1 ± 0.2 %	-	-	98.6 ± 0.5 %	1.4 ± 0.5 %	-	-	-	-	-
PS	96.0 ± 0.2 %	4.0 ± 0.2%	-	-	98.5 ± 0.3 %	0.9 ± 0.1 %	-	0.6 ± 0.1 %	-	-	-
PET	77.2 ± 0.4 %	22.8 ± 0.4 %	-	-	74.3 ± 1.1 %	24.8 ± 1.5 %	-	0.4 ± 0.4 %	0.5 ± 0.0 %	-	-
N6	77.3 ± 1.5 %	10.6 ± 0.4 %	11.3 ± 0.1 %	0.8 ± 1.0 %	73.1 ± 3.3 %	12.5 ± 1.4 %	5.6 ± 0.6 %	0.9 ± 0.2 %	7.4 ± 2.4 %	0.1 ± 0.2 %	0.3 ± 0.4 %

4.3.2.3. TFBA derivatisation of allylamine plasma polymer coatings

AApp coatings were derivatised by TFBA and XPS analyses were performed. Wide scans and high-resolution spectra (C1s, N1s, O1s, and F1s) were recorded.

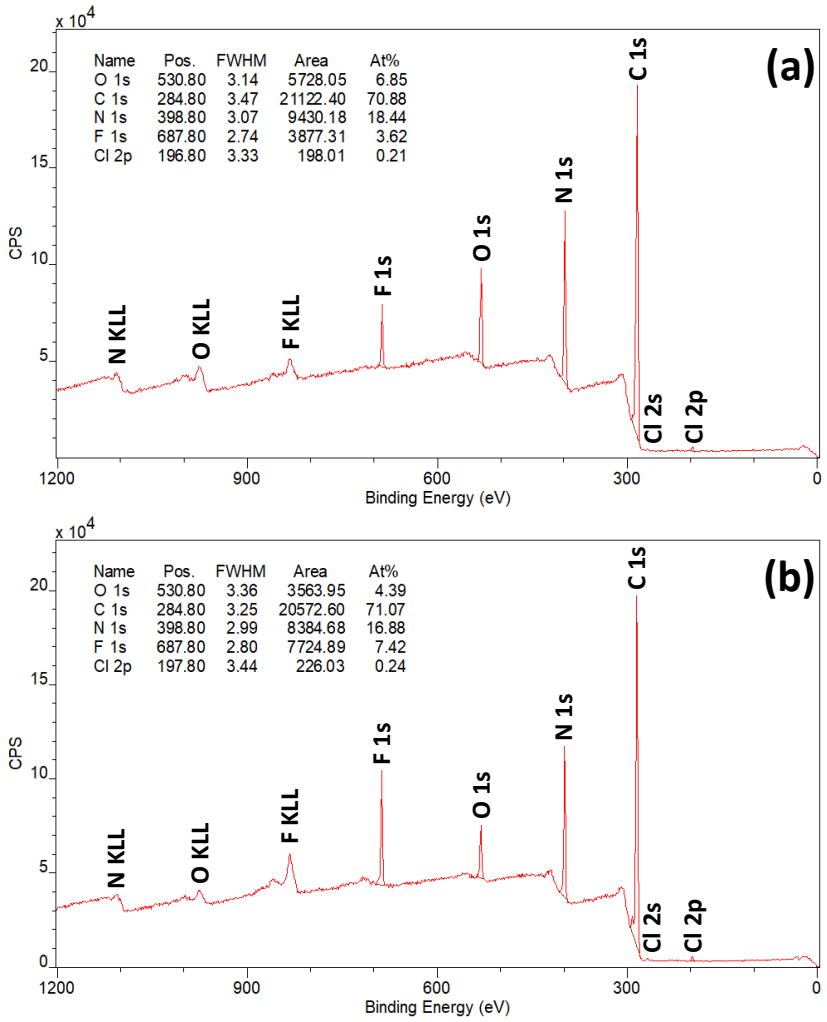

Figure 4.14: Representative XPS wide scan spectra of (a) AApp1 and (b) AApp2 deposited on Si wafer after 24h of TFBA derivatisation.

Figure 4.14 represents the XPS wide scan spectra of AApp after derivatisation. Before derivatisation, the compositions of AApp1 and AApp2 coatings were similar, as described in Section 4.3.1.2 After 24h of TFBA derivatisation, the appearance of a fluorine peak around 688 eV attested to the successful labelling, with 3.2% of F for AApp1 and 7.0% for AApp2 as summarised in Figure 4.15.

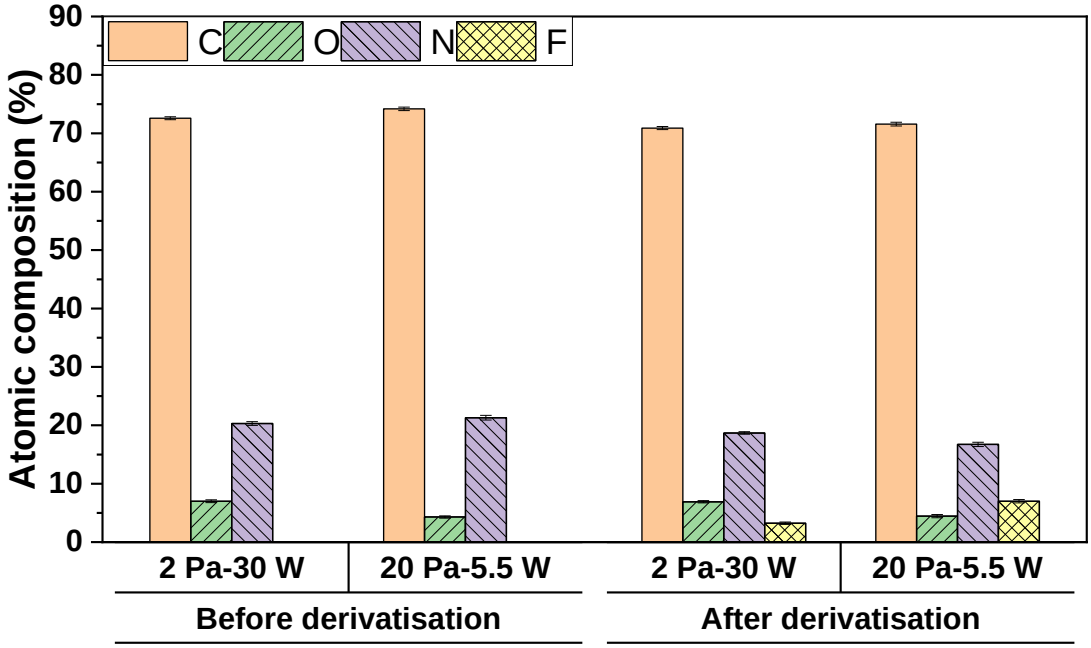

Figure 4.15: XPS wide scan data summary for AApp coatings before and after TFBA derivatisation (n = 3, with three locations on each sample).

The fluorine concentration for AApp2 was doubled compared to the one of AApp1 which may indicate higher primary amine retention for these plasma conditions, e.g high pressure and low power. Furthermore, by using Equation 5 and 6 as previously mentioned in Section 3.3.5, $\frac{[NH_2]}{[N]}$ was 5.8% for AApp1 and 13.9% for AApp2, and $\frac{[NH_2]}{[C]}$ was 1.7% for AApp1 and 4.4% for AApp2. Hence, it confirms the higher degree of -NH_2 retention with the γ regime (AApp2, 20 Pa - 5.5 W). Moreover, after derivatisation, a new peak was identified for both coatings in the C1s spectra around 293 eV which corresponds to -C-F_3 bonds, as shown in Figure 4.16a. For AApp1, -CF_3 was 1.2 ± 0.2% whereas for AApp2 it was 3.1 ± 0.2%. This is further confirmed by the F1s core line (Figure 4.16b) which shows a peak area doubled for AApp2 compared to AApp1 after derivatisation.

Overall, while both coatings had similar N content, these results indicate that the combination of high pressure and low power (γ regime) led to a higher primary amine content, more than doubled compared to the use of the α regime. This correlates with other studies which demonstrates higher functionalities retention

with γ regime for nitroxide radicals [55,56], epoxy [57], α-bromoisobutyryl [58], or ester functionalities [54] by using different monomers.

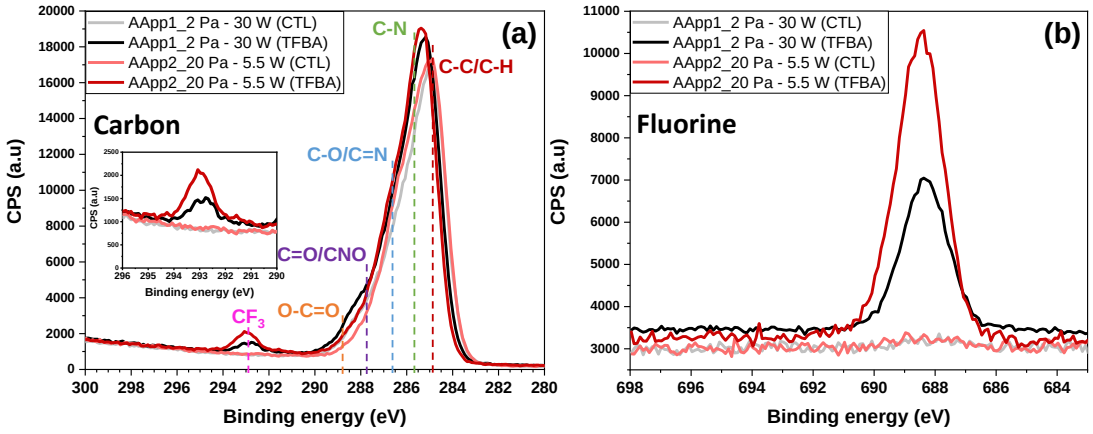

Figure 4.16: (a) C1s with an insert graph corresponding to the CF_3 peak, and (b) F1s high-resolution spectra of AApp coatings before (CTL) and after TFBA derivatisation. C1s peaks are fitted with different carbon-nitrogen and carbon-oxygen environments. CF_3 environment clearly appeared after derivatisation for both coatings. The areas of CF_3 and F peaks are doubled for AApp2 compared to AApp1.

4.3.3. TFBA derivatisation of allylamine plasma coatings (UoLiv)

As mentioned in Section 4.2, a number of AApp coatings were also produced at the University of Liverpool (UoLiv) in a different plasma reactor by using two conditions: 2.7 Pa and 20 W (AApp3), and 80 Pa and 5 W (AApp4). These coatings deposited on Si wafer were characterised by XPS before and after TFBA derivatisation. Wide scan spectra, as well as high-resolution spectra for C1s, N1s, and O1s, were recorded for both samples.

Typical wide scan spectra obtained for these AApp coatings before and after derivatisation are shown in Appendix B.2 and B.3. XPS data obtained from the wide scan spectra are summarised in Table 4.4. AApp coatings were mainly composed of carbon and nitrogen, as expected from the allylamine molecular structure. Small quantities of oxygen were detected due to residual oxygen species within the plasma and post-polymerisation oxidation with atmospheric oxygen. No silicon from the substrate was detected which indicates that the coatings were thicker

than the XPS sampling depth (> 10 nm), and free of gaps in the coatings which would give rise to a substrate signal.

AApp3 was consisted of 80.0 ± 0.2 % of C, 13.8 ± 0.1 % of N, 5.7 ± 0.3 % of O. AApp4 had similar content with 72.5 ± 0.3 % of C, 18.9 ± 0.3 % of N, and 8.1 ± 0.1 % of O (Table 4.4). However, the carbon is slightly higher for AApp3 compared to AApp4 (80.0 vs 72.5%), and nitrogen content is slightly higher for AApp4 compared to AApp3 (19.4 vs 13.2%).

Table 4.4: Summary of the main atomic elements of AApp coatings. Data is presented as mean ± STD. Three locations were analysed on each sample.

		C1s	N1s	O1s	F1s
Before derivatisation	**AApp3 2.7 Pa – 20 W**	80.0 ± 0.2 %	13.8 ± 0.1 %	5.7 ± 0.3 %	-
	AApp4 80 Pa – 5 W	72.5 ± 0.3 %	18.9 ± 0.3 %	8.1 ± 0.1 %	-
After derivatisation	**AApp3 2.7 Pa – 20 W**	78.3 ± 0.3 %	13.0 ± 0.7 %	5.2 ± 0.2 %	2.4 ± 0.7 %
	AApp4 80 Pa – 5 W	70.4 ± 0.4 %	17.4 ± 0.5 %	8.4 ± 0.1 %	3.3 ± 0.0 %

After derivatisation, fluorine was detected with 2.4 ± 0.7 % for AApp3 and 3.3 ± 0.0 % for AApp4. Small quantities of Cl (<1%) were also identified for both coating types after derivatisation which is due to possible contamination from chlorine compounds from the glove box where the TFBA derivatisation occurs.

The amount of fluorine was increased for AApp4 compared to AApp3 which suggests that AApp4 contains more -NH_2 groups. Indeed, by using Equation 5 and 6, $\frac{[NH_2]}{[N]}$ was 6.2% for AApp3 and AApp4. However, $\frac{[NH_2]}{[C]}$ was 1.8% for AApp4 and 1.1% for AApp3. Hence, it confirms the higher degree of -NH_2 retention with the γ regime (AApp4, 80 Pa - 5 W). This may also be explained by the higher nitrogen content observed in the atomic composition. The plasma phase during the allylamine plasma polymer deposition may also be interested to study as it may indicate the presence of the allylamine molecule or fragments of molecule depending on the plasma conditions. This study has been performed at UoLiv as

their plasma reactor possesses different equipment for the plasma study, which will be discussed in the next Section 4.3.4.

4.3.4. Chemical analysis of the allylamine plasma phase by mass spectrometry

The allylamine plasma phase was also studied by the UoLiv since the design of their cruciform reactor allows the plasma phase study by different equipment as mentioned in Section 4.2.

The effect of plasma power and pressure on the fragmentation of the allylamine molecule was investigated by plasma phase mass spectrometry. Figure 4.17 represents the mass spectra of neutral plasma species measured at two extremes of pressure and power ranges (6.7 Pa – 20 W, and 80 Pa – 5 W). As shown in Figure 4.17a, the spectrum displayed a significant amount of precursor dissociation, with only a small fraction that represents the intact allylamine molecule (*M*) at low pressure and high power (6.7 Pa – 20 W). Indeed, at high power, the electron energy is greater which leads to more fragmentation of the precursor by electron impact. At low pressure, the electron mean free path is greater which results in a higher degree of molecular dissociation due to the higher energy of the neutral/ionic species acquired from the electron impact. Groups of lower mass molecules around m/z 41, 28, and 18 amu formed the majority of the observed neutral content. Peaks from 15-18 amu were assigned to CH_3, NH_x, and H_2O. Signals at 41 and 28 amu were likely to be C_3H_5 and CH_2N respectively as C-C and C-N have the weakest bond strengths at 3.91 eV and 4.39 eV and were most likely to break from electron impact [43,50,191]. When the pressure increased up to 80 Pa (Figure 4.17b), the electron mean free path was reduced and more collisions occurred which led to a decrease in the average electron energy. Therefore, the fragmentation of the allylamine precursor was suppressed. Therefore, *M* at m/z 57 began to dominate the spectrum. Moreover, small peaks were observed at m/z 28, and 41 as described before, as well as more prominent signals from CH_4N at 30, and 39 amu, which may arise due to a loss of hydrogen from CH_2-CH_2-NH_2 [36]. The small signal beyond 57 amu implied radical oligomerisation was not occurring

to any appreciable level, which agrees with previously reported mass spectral analysis of allylamine neutral species [43].

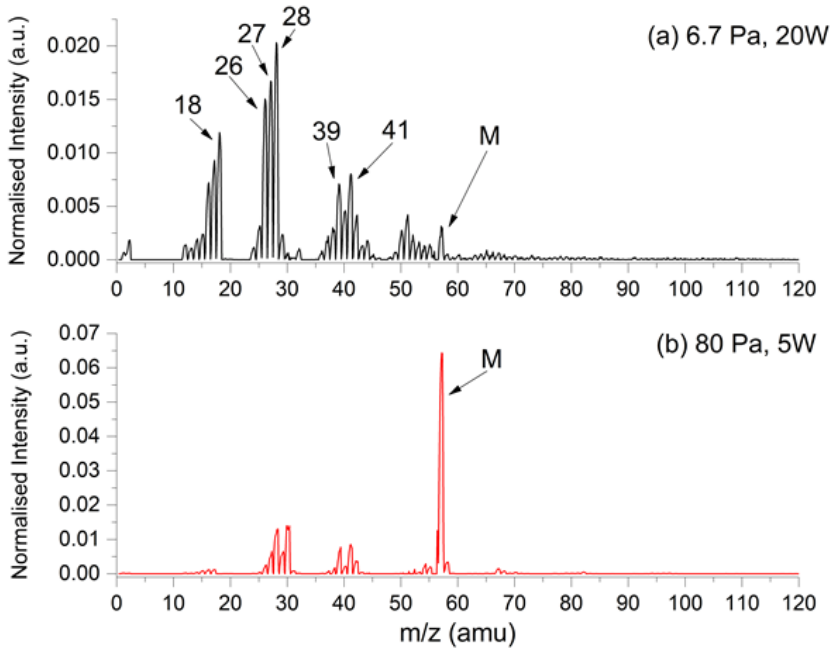

Figure 4.17: Recorded mass spectra of neutral species measured at a) 6.7 Pa 20 W, and b) 80 Pa, 5 W. High pressures and low powers suppresses the electron temperature which inhibits their ability to break molecular bonds in the plasma volume.

The fraction of the total mass spectrum signal attributed to the intact allylamine monomer *M* was studied for different plasma power (5, 10, and 20 W) and pressure (2.7 to 80 Pa) ranges. As shown in Figure 4.18, when the pressure increased and the plasma power decreased, *M* formed a larger fraction of the neutral particle flux with nearly 50% of the total flux at 80 Pa and 5 W. This indicates that high pressure and low power may lead to a higher fraction of intact allylamine monomer. If allylamine monomer is intact during the plasma deposition, the coating would have a high degree of retention of functional groups such as primary amines -NH_2 which correlates with the analyses of the AApp coatings by TFBA derivatisation.

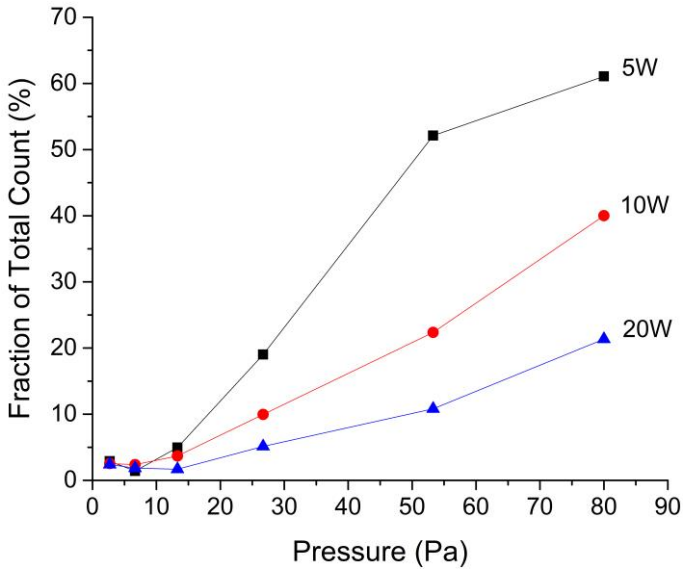

Figure 4.18: The total intensity of the intact monomer, M, as a percentage of the total recorded signal across the investigated pressure and power range. A synergistic combination of high pressure and low input power results in the protonated monomer forming most of the incident ion flux.

4.4. Conclusions

In this work, the effect of the different plasma regimes (α and γ) on the chemical composition of allylamine plasma polymer (AApp) coatings was investigated with AApp1 made at 2 Pa and 30 W, and AApp2 made at 20 Pa and 5.5 W. Primary amines $\frac{[NH_2]}{[N]}$ were estimated to 13.9% for AApp2 whereas only 5.8% for AApp1, and $\frac{[NH_2]}{[C]}$ were 4.4% AApp2 and only 1.7% for AApp1. Indeed, despite a similar atomic composition as shown by XPS, the concentration of -NH_2 was more than doubled for the coating made using the γ regime compared to the usual α regime. Therefore, the use of a combination of high pressure and low power during the plasma deposition process may result in better retention of chemical functionalities. These analyses were further compared with AApp coatings made at the UoLiv. The derivatisation of these coatings showed again that the use of γ regime may lead to a higher retention of primary amine groups. Furthermore, the analysis of the plasma phase clearly demonstrated that the combination of a higher pressure and lower power leads to less fragmentation of the allylamine molecule.

Chapter 5. Whey protein fibrillar coatings enriched with biomolecules

5.1. Overview

This chapter presents the production and characterisation of whey protein isolate (WPI) fibrillar coatings. WPI fibrillar coatings were produced by adsorption of WPI fibrils as described in Section 3.2.2. WPI fibrillar coatings were enriched with two different biomolecules, namely phloroglucinol (PG) and tannic acids (TAs). The coatings were analysed by XPS to investigate the influence of adsorption time, autoclave sterilisation, and incorporation of biomolecules on the WPI fibrillar coatings. The autoclave sterilisation and the addition of biomolecules did not impact the fibrils.

Regarding WPI/PG coatings, the incorporation of PG did not affect WPI fibrils. Moreover, cell tests were performed to check the influence of WPI fibrils containing PG adsorbed on Ti6Al4V alloy on cell behaviour as described in Section 3.2.2.5. The tests were performed on unstimulated and biofilm-stimulated cells. Results showed a significant decrease in metabolic activity when cells have been stimulated with biofilm, but no significant difference was observed between sample groups in unstimulated and biofilm-stimulated cells. WPI containing PG exhibited a general significant downregulation of pro-inflammatory markers compared to uncoated titanium. Susceptibility tests were not successful, but the attachment of bacteria was different depending on the sample group.

Finally, cell tests were performed on WPI/TAs coatings to see the influence of the coatings on cells as described in Section 3.2.2.8. For WPI/TAs coatings, TAs did not

affect WPI fibrils as for PG. Cell tests were performed to study the influence of such coatings adsorbed on glass on cell behaviour. Results did not show any negative impact of the coatings on cells. TNAP activity and calcium deposition were slightly increased in presence of the coatings, but no significant difference could be observed. Further investigation needs to be performed.

5.2. Methodology

Whey protein fibrillar coatings were produced as described in Section 3.2.2. The WPI coatings were characterised in terms of adsorption and stability. XPS analyses were used to characterise the chemical composition of the coatings and SEM images were produced to observe the fibrils.

Some coatings were also enriched with PG on Ti6Al4V alloy and cell tests using human bone marrow-derived mesenchymal stem cells (BM-MSCs) were performed including metabolic activity, gene expressions relative to bone formation and mineralisation, and pro-inflammatory response. Antibacterial tests such as susceptibility tests and bacterial attachment studies were attempted.

Other WPI coatings were enriched with TAs on glass substrates. The metabolic activity of human bone marrow stromal cells (hBMSCs) was studied after 2 and 4 days. Moreover, the enzyme activity of tissue non-specific alkaline phosphatase (TNAP) at day 11 and the calcium mineralisation at day 22 were measured.

5.3. Results and discussion

5.3.1. Adsorption and stability of WPI fibrils

5.3.1.1. Adsorption time

Different adsorption times were tested from 1h to 5h. The hypothesis was that a longer adsorption time would lead to a higher surface coverage and so a higher nitrogen content from the protein molecule which contains amine functionalities. In contact with the surface, a protein can undergo different conformational changes. Thus, the adsorption time may be an important factor to consider. However, by analysing the coating by XPS, no significant difference was observed

for the different adsorption times (Figure 5.1). N content increased from 0% (uncoated glass) to approximately 15% for all the coatings which indicates that 1h adsorption time leads to a saturated coating. Si was still detected for all the conditions, even after 5h of protein adsorption which indicates that the coating is either thin or not homogenous with gaps between fibrils. Protein-surface interaction has been widely studied in the biomaterial field. Roach *et al.* described that protein adsorption happens in two phases: rapid initial adsorption within an hour, followed by some time-dependent changes [192].

On the basis of these results, a 1h-adsorption time was used in further experiments in this project. Adsorption could also be improved by directly grafting the protein to the substrate [193]. However, in this study, the adsorption method will be used as a simple, quick, and economical method which does not require additional chemicals. Moreover, the adsorption method can be adapted to different substrate geometries.

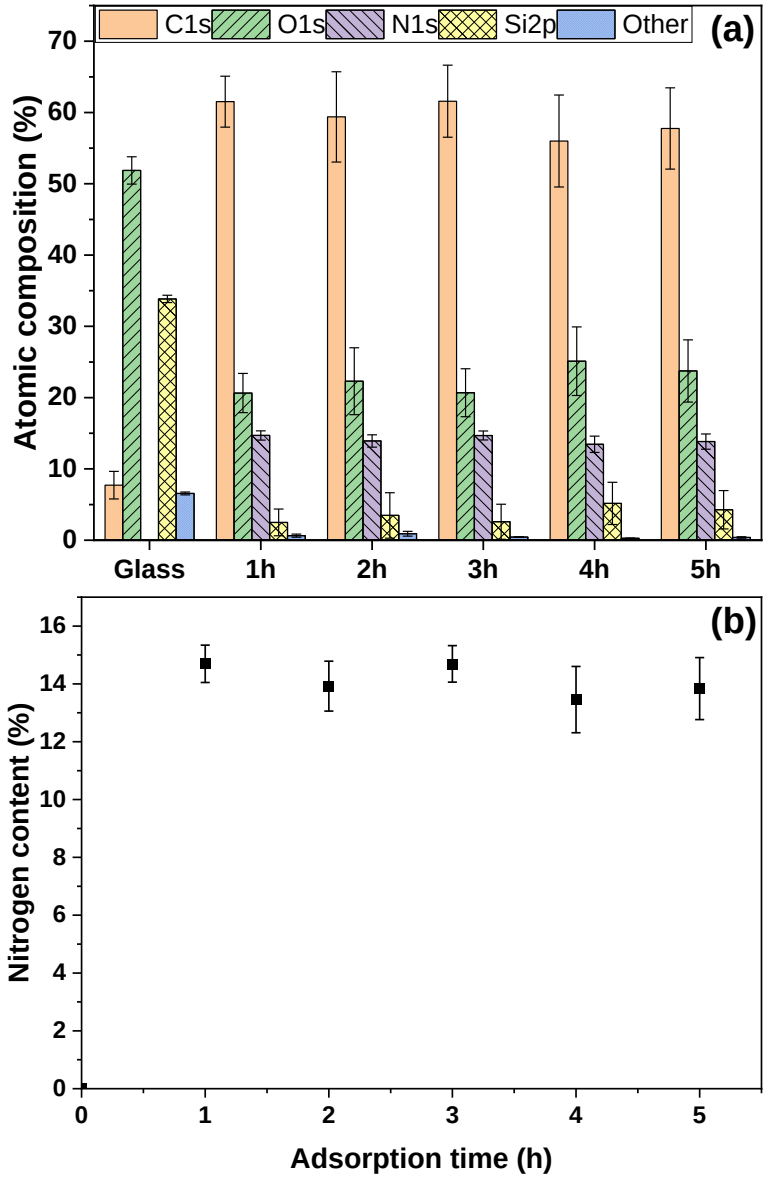

Figure 5.1: (a) XPS data of uncoated glass and WPI for different adsorption times (1h, 2h, 3h, 4h, and 5h). "Other" corresponds to other elements in low quantity which mainly originate from the glass substrate (S 2p, Cl 2p, Na 1s, Zn 2p, K 2s, Al 2p, P 2p, and Ti 2p). (b) Nitrogen content from the XPS data for the different adsorption times. Error bars represent standard deviation (n=5).

5.3.1.2. Stability study of the fibrils in suspension and as a coating

The stability of the WPI fibrils was studied after two months of storage at 4°C. A coating was made with a 2-month-old fibrillar suspension and imaged by SEM as shown in Figure 5.2. Fibrils were detected by SEM which attests their presence in the suspension. Thus, the WPI fibrillar suspension was stable for at least two

months of storage in the fridge. It is worth mentioning that the suspension was free of microbial growth, likely due to the acidic pH of the suspension (pH 2), which is an unfavourable environment for the growth of microbes.

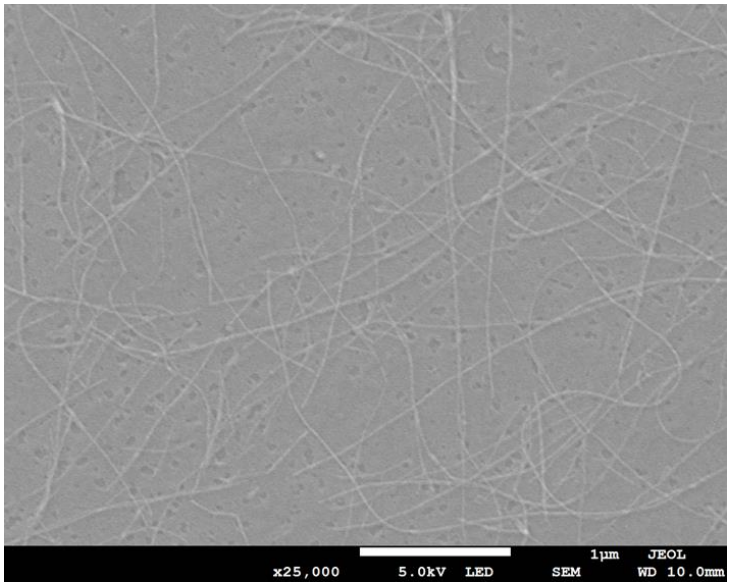

Figure 5.2: SEM image of WPI coating made with a 2-months old WPI fibrillar suspension. Small darker patterns may be from the glass structure. Scale bar: 1 µm.

Furthermore, the stability of the coating itself has been studied after 1h, 5h, and 24h of immersion in PBS which has a pH of 7.4, close to physiological pH (Figure 5.3). WPI fibrils were still present even after 24h of immersion as shown in Figure 5.3c. They seem thicker which may be due to salt deposition. In fact, at higher magnification, salt crystals were visible as indicated by the red arrow in Figures 5.3c and 5.3d. Since WPI fibrillar coatings are stable after 24h in PBS, they may be used to coat biomaterials to improve cell adhesion, proliferation, and differentiation, or to avoid microbial colonisation by incorporating other bioactive molecules like phloroglucinol (PG) or tannic acids (TAs).

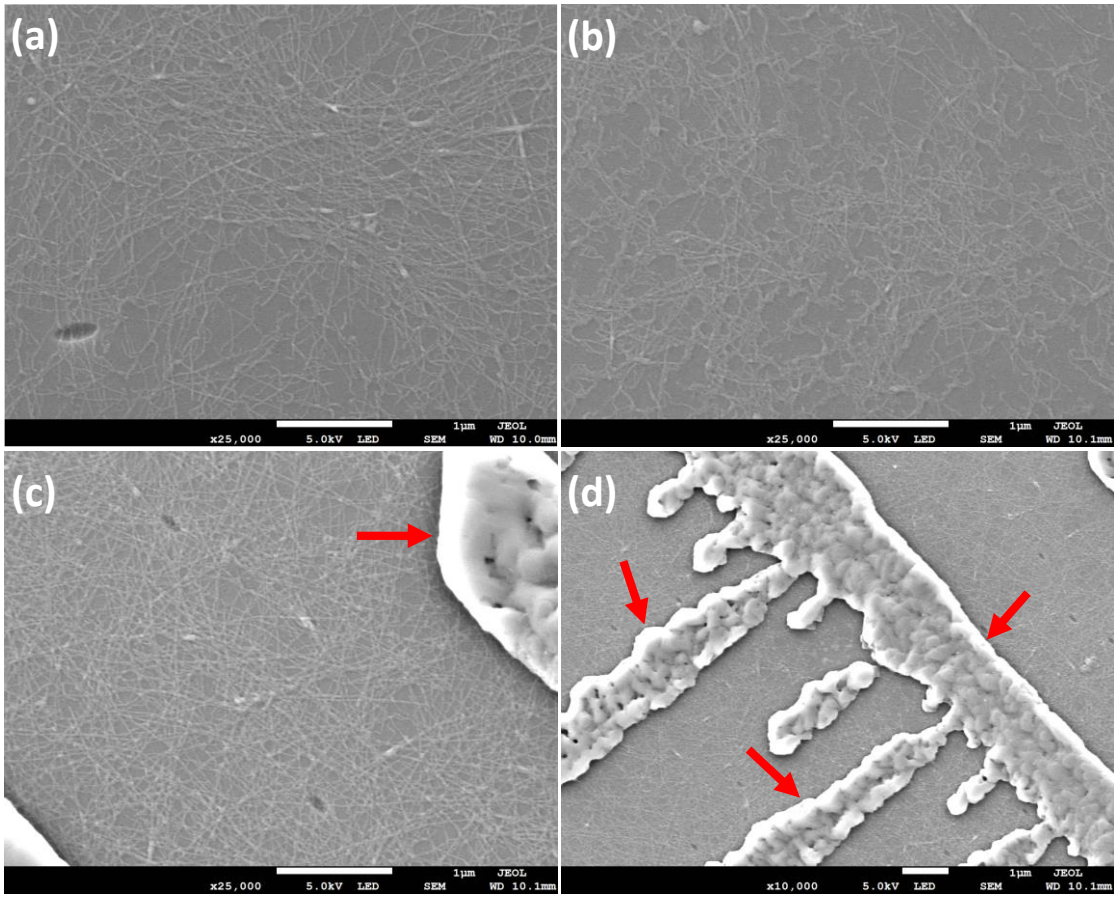

Figure 5.3: SEM images of the WPI coatings before autoclaving after (a) 1h, (b) 5h, and (c) 24h in PBS solution. (d) represents a lower magnification of image (c). Red arrows indicate possible salts. Scale bar: 1 µm.

5.3.2. Incorporation of phloroglucinol into the WPI fibrillar network

5.3.2.1. Characterisation of the WPI/PG coatings on glass

SEM analyses were performed to image the WPI fibrils adsorbed on glass substrates before and after sterilisation and with different concentrations of PG. The images confirmed the presence of WPI fibrils even after autoclave sterilisation and in the presence of PG as shown in Figure 5.4. Fibrils appeared on all coating types with a length in the micrometre range and a diameter in the nanometre range. They remained adsorbed on the glass substrate even after three successive washing steps and sterilisation by autoclaving, as already demonstrated in our previous study [82]. The use of autoclave sterilisation is a standard method in

hospitals since it is clinically accepted, therefore, the resistance of WPI fibrils to autoclaving is an important practical advantage.

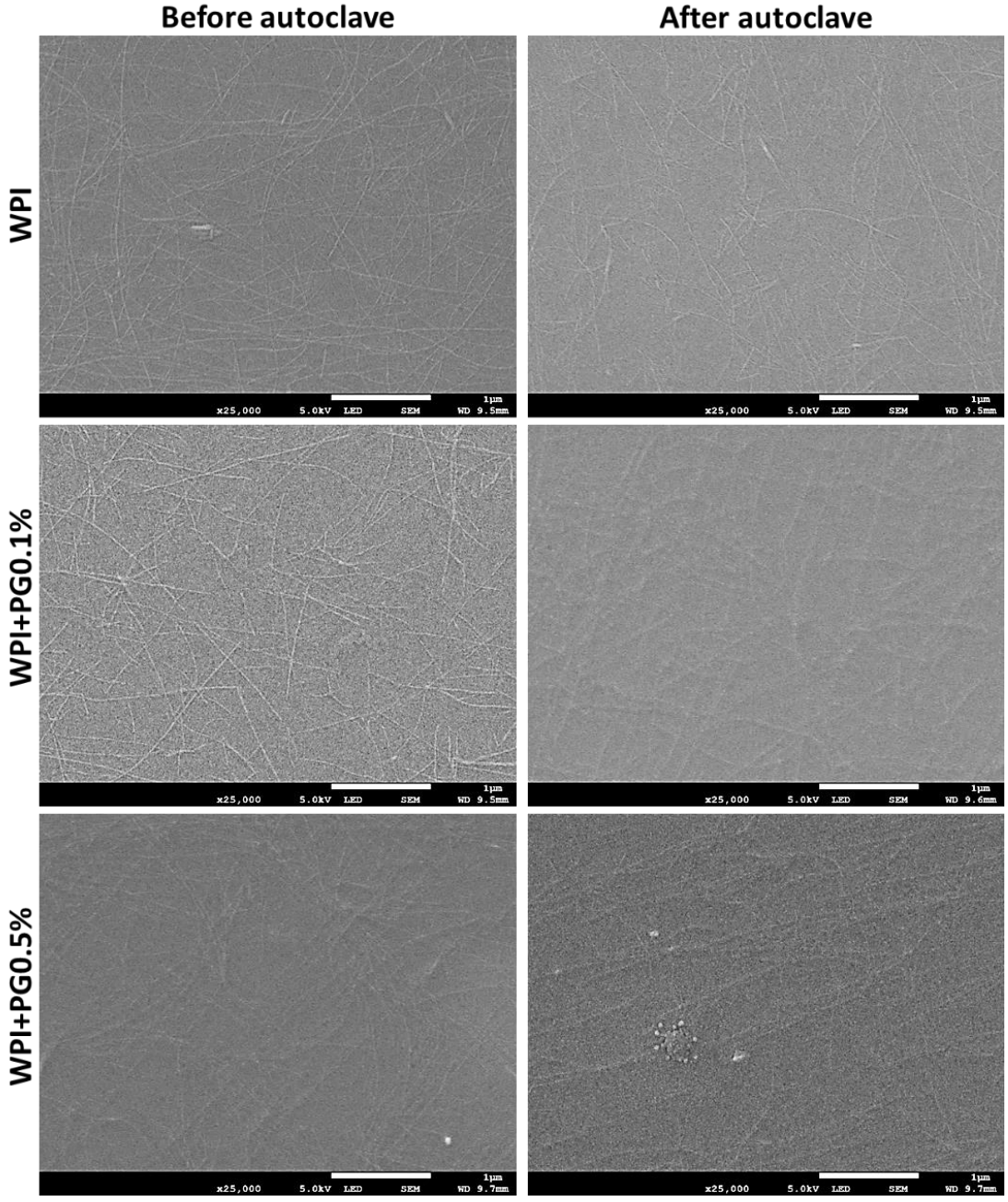

Figure 5.4: SEM images of WPI coatings before and after autoclaving for different PG concentrations. The first and second columns are before and after autoclaving, respectively. The first, second, and third rows are WPI, WPI with 0.1% of PG, and WPI with 0.5% of PG coatings, respectively. Scale bar: 1 µm.

Moreover, fibrils do not seem affected by the addition of PG for both concentrations (WPI+PG0.1% and WPI+PG0.5%). It is hypothesized that the gaps between the fibrils correspond to the glass substrate and the coatings are estimated to be one fibril thick. The gaps may also be covered by non-fibrillar proteins which are not visible by SEM. Fibril-surface interaction may be mainly due to non-covalent interactions such as electrostatic interactions, van der Waals, or hydrophobic interactions, which are the main interactions involved in protein adsorption processes [192].

The chemical composition of the coatings was analysed by XPS as presented in Figure 5.5 which represents a summary of XPS data for uncoated glass substrates and the different types of WPI coatings before and after sterilisation by autoclaving. Glass substrates consisted mainly of C (8%), O (52%), and Si (34%). Other components were also detected, such as Al, K, Na, P, Zn, and Ti in low quantities (< 7% in total). With the addition of WPI coatings on the glass, atomic percentage confirmed the presence of the protein with the introduction of N1s peak (more than 10% in all the coatings) due to the amine groups present in the molecular structure of the protein. The increase of C1s peak from 8% (glass) to 50-60% also attested to the presence of protein because of the carboxyl groups. Moreover, the characteristic Si peak from the glass decreased from 34% (glass) to 8-10% as well as other components such as K, Al, P, and Ti that are totally undetectable. The small quantity of Si still detectable after WPI coatings means that either the coating is thin (< 10-15 nm, due to the detection depth of XPS) or the coating is not homogeneous (so, the glass is also detected since the area of detection is 300 x 700 μm). The second hypothesis may be correct; since fibril diameters measured by AFM were about 20-22 nm the first hypothesis is unlikely to be correct (see Appendix C). Thus, the glass may be detected where there are no fibrils as hypothesized with the SEM images. In that case, surface coverage can be estimated since only glass in gaps between fibrils is detected, the loss of %Si corresponds to the surface coverage of fibrils which is about 2/3 of the coating. However, no clear difference was noticed between all the different conditions before/after sterilisation and after the addition of PG.

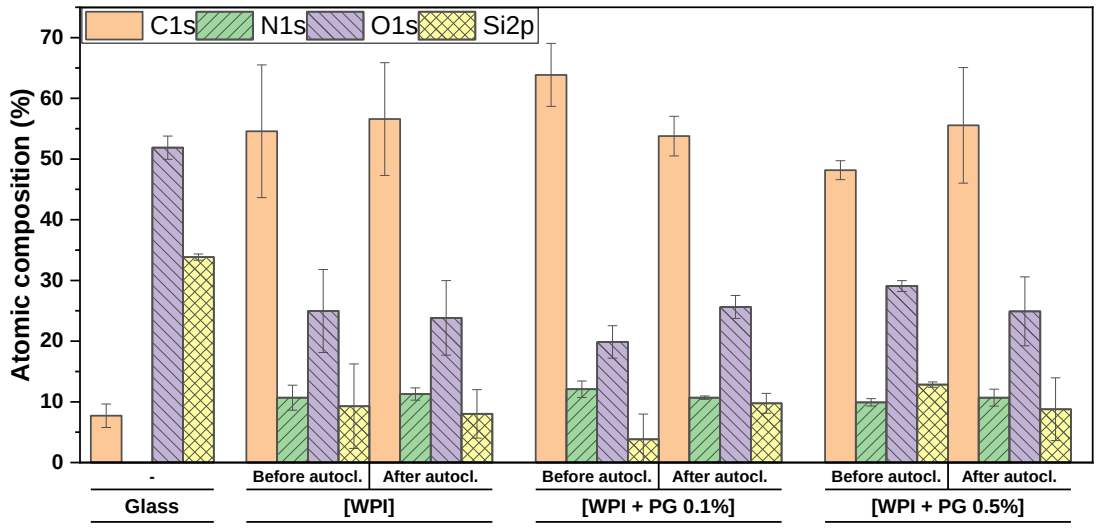

Figure 5.5: XPS data of uncoated glass and WPI coatings without PG, with 0.1% of PG and 0.5% of PG, before and after sterilisation by autoclaving (autocl.). Error bars represent standard deviation (n=3).

5.3.2.2. Characterisation of the WPI/PG coatings on Ti6Al4V alloy

Glass was used in previous experiments as an inexpensive substrate for the preliminary study. However, in orthopaedics or dental biomaterials, titanium alloy is often used. In the following part, Ti6Al4V (Ti) alloy was used as a more relevant material for bone contact to coat WPI fibrils with and without PG. As a reminder, sample denominations are presented in Table 5.1.

Table 5.1: WPI coatings denomination with and without PG.

Coating denomination	Description
$[WPI]_{autoclave}$	WPI fibrillar coating autoclaved
$[WPI + PG\ 0.1\%]_{autoclave}$	WPI + PG 0.1% mixed coating autoclaved
$[WPI + PG\ 0.5\%]_{autoclave}$	WPI + PG 0.5% mixed coating autoclaved
$[WPI]_{autoclave}$ + PG 0.1%	WPI fibrillar coating autoclaved + PG 0.1% added after
$[WPI]_{autoclave}$ + PG 0.5%	WPI fibrillar coating autoclaved + PG 0.5% added after

As shown in Figure 5.6, XPS was performed on WPI fibrils adsorbed on Ti. Different methods were used to sterilise the coating. Some coatings were autoclaved with

PG inside ([WPI + PG 0.X%]$_{autoclave}$), whereas others had PG added under sterile conditions on top of WPI fibrils which had been autoclaved ([WPI]$_{autoclave}$ + PG 0.X%). All coatings were mainly constituted of C, N, and O which demonstrates the presence of the protein layer. Indeed, nitrogen and carbon were detected from the protein constituted of a long chain of amino acids containing different molecular structures such as amine or carbonyl groups. Moreover, the decrease in %Ti from 15% (uncoated Ti) to less than 4% confirmed the presence of the coating. As Ti was still detected in the presence of WPI fibrils, the coating may be either thinner than 15 nm which is the depth detection limit, or non-uniform revealing gaps between the fibrils as already described on glass substrates in Section 5.3.2.1. No significant difference was observed between the different coatings. However, Ti decreased significantly from 3.6% (WPI) to 0.4% ([WPI]$_{autoclave}$ + PG 0.5%) which indicates that the coating may be thinner or more uniform. PG was not easily detectable as oxygen and carbon may come from the protein and Ti substrate.

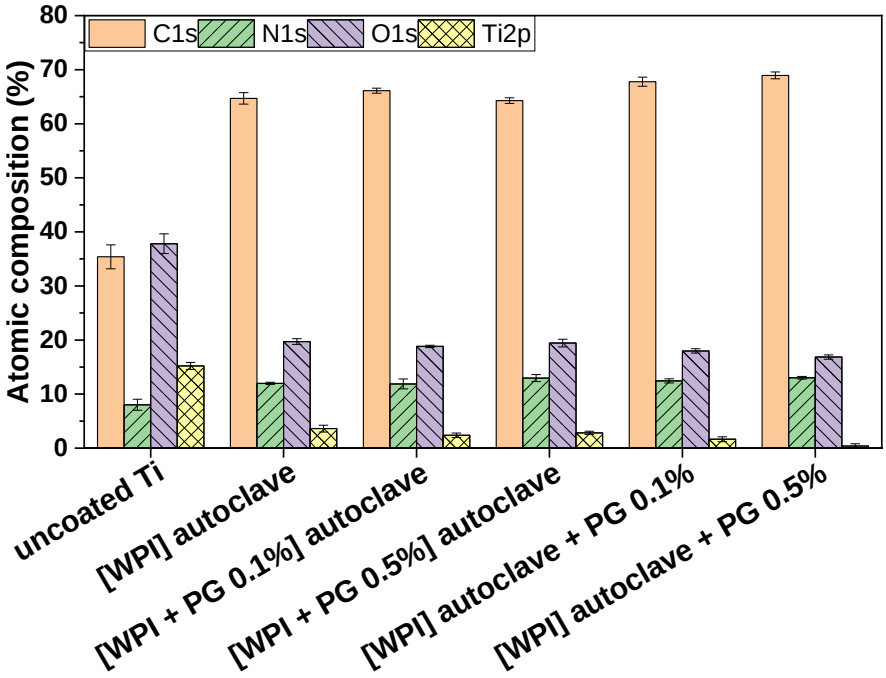

Figure 5.6: XPS data of uncoated Ti and WPI coatings without PG, with 0.1% of PG and 0.5% of PG. [WPI + PG 0.1%]$_{autoclave}$ and [WPI + PG 0.5%]$_{autoclave}$ mean that the coatings containing PG were autoclaved. [WPI]$_{autoclave}$ + PG 0.1% and [WPI]$_{autoclave}$ + PG 0.5% mean that only WPI coating was autoclaved, PG was added afterwards using a sterile filter and syringe. Error bars represent standard deviation.

5.3.2.3. In vitro tests

Cell tests were performed on WPI/PG coatings on porous Ti6Al4V alloy. The cells used were BM-MSCs which are cells that can undergo differentiation into multiple cell types and modulate host-immune responses by the secretion of pro-healing factors. However, due to the presence of biofilms the wound healing can be affected. Therefore, in this study, BM-MSCs were stimulated with biofilm to investigate the effect of the coatings on unstimulated and biofilm-stimulated cells' behaviour. The image of the biofilm is shown in Appendix D.

5.3.2.3.1. Cell morphology

SEM images were obtained to confirm the presence of BM-MSCs on uncoated Ti and WPI coatings with and without PG after 72h of culture (Figure 5.7). For all the conditions, BM-MSCs were attached in the pores of the Ti6Al4V alloy. Moreover, cells seemed to spread well on all coating types. However, no significant difference in the cell morphology between the sample groups was observed.

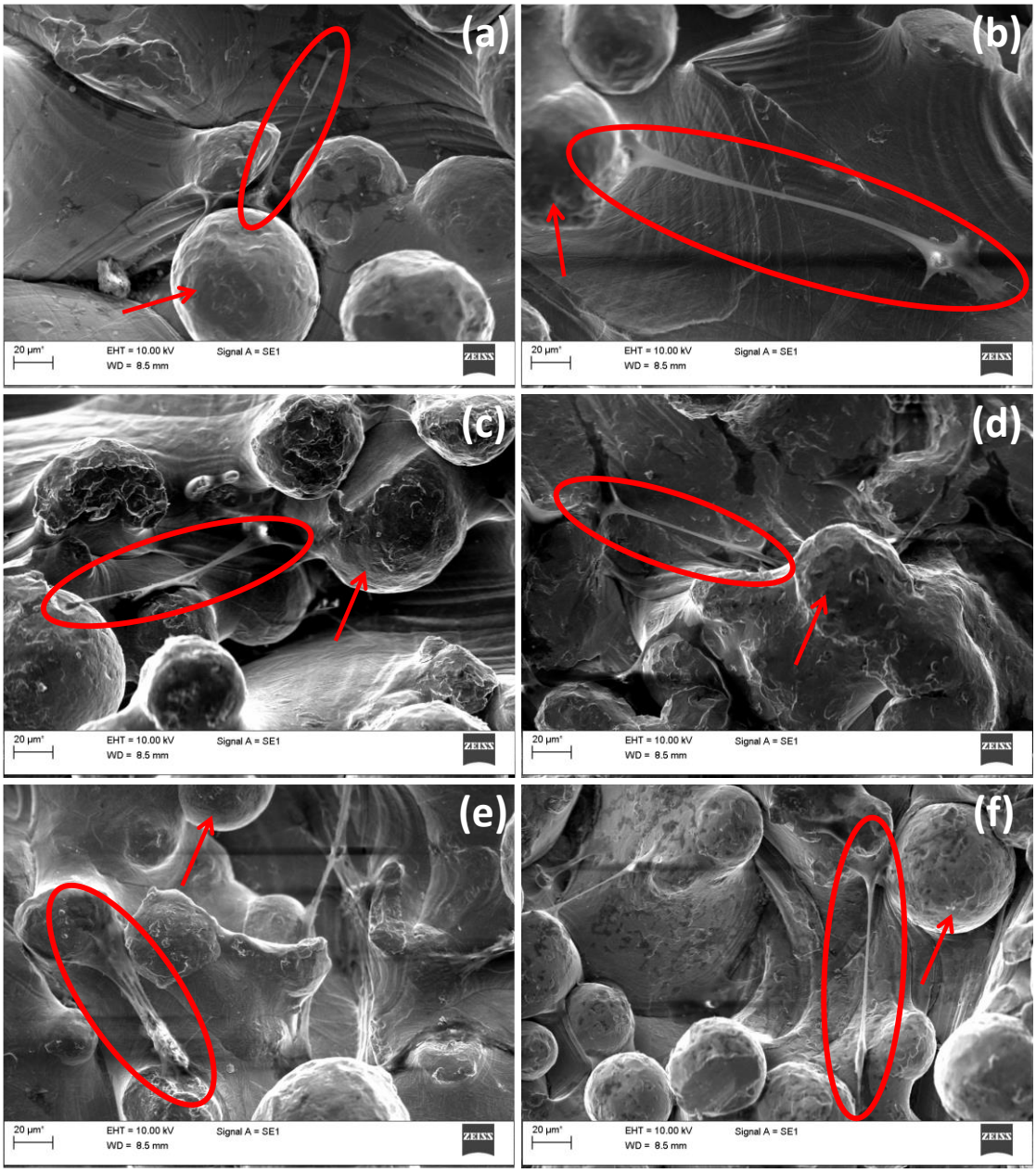

Figure 5.7: SEM images of unstimulated BM-MSCs on (a) uncoated Ti6Al4V, (b) WPI, (c) [WPI + PG 0.1%]$_{autoclave}$, (d) [WPI + PG 0.5%]$_{autoclave}$, (e) [WPI]$_{autoclave}$ + PG 0.1%, and (f) [WPI]$_{autoclave}$ + PG 0.5% coatings on Ti6Al4V. Ellipses indicate the cells and arrows show particles that form the Ti6Al4V alloy. Scale bar: 20 µm.

5.3.2.3.2. Metabolic activity

Metabolic activity of unstimulated and biofilm-stimulated BM-MSCs was investigated after 48h as summarised in Figure 5.8. Results showed a significant decrease in metabolic activity when cells had been stimulated with biofilm. This

may be due to the release of soluble factors from the biofilm which impact the cell function as already mentioned in a previous study [194]. They showed that mesenchymal stromal cells exposed to *S. aureus* and *P. aeruginosa* biofilm media had reduced cell viability due to activation of apoptosis and the migration and differentiation abilities were also reduced. Other studies investigated this effect especially in chronic wounds as biofilm seems to contribute to wound chronicity [195]. Moreover, no significant difference was observed between sample groups in unstimulated and biofilm-stimulated BM-MSCs, meaning that the coatings do not have a negative impact on cells compared to the uncoated Ti.

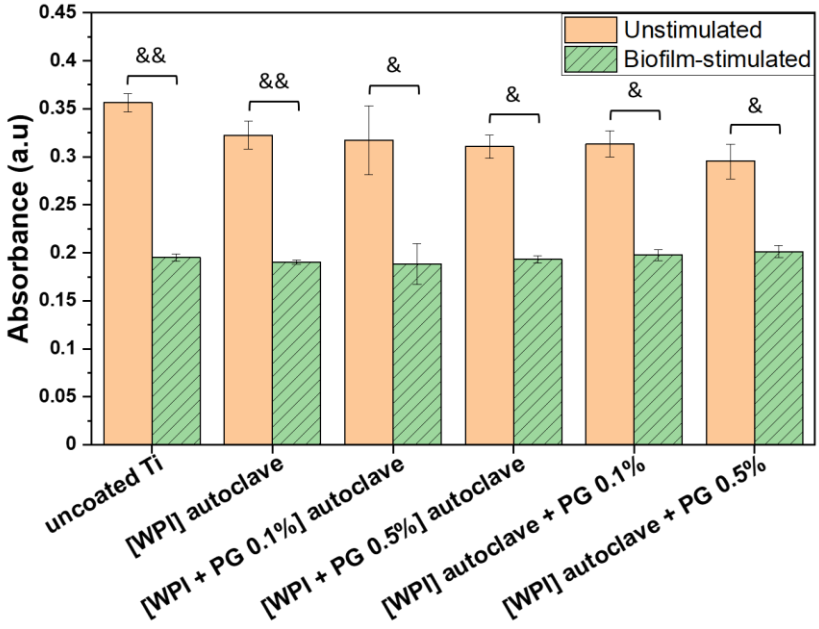

Figure 5.8: Metabolic activity of unstimulated and biofilm-stimulated BM-MSCs after 48h using MTT test. BM-MSCs were stimulated with biofilm for 2h and metabolic activity was analysed directly after biofilm stimulation. The results are shown as mean (n = 4, two technical repetitions) and bars represent standard error of the mean. Significant differences for unstimulated vs. biofilm-stimulated BM-MSCs are indicated with & ($p < 0.05$), and && ($p < 0.01$).

5.3.2.3.3. Matrix formation

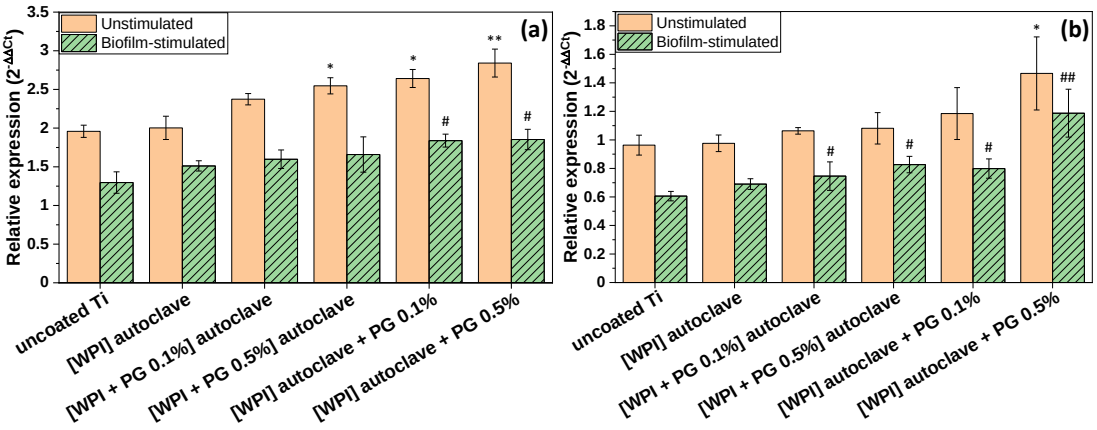

*Figure 5.9: Relative gene expression for matrix formation markers: (a) RUNX2, and (b) COL1A1. The results are shown as mean (n = 4, two technical repetitions) and bars represent the standard error of the mean. * and # represent statistical analyses between uncoated Ti and tested samples for unstimulated cells and biofilm-stimulated cells, respectively. (*,# p < 0.05; **,## p < 0.01).*

The expression of genes for bone matrix formation was studied for unstimulated and biofilm-stimulated cells. Runt-related transcription factor (*RUNX*) is an early marker of bone formation as it is detected in preosteoblast cells, and collagen type I alpha 1 chain (*COL1A1*) is known as a key marker of bone matrix production [196,197]. Both genes are important markers of the early stages of osseointegration. As shown in Figure 5.9, the expression of *RUNX* and *COL1A1* genes was reduced for biofilm-stimulated cells compared to unstimulated ones which may indicate that some factors released from the biofilm inhibit bone formation. However, in presence of PG, the expression of these genes increased especially when PG was not autoclaved with a concentration of 0.5%. This indicates that PG was more biologically active without being sterilised by autoclaving, and the heat may impact its activity. These results are in accordance with a previous study of PG added into collagen fibrillar coatings where *COL1A1* gene expression was studied [98].

5.3.2.3.4. Matrix mineralisation

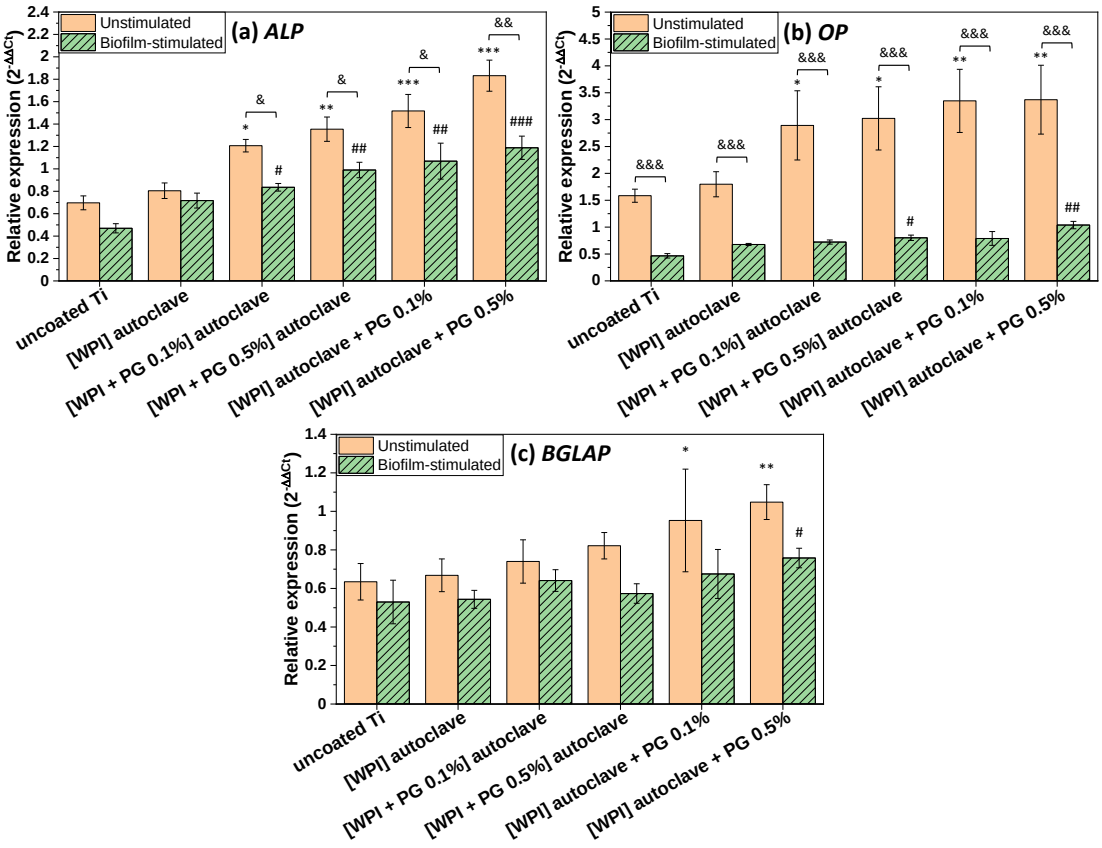

*Figure 5.10: Relative gene expression for matrix mineralisation markers: (a) ALP, (b) OP, and (c) BGLAP. The results are shown as mean (n = 4, two technical repetitions) and bars represent standard error of the mean. * and # represent statistical analyses between uncoated Ti and tested samples for unstimulated cells and biofilm-stimulated cells, respectively. (*,# p < 0.05; **,## p < 0.01).*

The expression of genes for matrix mineralisation was measured for unstimulated and biofilm-stimulated cells as shown in Figure 5.10. Alkaline phosphatase (*ALP*), osteopontin (*OP*), and bone gamma-carboxyglutamate protein (*BGLAP*) genes were used as they are osteogenic markers. *ALP* is an essential marker for bone mineralisation of osteoblastic cells [198], *OP* is a marker of osteogenic differentiation and is expressed during the maturation of osteoblastic cells [199], and *BGLAP* is involved in the regulation of the mineralisation process [200]. For all genes, their expressions were increased in presence of PG especially with 0.5% of PG which had been added after autoclaving. These results are in accordance with

a previous study of PG added into collagen fibrillar coatings where *BGLAP* gene expression was also studied [98].

5.3.2.3.5. Inflammatory response

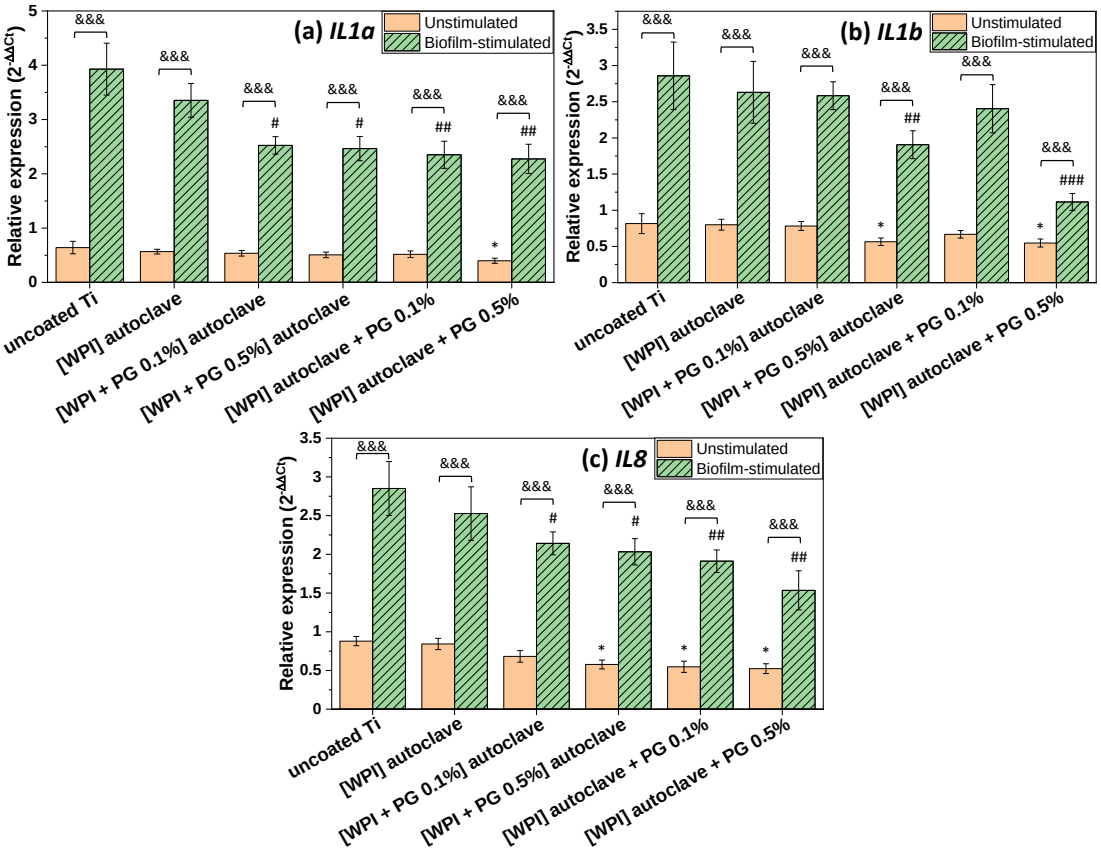

*Figure 5.11: Relative gene expression for pro-inflammatory markers: (a) IL1a, (b) IL1b, and (c) IL8. The results are shown as mean (n = 4, two technical repetitions) and bars represent standard error of the mean. * and # represent statistical analyses between uncoated Ti and tested samples for unstimulated cells and biofilm-stimulated cells, respectively. (*,# p < 0.05; **,## p < 0.01).*

The implantation of biomaterials such as Ti implants into the bone may trigger host responses such as inflammation which can interfere with the osseointegration process. The gene expressions of pro-inflammatory response were studied with three different markers: interleukin 1 alpha (*IL1a*), interleukin 1 beta (*IL1b*), and interleukin 8 (*IL8*) as shown in Figure 5.11. The expression of the three inflammatory markers was higher with biofilm-stimulated cells compared to unstimulated cells.

WPI containing PG exhibited a general significant downregulation of pro-inflammatory markers compared to uncoated titanium. Moreover, results suggested that WPI coatings containing a high amount of PG (0.5%) added after autoclaving may modulate the inflammatory response by downregulating pro-inflammatory genes, especially *IL1b* (Figure 5.11b).

As already described in the literature, PG may prevent inflammation by downregulating gene expression of inflammatory markers such as tumour necrosis factor-α, interleukin-1β, interleukin-6 and prostaglandin E2 via a possible reaction mechanism between hydroxyl groups and reactive oxygen species [139]. These results are also in accordance with a previous study on collagen fibrillar coatings containing PG [98].

Finally, the differences observed in gene expression suggested the presence of PG in the coatings even if it was not detectable by XPS analyses as mentioned in Section 5.3.2.2.

5.3.2.4. Antibacterial tests

5.3.2.4.1. Susceptibility tests

The minimum inhibitory concentration (MIC) of PG was estimated to be 2.5 mg/mL by following a clinical laboratory standards institute (CLSI) protocol against four species of bacteria (two Gram-positive species *S. aureus* and *E. faecalis,* and two Gram-negative species *P. aeruginosa* and *E. coli*) as described in Appendix E. Therefore, sensitivity tests were performed to investigate the possible antibacterial activity of WPI/PG coatings on four different bacteria: *S. epidermidis*, *MRSA*, *E. coli*, and *P. aeruginosa*. Two different agars (LB and DST) were tested since the type of agar may influence PG activity. The images of the tests are shown in Figure 5.12.

No ZOI was measured either on LB agar or on DST agar. Therefore, the coatings may not present antibacterial activity. The concentration of PG may be too low or most of PG may be lost during the washing steps which would explain why it was not detected by XPS. To increase PG concentration, the surface coverage of WPI fibrils could be increased by modifying the surface by plasma [201].

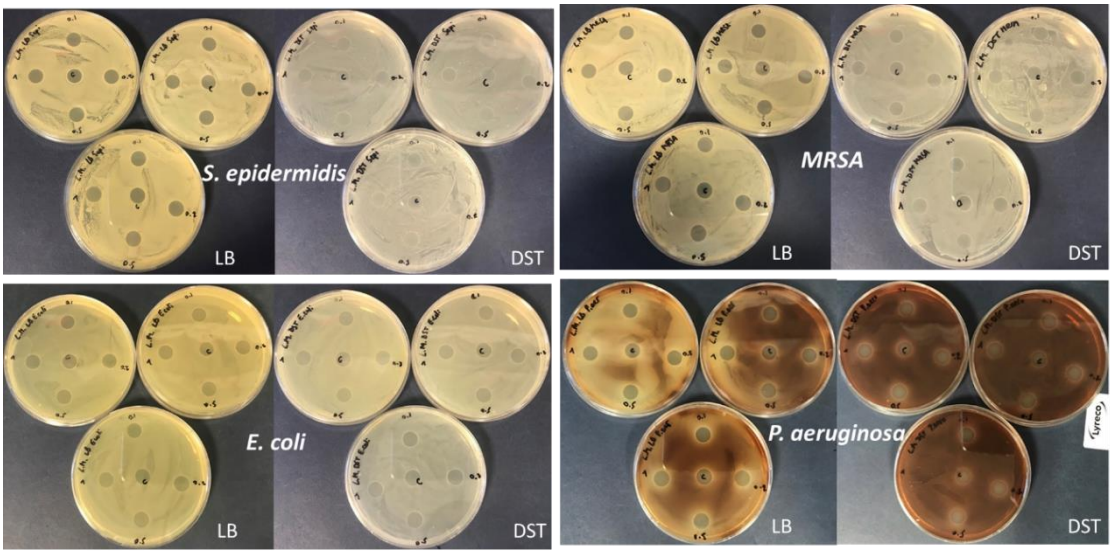

Figure 5.12: Sensitivity tests for S. epidermidis, MRSA, E. coli, and P. aeruginosa, as well as for two different types of agar LB (left image) and DST (right image)

5.3.2.4.2. Bacterial attachment study

The attachment of bacteria on the different coatings was studied after 24h of incubation with *S. epidermidis*. After crystal violet staining, the coatings were observed under microscope for qualitative analyses. The images in Figure 5.13 represent the bacteria attached on the coatings.

On glass, some bacteria were observed and attached on the sample. However, it can be observed that more bacteria were present on the WPI coating. The presence of the protein may act as a conditioning film for bacteria attachment. For [WPI + PG 0.1%]$_{autoclave}$, bacteria number may be slightly higher, and with 0.5%, the number of bacteria attached clearly increased. However, a clear decrease in bacteria attachment for [WPI]$_{autoclave}$ + PG 0.5% can be observed. This can indicate that PG added on top of the fibrils may hinder bacterial attachment. The high concentration may be necessary as it was not observed for PG 0.1%. Further work still needs to be performed to investigate the trend as the test also stains dead bacteria. Therefore, the bacteria attached may also be killed in contact with the coatings.

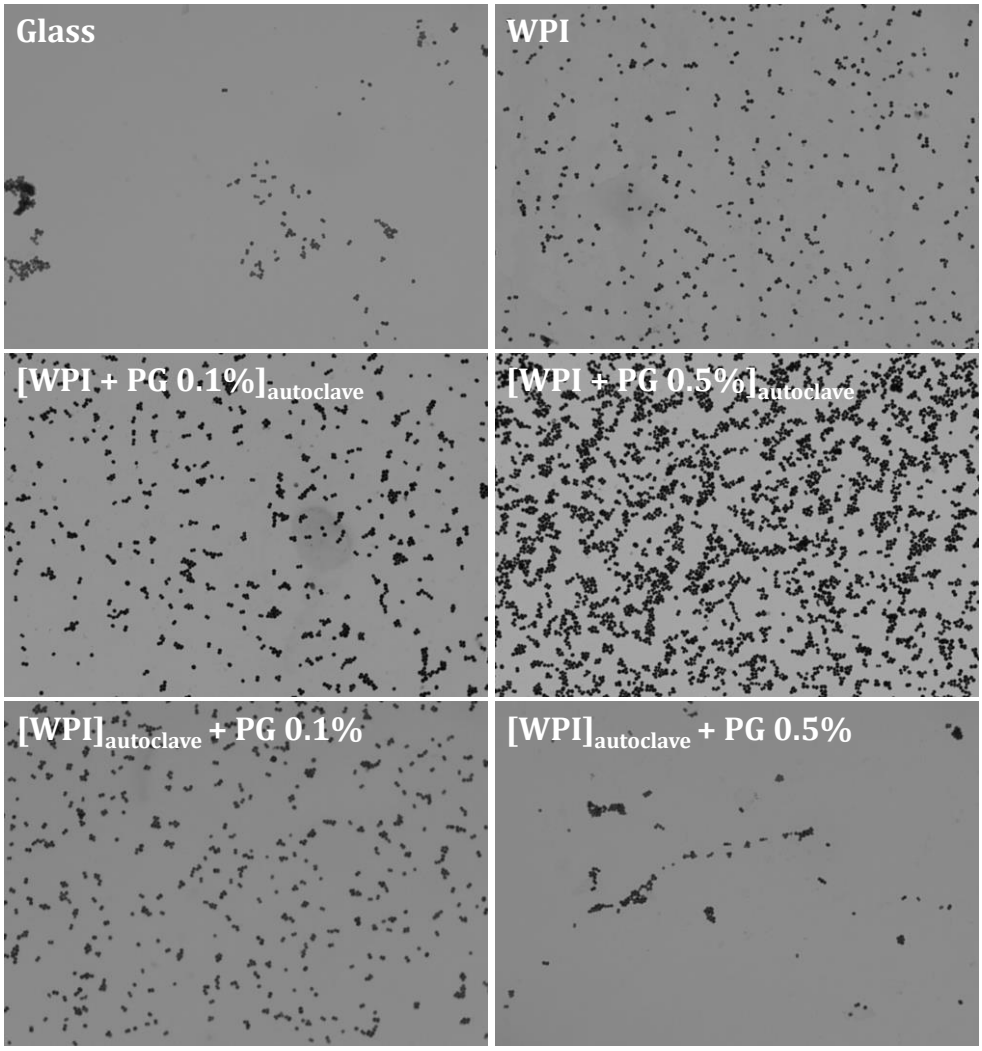

Figure 5.13: Attachment of S. epidermidis on uncoated glass and the different WPI coatings containing or not containing PG.

5.3.3. Incorporation of tannic acids into the WPI fibrillar network

This work was carried out with Zahin Absar as part of his MEng individual project "Fibril Coatings from Whey Protein Isolate on Biomaterial Surfaces", under my supervision and training. I supervised and trained Zahin to fabricate the coatings for characterisation. I provided guidance and feedback on his experimental plan and dissertation thesis. For the cell tests, the coatings were made by me for shipment to Germany. I would like to acknowledge Zahin for his work, which was awarded the

Stopford Prize 2022. The Stopford Prize is awarded annually to the student who undertakes the best Chemical Engineering project.

5.3.3.1. Characterisation of the WPI/TAs coatings on glass

Different WPI coatings were produced with the addition of tannic acids (TAs). Three different TAs were used: ALSOK2 (AL2), ALSOK4 (AL4), and BREWTAN F (BRW). A first set of coatings was produced with TAs added before fibril formation whereas a second set of coatings was made with TAs added after fibril formation, in the same manner as with PG. Samples were named as indicated in Table 5.2.

Table 5.2: WPI coating denominations as a function of TA type and when TA was added in the fibril formation process.

	TA type	**TA added before/after fibril formation**
WPI+AL2_bef	ALSOK2	Before
WPI+AL2_af	ALSOK2	After
WPI+AL4_bef	ALSOK4	Before
WPI+AL4_af	ALSOK4	After
WPI+BRW_bef	BREWTAN F	Before
WPI+BRW_af	BREWTAN F	After

SEM analyses were performed to image the WPI fibrils adsorbed on glass substrate with different TAs before sterilisation. The images confirmed the presence of WPI fibrils in the presence of TAs as shown in Figure 5.14. Fibrils appeared on all coating types but seem thicker for the ones containing ALSOK2 (Figure 5.14a-b) and ALSOK4 added before (Figure 5.14c) compared to the other conditions. For ALSOK2, no significant difference was observed when added before or after fibril formation. However, for ALSOK4, more WPI fibrils were observed when added before fibril formation (Figure 5.14c) with a thicker morphology compared to the one added after (Figure 5.14d). Regarding BREWTAN F, when added after fibril formation, small clear dots appeared on the image which may correspond to the TA (Figure 5.14f). Between the dots, fibrils seemed to form a thick mat which was not observed for the fibrillar coating with TA added before fibril formation (Figure 5.14e). However, for all the conditions, WPI fibrils remained adsorbed on the glass

substrate even after three successive washing steps, as already demonstrated earlier in 2.2.1. with PG. Moreover, fibrils were still present even in presence of TAs. When added before WPI fibril formation, TAs did not affect the formation of fibrils and when added after, they did not degrade the WPI fibril already formed.

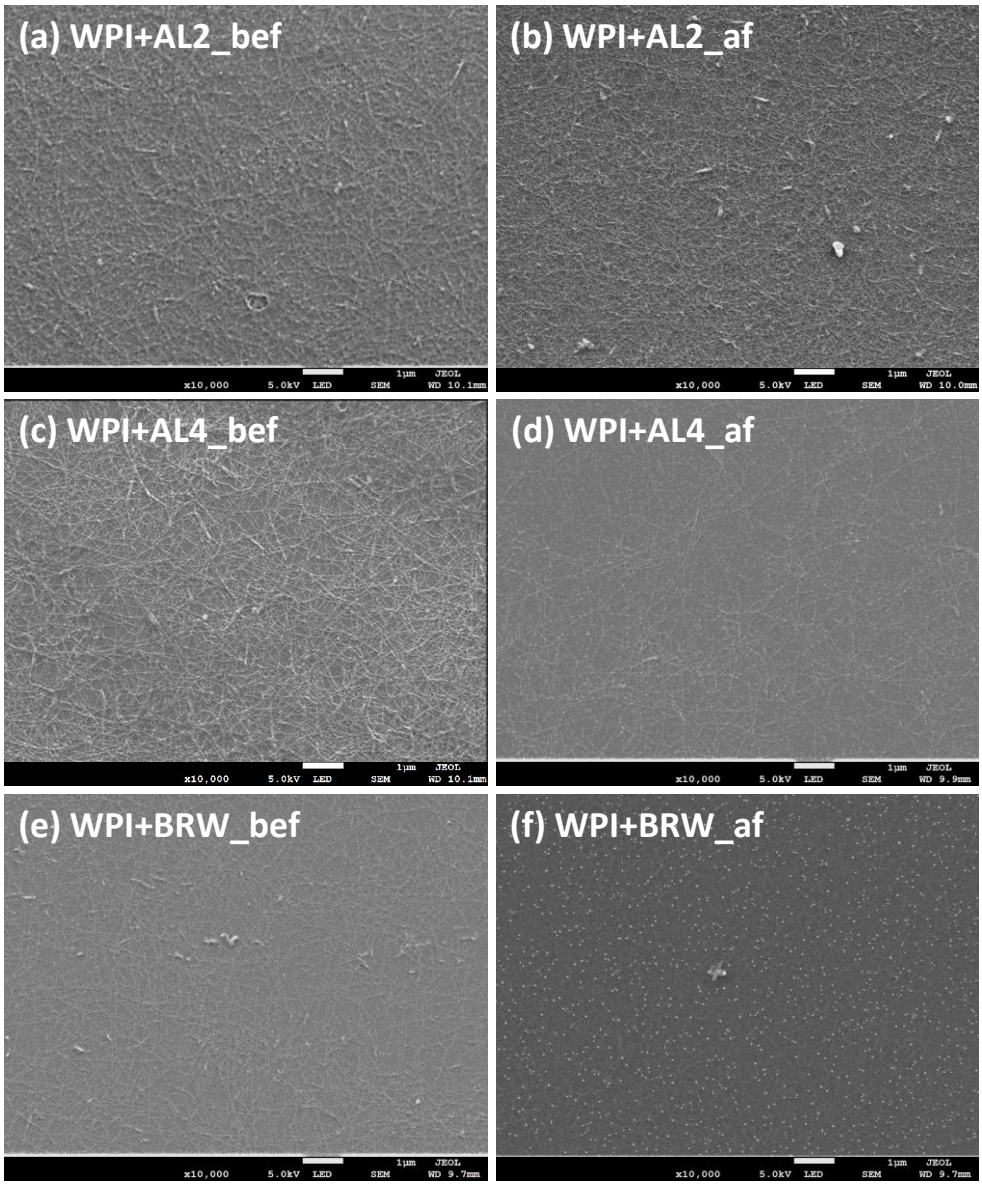

Figure 5.14: SEM images of WPI coatings with different tannic acids added before (first column - a, c, e) or after (second column - b, d, f) fibril formation: ALSOK2 (a, b), ALSOK4 (c, d), and BREWTAN F (e, f). Scale bar: 1 µm.

5.3.3.2. Cell tests

Cell tests were performed on WPI/TAs coatings on glass substrates. The cells used were hBMSCs from 4 different donors.

5.3.3.2.1. Metabolic activity

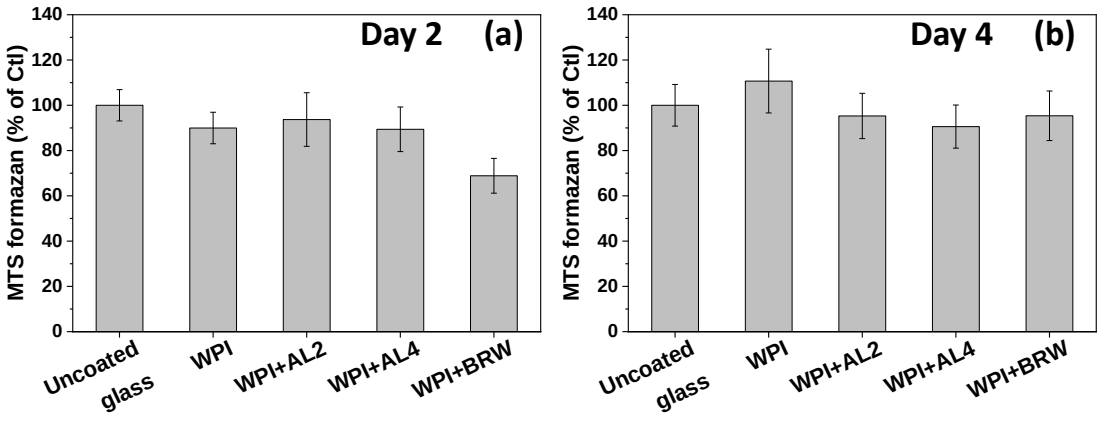

Figure 5.15: Metabolic activity of hBMSCs after (a) day 2 and (b) day 4 using MTS assay. The results are shown as mean (n = 4, two technical repetitions) and bars represent standard error of the mean. The values are percentage of Ctl (uncoated glass). No significant differences were observed.

Metabolic activity of hBMSCs was measured after 2 and 4 days of culture on the different WPI coatings. MTS assay measures the metabolic activity of cells which is an indication for cell number and cell viability [202]. Cell number increased on all samples from day 2 (Figure 5.15a) to day 4 (Figure 5.15b). The different WPI coatings have a marginal impact on cell number compared to uncoated glass and no significant differences were observed. However, after day 2, metabolic activity clearly decreased with WPI coating containing BRW meaning that BRW may impact cell viability. After day 4, the metabolic activity was similar for all the sample groups. These findings are similar to our previous studies which showed no significant difference in terms of metabolic activity for WPI coating on glass and WPI coating on Ti6Al4V containing heparin and tinzaparin [82,105]. However, it was observed a better organisation of the cytoskeleton on the glass coated with WPI fibrils [82].

5.3.3.2.2. Enzyme activity of TNAP and calcium deposition

The activity of tissue non-specific alkaline phosphatase (TNAP) enzyme was analysed after 11 days of culture on the different sample groups (Figure 5.16a). TNAP enzyme is used as an early marker of osteogenic differentiation which can indicate the potential of hBMSC to form hydroxyapatite, an essential component for bone regeneration [203]. Indeed, TNAP can hydrolyse pyrophosphate which then releases phosphate ions necessary for hydroxyapatite formation. TNAP activity is a prerequisite for bone mineralisation. A high TNAP activity is ideal since it will increase the bone mineralisation and improve the implant fixation into the body. A significant increase of TNAP activity was observed with WPI coating compared to uncoated glass as previously shown in other studies [82,105]. TNAP activity also slightly increased for coatings containing AL2, AL4, and BRW but no significant difference was noticed. Despite no clear TNAP increase for WPI/TAs coatings, TNAP activity did not decrease, meaning that hBMSC were not negatively impacted by the presence of the coatings.

TNAP activity is required for calcium phosphate deposition around the cells as previously shown [88]. Therefore, the study of the calcium phosphate accumulation should be directly linked to the TNAP activity. Calcium deposition was studied after day 22, as shown in Figure 5.16b. Calcium accumulation slightly increased in presence of all the coatings. However, no significant difference was observed.

Finally, the high statistical error observed in the different tests may be due to the high donor variance as cells were obtained from different donors. To overcome this issue, more data should be obtained from a larger number of donors.

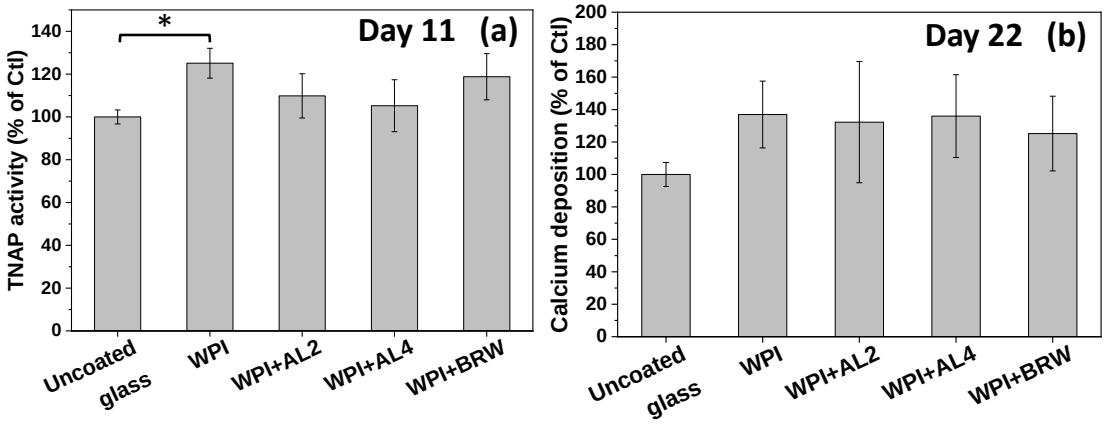

*Figure 5.16: (a) Enzyme activity of tissue non-specific alkaline phosphatase (TNAP) of hBMSC at day 11. (b) Calcium (phosphate) accumulation around hBMSC at day 22. The results are shown as mean (n = 4, two technical repetitions) and bars represent standard error of the mean. The values are percentage of Ctl (uncoated glass). Significant differences are indicated with * (p<0.05).*

5.4. Conclusions

WPI fibrils have been successfully produced and used to coat different substrates including glass and Ti6Al4V alloy discs. WPI fibrils withstood autoclave sterilisation which is an advantage as it is a clinically accepted method. WPI fibrillar coatings were also enriched with biomolecules such as PG and TAs, which do not affect the fibrils.

For WPI/PG coatings, SEM images clearly showed the presence of BM-MSCs attached to the coatings. Moreover, metabolic activity of unstimulated and biofilm-stimulated BM-MSCs was similar after 48h for all sample groups which suggest that the WPI/PG coatings do not have a negative impact on cells. These tests also demonstrated a significant decrease in metabolic activity when cells have been stimulated with biofilm likely due to the release of factors from the biofilm which may impact cell function. The expression of *RUNX* and *COL1A1* genes (early key markers of bone formation) increased in presence of PG, especially with the highest concentration (0.5%) which had been added after WPI autoclaving. The expression of genes relative to matrix mineralisation (*ALP*, *OP*, and *BGLAP*) was also significantly increased in the presence of the high concentration of PG. Hence,

a high PG concentration may promote early and late bone formation. Finally, the pro-inflammatory response, represented by the genes *IL1a*, *IL1b*, and *IL8,* was significantly reduced for the high concentration of PG which proves the anti-inflammatory properties of PG as previously shown [98].

Regarding WPI/TAs coatings, the metabolic activity of cells in contact with the coatings did not increase or decrease. Therefore, the coatings do not have a negative impact on cell viability. TNAP activity and calcium deposition slightly increased in presence of the coatings. However, a high statistical error was observed due to the high donor variance. Therefore, the number of cells and samples to be tested should be increased to overcome this issue.

To conclude, PG-enriched WPI fibrillar coatings constitute an inexpensive promising strategy to coat implants for bone repair as they may improve bone formation and mineralisation as well as reducing inflammatory response. WPI/TAs coatings may be another strategy to use, but further work needs to be performed to clearly identify the effect of the coatings on cells.

Chapter 6. General conclusion

The objective of this research was to develop coatings rich in primary amines by using two different strategies, namely plasma polymerisation and protein fibrils made from whey protein.

In Chapter 4, which concerned the plasma polymerisation technique, it was demonstrated that the retention of primary amines could be controlled by using specific plasma conditions (pressure and power). Allylamine plasma polymer coatings were produced and deposited onto silicon wafers by using two plasma regimes which are the α regime (2 Pa and 30 W), and the γ regime (20 Pa and 5.5 W). It was shown by XPS that the atomic composition of both coatings was similar in terms of carbon and nitrogen. The quantification of primary amines was performed by chemical derivatisation using TFBA. Despite a similar nitrogen composition, the concentration of primary amines was estimated to be doubled for the coatings made using the γ regime compared to the α regime. Moreover, same test was performed on allylamine samples made at the UoLiv for comparison as the reactors were not the same. The density of primary amine groups was higher on the samples made in the γ regime compared to the α regime. The analysis of the plasma phase made by the UoLiv clearly demonstrated that the use of high pressure and low power leads to less fragmentation of the allylamine molecule. Therefore, the use of a combination of high pressure and low power (γ regime) during the plasma deposition process may result in better retention of primary amines.

In Chapter 5, whey protein fibrillar coatings were successfully produced on glass and Ti6Al4V alloys. These coatings withstood autoclave sterilisation which is an important advantage since this sterilisation method is clinically accepted and

widely used in hospitals. Moreover, additional biomolecules were added such as PG and TAs. The addition of these biomolecules did not impact the fibrillar structure.

WPI/PG coatings seemed to positively influence cell behaviour. Indeed, SEM images clearly showed the presence of BM-MSCs attached to the coatings. Moreover, metabolic activity of unstimulated and biofilm-stimulated BM-MSCs was similar after 48h for all sample groups which suggest that the WPI/PG coatings do not have a negative impact on cells. Finally, the expression of genes related to bone matrix formation and mineralisation was significantly increased in the presence of PG, especially with the highest concentration (0.5%) which has been added after autoclaving of the coating. The expression of genes related to pro-inflammatory response was significantly reduced for the high concentration of PG added after autoclave sterilisation. Antibacterial tests such as susceptibility tests and bacterial attachment studies were performed. Susceptibility tests were not successful, but the attachment of bacteria was different depending on the sample group.

Regarding WPI/TAs coatings, the metabolic activity of cells was not impacted by the coatings which shows that they do not have a negative impact on cell viability. TNAP activity and calcium deposition slightly increased in the presence of the coatings, but a high statistical error was observed due to the high donor variance.

As a general conclusion, coatings rich in primary amines were successfully produced with two different strategies. One with plasma technology which is a technique that can be easily scalable to coat homogeneously a high variety of biomaterial geometries. Protein coating with whey protein fibrils constitutes a novel and promising method to coat biomaterials to improve cell behaviour such as for bone implant applications. Further work needs to be performed as it will be described in Chapter 7.

Chapter 7. Further work

Regarding plasma polymerisation to obtain coatings rich in primary amines, testing of the stability of the coatings needs to be performed in order to do biological tests. This could be performed at physiological pH in a cell culture medium. Cell tests may be further performed to check the differences in terms of cell behaviour on allylamine plasma polymer coatings made in the γ regime compared to the α regime. Further molecules could be linked to these chemical functionalities to endow new properties to the coating such as antimicrobial properties which would require antibacterial assays. A bacterial attachment study could also be performed to see if a difference can be observed between the coatings made at the different plasma regimes.

For whey protein fibrillar coatings, the adsorption of fibrils may be improved by activation of the surface by air or oxygen plasma before fibril adsorption. This would also help to increase the incorporation of molecules inside the fibrillar network. Moreover, further cell tests may be performed to avoid the problem of high donor variance. A complete microbiological study is also necessary to be conducted, for example by studying alive/dead bacteria on the coatings.

Chapter 8. Bibliography

1. Health care-associated infections - FACT SHEET Available online: https://www.who.int/gpsc/country_work/gpsc_ccisc_fact_sheet_en.pdf (accessed on Feb 14, 2020).

2. O' Neill, J. *Antimicrobial Resistance : Tackling a Crisis for the Health and Wealth of Nations*; 2014;

3. Monegro, A.F.; Regunath, H. Hospital Acquired Infections. *StatPearls [Internet]* **2020**.

4. ECDC *Annual epidemiological report on communicable diseases in Europe 2008. Report on the state of communicable diseases in the EU and EEA/EFTA countries*; 2008;

5. Badia, J.M.; Casey, A.L.; Petrosillo, N.; Hudson, P.M.; Mitchell, S.A.; Crosby, C. Impact of surgical site infection on healthcare costs and patient outcomes: a systematic review in six European countries. *J. Hosp. Infect.* **2017**, *96*, 1–15, doi:10.1016/j.jhin.2017.03.004.

6. Wertheimer, M.R.; St-Georges-Robillard, A.; Lerouge, S.; Mwale, F.; Elkin, B.; Oehr, C.; Wirges, W.; Gerhard, R. Fabrication and Characterization of Organic Thin Films for Applications in Tissue Engineering: Emphasis on Cell-Surface Interactions. *MRS Online Proc. Libr. 2012 14691* **2012**, *1469*, 43–48, doi:10.1557/OPL.2012.929.

7. Liu, X.; Feng, Q.; Bachhuka, A.; Vasilev, K. Surface Modification by Allylamine Plasma Polymerization Promotes Osteogenic Differentiation of Human Adipose-Derived Stem Cells. *ACS Appl. Mater. Interfaces* **2014**, *6*, 9733–9741, doi:10.1021/am502170s.

8. Siow, K.S.; Britcher, L.; Kumar, S.; Griesser, H.J. Plasma methods for the generation of chemically reactive surfaces for biomolecule immobilization and cell colonization - A review. *Plasma Process. Polym.* **2006**, *3*, 392–418, doi:10.1002/ppap.200600021.

9. Meyer-Plath, A.A.; Schröder, K.; Finke, B.; Ohl, A. Current trends in biomaterial surface functionalization - Nitrogen-containing plasma assisted processes with enhanced selectivity. *Vacuum* **2003**, *71*, 391–406, doi:10.1016/S0042-207X(02)00766-2.

10. Bílek, F.; Křížová, T.; Lehocký, M. Preparation of active antibacterial LDPE surface through multistep physicochemical approach: I. Allylamine grafting, attachment of antibacterial agent and antibacterial activity assessment. *Colloids Surfaces B Biointerfaces* **2011**, *88*, 440–447, doi:10.1016/j.colsurfb.2011.07.027.

11. Reis, R.; Dumée, L.F.; He, L.; She, F.; Orbell, J.D.; Winther-Jensen, B.; Duke, M.C. Amine Enrichment of Thin-Film Composite Membranes via Low Pressure Plasma Polymerization for Antimicrobial Adhesion. *ACS Appl. Mater. Interfaces* **2015**, *7*, 14644–14653, doi:10.1021/acsami.5b01603.

12. Vasilev, K.; Sah, V.R.; Goreham, R. V; Ndi, C.; Short, R.D.; Griesser, H.J. Antibacterial surfaces by adsorptive binding of polyvinyl-sulphonate-stabilized silver nanoparticles. *Nanotechnology* **2010**, *21*, 215102, doi:10.1088/0957-4484/21/21/215102.

13. Williams, D.F. Definitions in biomaterials: proceedings of a consensus conference of the European Society for Biomaterials.; Chester, England, 1987; Vol. 4, pp. 3–5.

14. Ratner, B.D.; Hoffman, A.S.; Schoen, F.J.; Lemons, J.E. *Biomaterials Science: An Introduction to Materials: Third Edition*; Elsevier Inc., 2013; ISBN 9780123746269.

15. Anderson, J.M.; Rodriguez, A.; Chang, D.T. Foreign body reaction to biomaterials. *Semin. Immunol.* 2008, *20*, 86–100.

16. Wei, Q.; Becherer, T.; Angioletti-Uberti, S.; Dzubiella, J.; Wischke, C.; Neffe, A.T.; Lendlein, A.; Ballauff, M.; Haag, R. Protein interactions with polymer coatings and biomaterials. *Angew. Chem. Int. Ed. Engl.* **2014**, *53*, 8004–8031, doi:10.1002/ANIE.201400546.

17. Felgueiras, H.P.; Antunes, J.C.; Martins, M.C.L.; Barbosa, M.A. Fundamentals of protein and cell interactions in biomaterials. *Pept. Proteins as Biomater. Tissue Regen. Repair* **2018**, 1–27, doi:10.1016/B978-0-08-100803-4.00001-2.

18. Lu, X.; Wu, Z.; Xu, K.; Wang, X.; Wang, S.; Qiu, H.; Li, X.; Chen, J. Multifunctional Coatings of Titanium Implants Toward Promoting Osseointegration and Preventing Infection: Recent Developments. *Front. Bioeng. Biotechnol.* **2021**, *9*, 1093, doi:10.3389/FBIOE.2021.783816/BIBTEX.

19. Raphel, J.; Holodniy, M.; Goodman, S.B.; Heilshorn, S.C. Multifunctional Coatings to Simultaneously Promote Osseointegration and Prevent Infection of Orthopaedic Implants. *Biomaterials* **2016**, *84*, 301, doi:10.1016/J.BIOMATERIALS.2016.01.016.

20. Keselowsky, B.G.; Collard, D.M.; García, A.J. Integrin binding specificity regulates biomaterial surface chemistry effects on cell differentiation. *Proc. Natl. Acad. Sci. U. S. A.* **2005**, *102*, 5953–5957, doi:10.1073/PNAS.0407356102/ASSET/EC917059-31B7-4BBB-8486-CACD11FB0A56/ASSETS/GRAPHIC/ZPQ0180581150004.JPEG.

21. Garrett, T.R.; Bhakoo, M.; Zhang, Z. Bacterial adhesion and biofilms on surfaces. *Prog. Nat. Sci.* **2008**, *18*, 1049–1056, doi:10.1016/j.pnsc.2008.04.001.

22. Filloux, A.; Vallet, I. Biofilm : mise en place et organisation d'une communauté bactérienne. *médecine/sciences* **2003**, *19*, 77–83, doi:10.1051/medsci/200319177.

23. Jamal, M.; Ahmad, W.; Andleeb, S.; Jalil, F.; Imran, M.; Nawaz, M.A.; Hussain, T.; Ali, M.; Rafiq, M.; Kamil, M.A. Bacterial biofilm and associated infections.

J. Chin. Med. Assoc. **2018**, *81*, 7–11, doi:10.1016/J.JCMA.2017.07.012.

24. Khatoon, Z.; McTiernan, C.D.; Suuronen, E.J.; Mah, T.-F.; Alarcon, E.I. Bacterial biofilm formation on implantable devices and approaches to its treatment and prevention. *Heliyon* **2018**, *4*, 1067, doi:10.1016/J.HELIYON.2018.E01067.

25. Habash, M.; Reid, G. Microbial Biofilms: Their Development and Significance for Medical Device-Related Infections. *J. Clin. Pharmacol.* **1999**, *39*, 887–898, doi:10.1177/00912709922008506.

26. Donlan, R.M. Biofilms: microbial life on surfaces. *Emerg. Infect. Dis.* **2002**, *8*, 1–88, doi:10.3201/eid0809.020063.

27. Huang, D.N.; Wang, J.; Ren, K.F.; Ji, J. Functionalized biomaterials to combat biofilms. *Biomater. Sci.* **2020**, *8*, 4052–4066, doi:10.1039/D0BM00526F.

28. Aziz, G.; De Geyter, N.; Morent, R. Incorporation of Primary Amines via Plasma Technology on Biomaterials. In *Advances in Bioengineering*; InTech, 2015.

29. Chu, P.K.; Chen, J.Y.; Wang, L.P.; Huang, N. Plasma-surface modification of biomaterials. *Mater. Sci. Eng. R Reports* **2002**, *36*, 143–206, doi:10.1016/S0927-796X(02)00004-9.

30. Lieberman, M.A.; Lichtenberg, A.J. *Principles of Plasma Discharges and Materials Processing*; John Wiley & Sons, Inc.: Hoboken, NJ, USA, 2005; ISBN 978-0-471-72425-4 978-0-471-72001-0.

31. Friedrich, J. Mechanisms of Plasma Polymerization – Reviewed from a Chemical Point of View. *Plasma Process. Polym.* **2011**, *8*, 783–802, doi:10.1002/PPAP.201100038.

32. Szili, E.; Short, R.; Steele, D.; Bradley, J. Surface modification of biomaterials by plasma polymerization. *Surf. Modif. Biomater. Methods Anal. Appl.* **2011**, 3–39, doi:10.1533/9780857090768.1.3.

33. Naderi, J.; Giles, C.; Saboohi, S.; Griesser, H.J.; Coad, B.R. Combatting fungal biofilm formation by diffusive release of fluconazole from heptylamine plasma polymer coating. *Biointerphases* **2020**, *15*, 061012, doi:10.1116/6.0000511.

34. Michelmore, A.; Steele, D.A.; Whittle, J.D.; Bradley, J.W.; Short, R.D. Nanoscale deposition of chemically functionalised films via plasma polymerisation. **2013**, *3*, 13540, doi:10.1039/c3ra41563e.

35. Gengenbach, T.R.; Griesser, H.J. Aging of 1,3-Diaminopropane Plasma-Deposited Polymer Films: Mechanisms and Reaction Pathways. *J Polym Sci A Polym Chem* **1999**, *37*, 2191–2206, doi:10.1002/(SICI)1099-0518(19990701)37:13.

36. Ryssy, J.; Prioste-Amaral, E.; Assuncao, D.F.N.; Rogers, N.; Kirby, G.T.S.; Smith, L.E.; Michelmore, A. Chemical and physical processes in the retention of functional groups in plasma polymers studied by plasma phase mass spectroscopy. *Phys. Chem. Chem. Phys.* **2016**, *18*, 4496–4504, doi:10.1039/C5CP05850C.

37. Shen, M.; Bell, A.T. A Review of Recent Advances in Plasma Polymerization. *ACS Symp. Ser.* **1979**, *108*, 1–33, doi:10.1021/BK-1979-0108.CH001.

38. Asad, A.; Sameoto, D.; Sadrzadeh, M. Overview of membrane technology. *Nanocomposite Membr. Water Gas Sep.* **2020**, 1–28, doi:10.1016/B978-0-12-816710-6.00001-8.

39. Jin Ho Lee; Jong Woo Park; Hai Bang Lee Cell adhesion and growth on polymer surfaces with hydroxyl groups prepared by water vapour plasma treatment. *Biomaterials* **1991**, *12*, 443–448, doi:10.1016/0142-9612(91)90140-6.

40. Rossini, P.; Colpo, P.; Ceccone, G.; Jandt, K.D.; Rossi, F. Surfaces engineering of polymeric films for biomedical applications. *Mater. Sci. Eng. C* **2003**, *23*, 353–358, doi:10.1016/S0928-4931(02)00286-2.

41. Saboohi, S.; Jasieniak, M.; Coad, B.R.; Griesser, H.J.; Short, R.D.; Michelmore, A. Comparison of Plasma Polymerization under Collisional and Collision-Less Pressure Regimes. *J. Phys. Chem. B* **2015**, *119*, 15359–15369, doi:10.1021/acs.jpcb.5b07309.

42. Leich, M.A.; Mackie, N.M.; Williams, K.L.; Fisher, E.R. Pulsed plasma polymerization of benzaldehyde for retention of the aldehyde functional group. *Macromolecules* **1998**, *31*, 7618–7626, doi:10.1021/ma980332c.

43. Denis, L.; Cossement, D.; Godfroid, T.; Renaux, F.; Bittencourt, C.; Snyders, R.; Hecq, M. Synthesis of allylamine plasma polymer films: Correlation between plasma diagnostic and film characteristics. *Plasma Process. Polym.* **2009**, *6*, 199–208, doi:10.1002/ppap.200800137.

44. Haddow, D.B.; France, R.M.; Short, R.D.; Bradley, J.W.; Barton, D. Mass spectrometric and ion energy study of the continuous wave plasma polymerization of acrylic acid. *Langmuir* **2000**, *16*, 5654–5660, doi:10.1021/la991537x.

45. Choukourov, A.; Biederman, H.; Slavinska, D.; Hanley, L.; Grinevich, A.; Boldyryeva, H.; Mackova, A. Mechanistic studies of plasma polymerization of allylamine. *J. Phys. Chem. B* **2005**, *109*, 23086–23095, doi:10.1021/jp0535691.

46. Voronin, S.A.; Zelzer, M.; Fotea, C.; Alexander, M.R.; Bradley, J.W. Pulsed and continuous wave acrylic acid radio frequency plasma deposits: Plasma and surface chemistry. *J. Phys. Chem. B* **2007**, *111*, 3419–3429, doi:10.1021/jp068488z.

47. Carletto, A.; Badyal, J.P.S. Ultra-high selectivity pulsed plasmachemical deposition reaction pathways. *Phys. Chem. Chem. Phys.* **2019**, *21*, 16468–16476, doi:10.1039/c9cp02192b.

48. Yasuda, H. *Plasma Polymerization*; Elsevier, 1985;

49. Michelmore, A.; Steele, D.A.; Robinson, D.E.; Whittle, J.D.; Short, R.D. The link

between mechanisms of deposition and the physico-chemical properties of plasma polymer films. *Soft Matter* **2013**, *9*, 6167–6175, doi:10.1039/C3SM51039E.

50. Daunton, C.; Smith, L.E.; Whittle, J.D.; Short, R.D.; Steele, D.A.; Michelmore, A. Plasma parameter aspects in the fabrication of stable amine functionalized plasma polymer films. *Plasma Process. Polym.* **2015**, *12*, 817–826, doi:10.1002/ppap.201400215.

51. Saboohi, S.; Coad, B.R.; Griesser, H.J.; Michelmore, A.; Short, R.D. Synthesis of highly functionalised plasma polymer films from protonated precursor ions: Via the plasma α-γ Transition. *Phys. Chem. Chem. Phys.* **2017**, *19*, 5637–5646, doi:10.1039/c6cp08630f.

52. Alexander, M.R.; Duc, T.M. A study of the interaction of acrylic acid/1,7-octadiene plasma deposits with water and other solvents. *Polymer (Guildf).* **1999**, *40*, 5479–5488, doi:10.1016/S0032-3861(98)00784-8.

53. Whittle, J.D.; Short, R.D.; Steele, D.A.; Bradley, J.W.; Bryant, P.M.; Jan, F.; Biederman, H.; Serov, A.A.; Choukurov, A.; Hook, A.L.; et al. Variability in plasma polymerization processes - An international round-robin study. *Plasma Process. Polym.* **2013**, *10*, 767–778, doi:10.1002/PPAP.201300029.

54. Saboohi, S.; Coad, B.R.; Short, R.D.; Michelmore, A.; Griesser, H.J. Rational approaches for optimizing chemical functionality of plasma polymers: A case study with ethyl trimethylacetate. *Plasma Process. Polym.* **2021**, *18*, 2000195, doi:10.1002/ppap.202000195.

55. Barnes, M.J.; Robson, A.J.; Naderi, J.; Short, R.D.; Bradley, J.W. Plasma polymerization of (2,2,6,6-tetramethylpiperidin-1-yl)oxyl in a collisional, capacitively coupled radio frequency discharge. *Biointerphases* **2020**, *15*, 061007, doi:10.1116/6.0000662.

56. Michl, T.D.; Tran, D.T.T.; Böttle, K.; Kuckling, H.F.; Zhalgasbaikyzy, A.; Ivanovská, B.; Cavallaro, A.A.; Toledo, M.A.A.; Sherman, P.J.; Al-Bataineh, S.A.; et al. To be a radical or not to be one? The fate of the stable nitroxide radical

TEMPO [(2,2,6,6-Tetramethylpiperidin-1-yl)oxyl] undergoing plasma polymerization into thin-film coatings. *Biointerphases* **2020**, *15*, 031015, doi:10.1116/6.0000259.

57. Thierry, B.; Jasieniak, M.; De Smet, L.C.P.M.; Vasilev, K.; Griesser, H.J. Reactive epoxy-functionalized thin films by a pulsed plasma polymerization process. *Langmuir* **2008**, *24*, 10187–10195, doi:10.1021/la801140u.

58. Saboohi, S.; Coad, B.R.; Michelmore, A.; Short, R.D.; Griesser, H.J. Hyperthermal Intact Molecular Ions Play Key Role in Retention of ATRP Surface Initiation Capability of Plasma Polymer Films from Ethyl α-Bromoisobutyrate. *ACS Appl. Mater. Interfaces* **2016**, *8*, 16493–16502, doi:10.1021/acsami.6b04477.

59. Song, H.; Jung, S.C.; Kim, B.H. Focal adhesion of osteoblastic cells on titanium surface with amine functionalities formed by plasma polymerization. *Jpn. J. Appl. Phys.* **2012**, *51*, 08HE01, doi:10.1143/JJAP.51.08HE01.

60. Ren, T.B.; Weigel, T.; Groth, T.; Lendlein, A. Microwave plasma surface modification of silicone elastomer with allylamine for improvement of biocompatibility. *J. Biomed. Mater. Res. Part A* **2008**, *86A*, 209–219, doi:10.1002/jbm.a.31508.

61. Aziz, G.; De Geyter, N.; Declercq, H.; Cornelissen, R.; Morent, R. Incorporation of amine moieties onto ultra-high molecular weight polyethylene (UHMWPE) surface via plasma and UV polymerization of allylamine. *Surf. Coatings Technol.* **2015**, *271*, 39–47, doi:10.1016/j.surfcoat.2015.01.027.

62. Aziz, G.; Thukkaram, M.; De Geyter, N.; Morent, R. Plasma parameters effects on the properties, aging and stability behaviors of allylamine plasma coated ultra-high molecular weight polyethylene (UHMWPE) films. *Appl. Surf. Sci.* **2017**, *409*, 381–395, doi:10.1016/j.apsusc.2017.03.027.

63. Vasilev, K.; Michelmore, A.; Martinek, P.; Chan, J.; Sah, V.; Griesser, H.J.; Short, R.D. Early Stages of Growth of Plasma Polymer Coatings Deposited from Nitrogen- and Oxygen-Containing Monomers. *Plasma Process. Polym.* **2010**,

7, 824–835, doi:10.1002/ppap.201000030.

64. Zhao, J.H.; Michalski, W.P.; Williams, C.; Li, L.; Xu, H.S.; Lamb, P.R.; Jones, S.; Zhou, Y.M.; Dai, X.J. Controlling cell growth on titanium by surface functionalization of heptylamine using a novel combined plasma polymerization mode. *J. Biomed. Mater. Res. - Part A* **2011**, *97 A*, 127–134, doi:10.1002/jbm.a.33035.

65. Finke, B.; Hempel, F.; Testrich, H.; Artemenko, A.; Rebl, H.; Kylián, O.; Meichsner, J.; Biederman, H.; Nebe, B.; Weltmann, K.D.; et al. Plasma processes for cell-adhesive titanium surfaces based on nitrogen-containing coatings. *Surf. Coatings Technol.* **2011**, *205*, doi:10.1016/j.surfcoat.2010.12.044.

66. Testrich, H.; Rebl, H.; Finke, B.; Hempel, F.; Nebe, B.; Meichsner, J. Aging effects of plasma polymerized ethylenediamine (PPEDA) thin films on cell-adhesive implant coatings. *Mater. Sci. Eng. C* **2013**, *33*, 3875–3880, doi:10.1016/j.msec.2013.05.024.

67. Gigout, A.; Ruiz, J.-C.; Wertheimer, M.R.; Jolicoeur, M.; Lerouge, S. Nitrogen-Rich Plasma-Polymerized Coatings on PET and PTFE Surfaces Improve Endothelial Cell Attachment and Resistance to Shear Flow. *Macromol. Biosci.* **2011**, *11*, 1110–1119, doi:10.1002/mabi.201000512.

68. Truica-Marasescu, F.; Wertheimer, M.R. Nitrogen-rich plasma-polymer films for biomedical applications. *Plasma Process. Polym.* **2008**, *5*, 44–57, doi:10.1002/ppap.200700077.

69. Ruiz, J.C.; St-Georges-Robillard, A.; Thérésy, C.; Lerouge, S.; Wertheimer, M.R. Fabrication and characterisation of amine-rich organic thin films: Focus on stability. *Plasma Process. Polym.* **2010**, *7*, 737–753, doi:10.1002/ppap.201000042.

70. Babaei, S.; Girard-Lauriault, P.L. Tuning the Surface Properties of Oxygen-Rich and Nitrogen-Rich Plasma Polymers: Functional Groups and Surface Charge. *Plasma Chem. Plasma Process.* **2016**, *36*, 651–666,

doi:10.1007/s11090-015-9682-1.

71. Nemcakova, I.; Blahova, L.; Rysanek, P.; Blanquer, A.; Bacakova, L.; Zajíčková, L. Behaviour of Vascular Smooth Muscle Cells on Amine Plasma-Coated Materials with Various Chemical Structures and Morphologies. *Int. J. Mol. Sci. 2020, Vol. 21, Page 9467* **2020**, *21*, 9467, doi:10.3390/IJMS21249467.

72. Charbonneau, C.; Ruiz, J.-C.; Lequoy, P.; Hébert, M.-J.; Crescenzo, G. De; Wertheimer, M.R.; Lerouge, S. Chondroitin Sulfate and Epidermal Growth Factor Immobilization after Plasma Polymerization: A Versatile Anti-Apoptotic Coating to Promote Healing Around Stent Grafts. *Macromol. Biosci.* **2012**, *12*, 812–821, doi:10.1002/MABI.201100447.

73. Abbas, A.; Vercaigne-Marko, D.; Supiot, P.; Bocquet, B.; Vivien, C.; Guillochon, D. Covalent attachment of trypsin on plasma polymerized allylamine. *Colloids Surfaces B Biointerfaces* **2009**, *73*, 315–324, doi:10.1016/j.colsurfb.2009.06.007.

74. Gancarz, I.; Bryjak, J.; Poźniak, G.; Tylus, W. Plasma modified polymers as a support for enzyme immobilization II. Amines plasma. *Eur. Polym. J.* **2003**, *39*, 2217–2224, doi:10.1016/S0014-3057(03)00160-5.

75. Yang, J.; Bei, J.; Wang, S. Enhanced cell affinity of poly (D,L-lactide) by combining plasma treatment with collagen anchorage. *Biomaterials* **2002**, *23*, 2607–2614, doi:10.1016/S0142-9612(01)00400-8.

76. Simovic, S.; Losic, D.; Vasilev, K. Controlled drug release from porous materials by plasma polymer deposition. *Chem. Commun.* **2010**, *46*, 1317–1319, doi:10.1039/b919840g.

77. Girard-Lauriault, P.-L.; Truica-Marasescu, F.; Petit, A.; Wang, H.T.; Desjardins, P.; Antoniou, J.; Mwale, F.; Wertheimer, M.R. Adhesion of Human U937 Monocytes to Nitrogen-Rich Organic Thin Films: Novel Insights into the Mechanism of Cellular Adhesion. *Macromol. Biosci.* **2009**, *9*, 911–921, doi:10.1002/MABI.200800359.

78. Girard-Lauriault, P.-L.; Mwale, F.; Iordanova, M.; Demers, C.; Desjardins, P.; Wertheimer, M.R. Atmospheric Pressure Deposition of Micropatterned Nitrogen-Rich Plasma-Polymer Films for Tissue Engineering. *Plasma Process. Polym.* **2005**, *2*, 263–270.

79. Bílek, F.; Sulovská, K.; Lehocký, M.; Sáha, P.; Humpolíček, P.; Mozetič, M.; Junkar, I. Preparation of active antibacterial LDPE surface through multistep physicochemical approach II: Graft type effect on antibacterial properties. *Colloids Surfaces B Biointerfaces* **2013**, *102*, 842–848, doi:10.1016/j.colsurfb.2012.08.026.

80. Ghomi, E.R.; Nourbakhsh, N.; Kenari, M.A.; Zare, M.; Ramakrishna, S. Collagen-based biomaterials for biomedical applications. *J. Biomed. Mater. Res. Part B Appl. Biomater.* **2021**, doi:10.1002/JBM.B.34881.

81. Hay, E.. *Cell Biology of Extracellular Matrix*; Springer US, 1981; ISBN 978-1-4612-8226-6.

82. Rabe, R.; Hempel, U.; Martocq, L.; Keppler, J.K.; Aveyard, J.; Douglas, T.E.L. Dairy-Inspired Coatings for Bone Implants from Whey Protein Isolate-Derived Self-Assembled Fibrils. *Int. J. Mol. Sci.* **2020**, *21*, 5544, doi:10.3390/ijms21155544.

83. Vandrovcova, M.; Douglas, T.E.L.; Heinemann, S.; Scharnweber, D.; Dubruel, P.; Bacakova, L. Collagen-lactoferrin fibrillar coatings enhance osteoblast proliferation and differentiation. *J. Biomed. Mater. Res. - Part A* **2015**, *103*, 525–533, doi:10.1002/jbm.a.35199.

84. Douglas, T.; Heinemann, S.; Mietrach, C.; Hempel, U.; Bierbaum, S.; Scharnweber, D.; Worch, H. Interactions of collagen types I and II with chondroitin sulfates A-C and their effect on osteoblast adhesion. *Biomacromolecules* **2007**, *8*, 1085–1092, doi:10.1021/bm0609644.

85. Haynes, C.A.; Norde, W. Globular proteins at solid/liquid interfaces. *Colloids Surfaces B Biointerfaces* **1994**, *2*, 517–566, doi:10.1016/0927-7765(94)80066-9.

86. Norde, W. Adsorption of proteins from solution at the solid-liquid interface. *Adv. Colloid Interface Sci.* **1986**, *25*, 267–340, doi:10.1016/0001-8686(86)80012-4.

87. Hempel, U.; Preissler, C.; Vogel, S.; Möller, S.; Hintze, V.; Becher, J.; Schnabelrauch, M.; Rauner, M.; Hofbauer, L.C.; Dieter, P. Artificial extracellular matrices with oversulfated glycosaminoglycan derivatives promote the differentiation of osteoblast-precursor cells and premature osteoblasts. *Biomed Res. Int.* **2014**, *2014*, doi:10.1155/2014/938368.

88. Hempel, U.; Matthäus, C.; Preissler, C.; Möller, S.; Hintze, V.; Dieter, P. Artificial matrices with high-sulfated glycosaminoglycans and collagen are anti-inflammatory and pro-osteogenic for human mesenchymal stromal cells. *J. Cell. Biochem.* **2014**, *115*, 1561–1571, doi:10.1002/jcb.24814.

89. Knowles, T.P.J.; Oppenheim, T.W.; Buell, A.K.; Chirgadze, D.Y.; Welland, M.E. Nanostructured films from hierarchical self-assembly of amyloidogenic proteins. *Nat. Nanotechnol.* **2010**, *5*, 204–207, doi:10.1038/nnano.2010.26.

90. Reynolds, N.P.; Styan, K.E.; Easton, C.D.; Li, Y.; Waddington, L.; Lara, C.; Forsythe, J.S.; Mezzenga, R.; Hartley, P.G.; Muir, B.W. Nanotopographic surfaces with defined surface chemistries from amyloid fibril networks can control cell attachment. *Biomacromolecules* **2013**, *14*, 2305–2316, doi:10.1021/bm400430t.

91. Reynolds, N.P.; Charnley, M.; Mezzenga, R.; Hartley, P.G. Engineered lysozyme amyloid fibril networks support cellular growth and spreading. *Biomacromolecules* **2014**, *15*, 599–608, doi:10.1021/bm401646x.

92. Reynolds, N.P.; Charnley, M.; Bongiovanni, M.N.; Hartley, P.G.; Gras, S.L. Biomimetic topography and chemistry control cell attachment to amyloid fibrils. *Biomacromolecules* **2015**, *16*, 1556–1565, doi:10.1021/acs.biomac.5b00114.

93. Hindié, M.; Degat, M.C.; Gaudire, F.; Gallet, O.; Van Tassel, P.R.; Pauthe, E. Pre-osteoblasts on poly(l-lactic acid) and silicon oxide: Influence of fibronectin

and albumin adsorption. *Acta Biomater.* **2011**, *7*, 387–394, doi:10.1016/j.actbio.2010.08.001.

94. Sima, F.; Davidson, P.; Pauthe, E.; Sima, L.E.; Gallet, O.; Mihailescu, I.N.; Anselme, K. Fibronectin layers by matrix-assisted pulsed laser evaporation from saline buffer-based cryogenic targets. *Acta Biomater.* **2011**, *7*, 3780–3788, doi:10.1016/j.actbio.2011.06.016.

95. Montaño-Machado, V.; Chevallier, P.; Mantovani, D.; Pauthe, E. On the potential for fibronectin/phosphorylcholine coatings on PTFE substrates to jointly modulate endothelial cell adhesion and hemocompatibility properties. *Biomatter* **2015**, *5*, e979679, doi:10.4161/21592535.2014.979679.

96. Geißler, U.; Hempel, U.; Wolf, C.; Scharnweber, D.; Worch, H.; Wenzel, K.W. Collagen type I-coating of Ti6A14V promotes adhesion of osteoblasts. *J. Biomed. Mater. Res.* **2000**, *51*, 752–760, doi:10.1002/1097-4636(20000915)51:4<752::AID-JBM25>3.0.CO;2-7.

97. Roehlecke, C.; Witt, M.; Kasper, M.; Schulze, E.; Wolf, C.; Hofer, A.; Funk, R.H.W. Synergistic effect of titanium alloy and collagen type I on cell adhesion, proliferation and differentiation of osteoblast-like cells. *Cells Tissues Organs* **2001**, *168*, 178–187, doi:10.1159/000047833.

98. Mieszkowska, A.; Beaumont, H.; Martocq, L.; Koptyug, A.; Surmeneva, M.A.; Surmenev, R.A.; Naderi, J.; Douglas, T.E.L.; Gurzawska-Comis, K.A. Phenolic-Enriched Collagen Fibrillar Coatings on Titanium Alloy to Promote Osteogenic Differentiation and Reduce Inflammation. *Int. J. Mol. Sci.* **2020**, *21*, 6406, doi:10.3390/ijms21176406.

99. Morra, M.; Cassinelli, C.; Cascardo, G.; Cahalan, P.; Cahalan, L.; Fini, M.; Giardino, R. Surface engineering of titanium by collagen immobilization. Surface characterization and in vitro and in vivo studies. *Biomaterials* **2003**, *24*, 4639–4654, doi:10.1016/S0142-9612(03)00360-0.

100. Hsueh, Y.H.; Cheng, C.Y.; Chien, H.W.; Huang, X.H.; Huang, C.W.; Wu, C.H.;

Chen, S.T.; Ou, S.F. Synergistic effects of collagen and silver on the deposition characteristics, antibacterial ability, and cytocompatibility of a collagen/silver coating on titanium. *J. Alloys Compd.* **2020**, *830*, 154490, doi:10.1016/j.jallcom.2020.154490.

101. Douglas, T.E.L.; Vandrovcová, M.; Kročilová, N.; Keppler, J.K.; Zárubová, J.; Skirtach, A.G.; Bačáková, L. Application of whey protein isolate in bone regeneration: Effects on growth and osteogenic differentiation of bone-forming cells. *J. Dairy Sci.* **2018**, *101*, 28–36, doi:10.3168/jds.2017-13119.

102. Gupta, D.; Kocot, M.; Tryba, A.M.; Serafim, A.; Stancu, I.C.; Jaegermann, Z.; Pamuła, E.; Reilly, G.C.; Douglas, T.E.L. Novel naturally derived whey protein isolate and aragonite biocomposite hydrogels have potential for bone regeneration. *Mater. Des.* **2020**, *188*, 108408, doi:10.1016/j.matdes.2019.108408.

103. Gadang, V.P.; Hettiarachchy, N.S.; Johnson, M.G.; Owens, C. Evaluation of Antibacterial Activity of Whey Protein Isolate Coating Incorporated with Nisin, Grape Seed Extract, Malic Acid, and EDTA on a Turkey Frankfurter System. *J. Food Sci.* **2008**, *73*, M389–M394.

104. Seydim, A.C.; Sarikus, G. Antimicrobial activity of whey protein based edible films incorporated with oregano, rosemary and garlic essential oils. *Food Res. Int.* **2006**, *39*, 639–644.

105. Facchetti, D.; Hempel, U.; Martocq, L.; Smith, A.M.; Koptyug, A.; Surmenev, R.A.; Surmeneva, M.A.; Douglas, T.E.L. Heparin enriched-wpi coating on ti6al4v increases hydrophilicity and improves proliferation and differentiation of human bone marrow stromal cells. *Int. J. Mol. Sci.* **2022**, *23*, 139, doi:10.3390/ijms23010139.

106. Zhou, W.; Jia, Z.; Xiong, P.; Yan, J.; Li, Y.; Li, M.; Cheng, Y.; Zheng, Y. Bioinspired and Biomimetic AgNPs/Gentamicin-Embedded Silk Fibroin Coatings for Robust Antibacterial and Osteogenetic Applications. *ACS Appl. Mater. Interfaces* **2017**, *9*, 25830–25846, doi:10.1021/acsami.7b06757.

107. Wang, C.; Wang, S.; Yang, Y.; Jiang, Z.; Deng, Y.; Song, S.; Yang, W.; Chen, Z.G. Bioinspired, biocompatible and peptide-decorated silk fibroin coatings for enhanced osteogenesis of bioinert implant. *J. Biomater. Sci. Polym. Ed.* **2018**, *29*, 1595–1611, doi:10.1080/09205063.2018.1477316.

108. Wang, S.D.; Ma, Q.; Wang, K.; Chen, H.W. Improving Antibacterial Activity and Biocompatibility of Bioinspired Electrospinning Silk Fibroin Nanofibers Modified by Graphene Oxide. *ACS Omega* **2017**, *3*, 406–413, doi:10.1021/acsomega.7b01210.

109. Cestari, M.; Muller, V.; Rodrigues, J.H.D.S.; Nakamura, C. V.; Rubira, A.F.; Muniz, E.C. Preparing silk fibroin nanofibers through electrospinning: Further heparin immobilization toward hemocompatibility improvement. *Biomacromolecules* **2014**, *15*, 1762–1767, doi:10.1021/bm500132g.

110. Sottile, J.; Hocking, D.C. Fibronectin polymerization regulates the composition and stability of extracellular matrix fibrils and cell-matrix adhesions. *Mol. Biol. Cell* **2002**, *13*, 3546–3559, doi:10.1091/mbc.E02-01-0048.

111. Ward, M.; Marcey, D. Fibronectin, an Extracellular Adhesion Molecule Available online: http://biology.kenyon.edu/BMB/Chime/Fibronectin/frames/fibrotxt.htm (accessed on Apr 27, 2018).

112. An, Y.H.; Friedman, R.J. Concise review of mechanisms of bacterial adhesion to biomaterial surfaces. *J. Biomed. Mater. Res.* **1998**, *43*, 338–348, doi:10.1002/(SICI)1097-4636(199823)43:3<338::AID-JBM16>3.0.CO;2-B.

113. Hay, E.. *Cell Biology of Extracellular Matrix: Second Edition*; Springer Science & Business Media, 1991; ISBN 978-0-306-43951-3.

114. Parisi, L.; Toffoli, A.; Ghezzi, B.; Mozzoni, B.; Lumetti, S.; Macaluso, G.M. A glance on the role of fibronectin in controlling cell response at biomaterial interface. *Jpn. Dent. Sci. Rev.* **2020**, *56*, 50–55, doi:10.1016/J.JDSR.2019.11.002.

115. García, A.J.; Vega, M.D.; Boettiger, D. Modulation of cell proliferation and differentiation through substrate- dependent changes in fibronectin conformation. *Mol. Biol. Cell* **1999**, *10*, 785–798, doi:10.1091/mbc.10.3.785.

116. Ricard-Blum, S. The Collagen Family. *Cold Spring Harb. Perspect. Biol.* **2011**, *3*, 1–19, doi:10.1101/CSHPERSPECT.A004978.

117. Brett, D. A review of collagen and collagen-based wound dressings. *Wounds* 2008, *20*, 347–356.

118. Khan, R.; Khan, M.H. Use of collagen as a biomaterial: An update. *J. Indian Soc. Periodontol.* **2013**, *17*, 539, doi:10.4103/0972-124X.118333.

119. Akkermans, C.; Venema, P.; van der Goot, A.J.; Gruppen, H.; Bakx, E.J.; Boom, R.M.; van der Linden, E. Peptides are building blocks of heat-induced fibrillar protein aggregates of β-lactoglobulin formed at pH 2. *Biomacromolecules* **2008**, *9*, 1474–1479, doi:10.1021/bm7014224.

120. Heyn, T.R.; Garamus, V.M.; Neumann, H.R.; Uttinger, M.J.; Guckeisen, T.; Heuer, M.; Selhuber-Unkel, C.; Peukert, W.; Keppler, J.K. Influence of the polydispersity of pH 2 and pH 3.5 beta-lactoglobulin amyloid fibril solutions on analytical methods. *Eur. Polym. J.* **2019**, *120*, doi:10.1016/j.eurpolymj.2019.08.038.

121. Keppler, J.K.; Heyn, T.R.; Meissner, P.M.; Schrader, K.; Schwarz, K. Protein oxidation during temperature-induced amyloid aggregation of beta-lactoglobulin. *Food Chem.* **2019**, *289*, 223–231, doi:10.1016/j.foodchem.2019.02.114.

122. Serfert, Y.; Lamprecht, C.; Tan, C.P.; Keppler, J.K.; Appel, E.; Rossier-Miranda, F.J.; Schroen, K.; Boom, R.M.; Gorb, S.; Selhuber-Unkel, C.; et al. Characterisation and use of β-lactoglobulin fibrils for microencapsulation of lipophilic ingredients and oxidative stability thereof. *J. Food Eng.* **2014**, *143*, 53–61, doi:10.1016/j.jfoodeng.2014.06.026.

123. Keppler, J.K.; Martin, D.; Garamus, V.M.; Berton-Carabin, C.; Nipoti, E.;

Coenye, T.; Schwarz, K. Functionality of whey proteins covalently modified by allyl isothiocyanate. Part 1 physicochemical and antibacterial properties of native and modified whey proteins at pH 2 to 7. *Food Hydrocoll.* **2017**, *65*, 130–143, doi:10.1016/j.foodhyd.2016.11.016.

124. Loveday, S.M.; Wang, X.L.; Rao, M.A.; Anema, S.G.; Singh, H. β-Lactoglobulin nanofibrils: Effect of temperature on fibril formation kinetics, fibril morphology and the rheological properties of fibril dispersions. *Food Hydrocoll.* **2012**, *27*, 242–249, doi:10.1016/j.foodhyd.2011.07.001.

125. Li, T.; Wang, L.; Zhang, X.; Geng, H.; Xue, W.; Chen, Z. Assembly behavior, structural characterization and rheological properties of legume proteins based amyloid fibrils. *Food Hydrocoll.* **2021**, *111*, 106396, doi:10.1016/j.foodhyd.2020.106396.

126. Nguyen, T.P.; Nguyen, Q.V.; Nguyen, V.H.; Le, T.H.; Huynh, V.Q.N.; Vo, D.V.N.; Trinh, Q.T.; Kim, S.Y.; Van Le, Q. Silk fibroin-based biomaterials for biomedical applications: A review. *Polymers (Basel).* 2019, *11*.

127. Lee, H.; Dellatore, S.M.; Miller, W.M.; Messersmith, P.B. Mussel-inspired surface chemistry for multifunctional coatings. *Science (80-.).* **2007**, *318*, 426–430, doi:10.1126/science.1147241.

128. Cong, Y.; Xia, T.; Zou, M.; Li, Z.; Peng, B.; Guo, D.; Deng, Z. Mussel-inspired polydopamine coating as a versatile platform for synthesizing polystyrene/Ag nanocomposite particles with enhanced antibacterial activities. *J. Mater. Chem. B* **2014**, *2*, 3450–3461, doi:10.1039/c4tb00460d.

129. Xu, H.; Shi, X.; Ma, H.; Lv, Y.; Zhang, L.; Mao, Z. The preparation and antibacterial effects of dopa-cotton/AgNPs. *Appl. Surf. Sci.* **2011**, *257*, 6799–6803, doi:10.1016/j.apsusc.2011.02.129.

130. Sileika, T.S.; Kim, H.-D.; Maniak, P.; Messersmith, P.B. Antibacterial Performance of Polydopamine-Modified Polymer Surfaces Containing Passive and Active Components. *ACS Appl. Mater. Interfaces* **2011**, *3*, 4602–4610, doi:10.1021/am200978h.

131. Su, L.; Yu, Y.; Zhao, Y.; Liang, F.; Zhang, X. Strong Antibacterial Polydopamine Coatings Prepared by a Shaking-assisted Method. *Sci. Rep.* **2016**, *6*, doi:10.1038/srep24420.

132. Dong, P.; Hao, W.; Wang, X.; Wang, T. Fabrication and biocompatibility of polyethyleneimine/heparin self-assembly coating on NiTi alloy. *Thin Solid Films* **2008**, *516*, 5168–5171, doi:10.1016/j.tsf.2007.07.084.

133. Dong, P.; Hao, W.; Xia, Y.; Da, G.; Wang, T. Comparison Study of Corrosion Behavior and Biocompatibility of Polyethyleneimine (PEI)/Heparin and Chitosan/Heparin Coatings on NiTi alloy. *J. Mater. Sci. Technol.* **2010**, *26*, 1027–1031, doi:10.1016/S1005-0302(10)60169-7.

134. Hernandez-Montelongo, J.; Lucchesi, E.G.; Nascimento, V.F.; França, C.G.; Gonzalez, I.; Macedo, W.A.A.; Machado, D.; Lancellotti, M.; Moraes, A.M.; Beppu, M.M.; et al. Antibacterial and non-cytotoxic ultra-thin polyethylenimine film. *Mater. Sci. Eng. C* **2017**, *71*, 718–724, doi:10.1016/j.msec.2016.10.064.

135. Forrest, M.L.; Koerber, J.T.; Pack, D.W. A degradable polyethylenimine derivative with low toxicity for highly efficient gene delivery. *Bioconjug. Chem.* **2003**, *14*, 934–940, doi:10.1021/bc034014g.

136. Brunot, C.; Ponsonnet, L.; Lagneau, C.; Farge, P.; Picart, C.; Grosgogeat, B. Cytotoxicity of polyethyleneimine (PEI), precursor base layer of polyelectrolyte multilayer films. *Biomaterials* **2007**, *28*, 632–640, doi:10.1016/j.biomaterials.2006.09.026.

137. Liu, Z.M.; Lee, S.Y.; Sarun, S.; Peschel, D.; Groth, T. Immobilization of poly (ethylene imine) on poly (l-lactide) promotes MG63 cell proliferation and function. *J. Mater. Sci. Mater. Med.* **2009**, *20*, 2317–2326, doi:10.1007/s10856-009-3806-1.

138. Liudmila M, M.; Dmitriy A, R.; Maria G, F.; Evgeniy E, F. Ultrathin polyethyleneimine (PEI) films for culturing of the human mesenchymal stromal cells (hMSCs). *J. Cardiovasc. Med. Cardiol.* **2020**, 255–261,

doi:10.17352/2455-2976.000148.

139. Kim, M.M.; Kim, S.K. Effect of phloroglucinol on oxidative stress and inflammation. *Food Chem. Toxicol.* **2010**, *48*, 2925–2933, doi:10.1016/j.fct.2010.07.029.

140. Kang, K.A.; Lee, K.H.; Chae, S.; Zhang, R.; Jung, M.S.; Ham, Y.M.; Baik, J.S.; Lee, N.H.; Hyun, J.W. Cytoprotective effect of phloroglucinol on oxidative stress induced cell damage via catalase activation. *J. Cell. Biochem.* **2006**, *97*, 609–620, doi:10.1002/jcb.20668.

141. Mody, N.; Parhami, F.; Sarafian, T.A.; Demer, L.L. Oxidative stress modulates osteoblastic differentiation of vascular and bone cells. *Free Radic. Biol. Med.* **2001**, *31*, 509–519, doi:10.1016/S0891-5849(01)00610-4.

142. Bai, X.C.; Lu, D.; Bai, J.; Zheng, H.; Ke, Z.Y.; Li, X.M.; Luo, S.Q. Oxidative stress inhibits osteoblastic differentiation of bone cells by ERK and NF-κB. *Biochem. Biophys. Res. Commun.* **2004**, *314*, 197–207, doi:10.1016/j.bbrc.2003.12.073.

143. Kim, M.; Kim, G. Electrospun PCL/phlorotannin nanofibres for tissue engineering: Physical properties and cellular activities. *Carbohydr. Polym.* **2012**, *90*, 592–601, doi:10.1016/j.carbpol.2012.05.082.

144. Yeo, M.; Jung, W.K.; Kim, G. Fabrication, characterisation and biological activity of phlorotannin-conjugated PCL/β-TCP composite scaffolds for bone tissue regeneration. *J. Mater. Chem.* **2012**, *22*, 3568–3577, doi:10.1039/c2jm14725d.

145. Fraser, J.H.E.; Helfrich, M.H.; Wallace, H.M.; Ralston, S.H. Hydrogen peroxide, but not superoxide, stimulates bone resorption in mouse calvariae. *Bone* **1996**, *19*, 223–226, doi:10.1016/8756-3282(96)00177-9.

146. Douglas, T.E.L.; Dokupil, A.; Reczyńska, K.; Brackman, G.; Krok-Borkowicz, M.; Keppler, J.K.; Božič, M.; Van Der Voort, P.; Pietryga, K.; Samal, S.K.; et al. Enrichment of enzymatically mineralized gellan gum hydrogels with

phlorotannin-rich Ecklonia cava extract Seanol® to endow antibacterial properties and promote mineralization. *Biomed. Mater.* **2016**, *11*, doi:10.1088/1748-6041/11/4/045015.

147. Eom, S.H.; Kim, Y.M.; Kim, S.K. Antimicrobial effect of phlorotannins from marine brown algae. *Food Chem. Toxicol.* 2012, *50*, 3251–3255.

148. Lopes, G.; Sousa, C.; Silva, L.R.; Pinto, E.; Andrade, P.B.; Bernardo, J.; Mouga, T.; Valentão, P. Can phlorotannins purified extracts constitute a novel pharmacological alternative for microbial infections with associated inflammatory conditions? *PLoS One* **2012**, *7*, e31145, doi:10.1371/journal.pone.0031145.

149. Lee, D.S.; Cho, Y.S.; Je, J.Y. Antioxidant and Antibacterial Activities of Chitosan-Phloroglucinol Conjugate. *Fish. Aquat. Sci.* **2013**, *16*, 229–235, doi:10.5657/FAS.2013.0229.

150. Lišková, J.; Douglas, T.E.L.; Beranová, J.; Skwarczyńska, A.; Božič, M.; Samal, S.K.; Modrzejewska, Z.; Gorgieva, S.; Kokol, V.; Bačáková, L. Chitosan hydrogels enriched with polyphenols: Antibacterial activity, cell adhesion and growth and mineralization. *Carbohydr. Polym.* **2015**, *129*, 135–142, doi:10.1016/j.carbpol.2015.04.043.

151. Douglas, T.E.L.; Keppler, J.K.; Vandrovcová, M.; Plencner, M.; Beranová, J.; Feuereisen, M.; Parakhonskiy, B. V.; Svenskaya, Y.; Atkin, V.; Ivanova, A.; et al. Enhancement of Biomimetic Enzymatic Mineralization of Gellan Gum Polysaccharide Hydrogels by Plant-Derived Gallotannins. *Int. J. Mol. Sci. 2020, Vol. 21, Page 2315* **2020**, *21*, 2315, doi:10.3390/IJMS21072315.

152. Chai, Y.; Lee, H.J.; Shaik, A.A.; Nkhata, K.; Xing, C.; Zhang, J.; Jeong, S.J.; Kim, S.H.; Lü, J. Penta-O-galloyl-β-D-glucose induces G1arrest and DNA replicative S-phase arrest independently of P21 cyclin-dependent kinase inhibitor 1A, P27 cyclin-dependent kinase inhibitor 1B and P53 in human breast cancer cells and is orally active against triple-negative xenograft growth. *Breast Cancer Res.* **2010**, *12*, 1–11,

doi:10.1186/BCR2634/FIGURES/7.

153. Mayorova, O.A.; Jolly, B.C.N.; Verkhovskii, R.A.; Plastun, V.O.; Sindeeva, O.A.; Douglas, T.E.L. pH-Sensitive Dairy-Derived Hydrogels with a Prolonged Drug Release Profile for Cancer Treatment. *Mater. 2021, Vol. 14, Page 749* **2021**, *14*, 749, doi:10.3390/MA14040749.

154. Hagerman, A.E. Chemistry of Tannin-Protein Complexation. *Chem. Significance Condens. Tann.* **1989**, 323–333, doi:10.1007/978-1-4684-7511-1_20.

155. Kwok, D.Y.; Neumann, A.W. Contact angle measurement and contact angle interpretation. *Adv. Colloid Interface Sci.* **1999**, *81*, 167–249, doi:10.1016/S0001-8686(98)00087-6.

156. Ferrari, M.; Cirisano, F.; Morán, M.C. Mammalian Cell Behavior on Hydrophobic Substrates: Influence of Surface Properties. *Colloids and Interfaces* **2019**, *3*, 48, doi:10.3390/colloids3020048.

157. Briggs, D. *Surface Analysis of Polymers by XPS and Static SIMS*; Cambridge University Press, 1998; ISBN 9780521352222.

158. Stevie, F.A.; Donley, C.L. Introduction to x-ray photoelectron spectroscopy. *J. Vac. Sci. Technol. A Vacuum, Surfaces, Film.* **2020**, *38*, 063204, doi:10.1116/6.0000412.

159. Easton, C.D.; Kinnear, C.; McArthur, S.L.; Gengenbach, T.R. Practical guides for x-ray photoelectron spectroscopy: Analysis of polymers. *J. Vac. Sci. Technol. A Vacuum, Surfaces, Film.* **2020**, *38*, 023207, doi:10.1116/1.5140587.

160. Kim, J.; Jung, D.; Park, Y.; Kim, Y.; Moon, D.W.; Lee, T.G. Quantitative analysis of surface amine groups on plasma-polymerized ethylenediamine films using UV–visible spectroscopy compared to chemical derivatization with FT-IR spectroscopy, XPS and TOF-SIMS. *Appl. Surf. Sci.* **2007**, *253*, 4112–4118, doi:10.1016/J.APSUSC.2006.09.011.

161. Graf, N.; Yegen, E.; Gross, T.; Lippitz, A.; Weigel, W.; Krakert, S.; Terfort, A.; Unger, W.E.S. XPS and NEXAFS studies of aliphatic and aromatic amine species on functionalized surfaces. *Surf. Sci.* **2009**, *603*, 2849–2860, doi:10.1016/j.susc.2009.07.029.

162. Briggs, D.; Seah, M.P. Practical Surface Analysis, Auger and X-ray Photoelectron Spectroscopy (Volume 1). **1996**, 674.

163. Ghobeira, R.; Esbah Tabaei, P.S.; Morent, R.; De Geyter, N. Chemical characterization of plasma-activated polymeric surfaces via XPS analyses: A review. *Surfaces and Interfaces* **2022**, *31*, doi:10.1016/J.SURFIN.2022.102087.

164. Beamson, G.; Briggs, D. *High Resolution XPS of Organic Polymers: The Scienta ESCA300 Database*; American Chemical Society (ACS), 1992; Vol. 70;.

165. Norris, K.; Mishukova, O.I.; Zykwinska, A.; Colliec-Jouault, S.; Sinquin, C.; Koptioug, A.; Cuenot, S.; Kerns, J.G.; Surmeneva, M.A.; Surmenev, R.A.; et al. Marine polysaccharide-collagen coatings on Ti6Al4V alloy formed by self-assembly. *Micromachines* **2019**, *10*, 68, doi:10.3390/mi10010068.

166. Michelmore, A.; Martinek, P.; Sah, V.; Short, R.D.; Vasilev, K. Surface morphology in the early stages of plasma polymer film growth from amine-containing monomers. *Plasma Process. Polym.* **2011**, *8*, 367–372, doi:10.1002/ppap.201000140.

167. Wu, S.; Zhang, B.; Liu, Y.; Suo, X.; Li, H. Influence of surface topography on bacterial adhesion: A review (Review). *Biointerphases* **2018**, *13*, 060801, doi:10.1116/1.5054057.

168. Barth, A. Infrared spectroscopy of proteins. *Biochim. Biophys. Acta - Bioenerg.* **2007**, *1767*, 1073–1101, doi:10.1016/j.bbabio.2007.06.004.

169. Abbas, A.; Vivien, C.; Bocquet, B.; Guillochon, D.; Supiot, P. Preparation and Multi-Characterization of Plasma Polymerized Allylamine Films. *Plasma Process. Polym.* **2009**, *6*, 593–604, doi:10.1002/ppap.200900016.

170. Noel, S.; Liberelle, B.; Robitaille, L.; De Crescenzo, G. Quantification of primary amine groups available for subsequent biofunctionalization of polymer surfaces. *Bioconjug. Chem.* **2011**, *22*, 1690–1699, doi:10.1021/bc200259c.

171. Coussot, G.; Perrin, C.; Moreau, T.; Dobrijevic, M.; Le Postollec, A.; Vandenabeele-Trambouze, O. A rapid and reversible colorimetric assay for the characterization of aminated solid surfaces. *Anal. Bioanal. Chem.* **2011**, *399*, 1061–1069, doi:10.1007/s00216-010-4363-7.

172. Klages, C.P.; Kotula, S. Critical remarks on chemical derivatization analysis of plasma-treated polymer surfaces and plasma polymers. *Plasma Process. Polym.* **2016**, *13*, 1213–1223, doi:10.1002/PPAP.201600210.

173. Manakhov, A.; Michlíček, M.; Felten, A.; Pireaux, J.J.; Nečas, D.; Zajíčková, L. XPS depth profiling of derivatized amine and anhydride plasma polymers: Evidence of limitations of the derivatization approach. *Appl. Surf. Sci.* **2017**, *394*, 578–585, doi:10.1016/j.apsusc.2016.10.099.

174. Girard-Lauriault, P.L.; Unger, W.E.S.; Dietrich, P.M.; Holländer, A. Innovative and Established Strategies for the Surface Analysis of Nitrogen and Oxygen-Rich Plasma Polymer Films by XPS: An Introductory Guide. *Plasma Process. Polym.* **2015**, *12*, 953–967, doi:10.1002/ppap.201500115.

175. Ruiz, J.C.; Taheri, S.; Michelmore, A.; Robinson, D.E.; Short, R.D.; Vasilev, K.; Förch, R. Approaches to quantify amine groups in the presence of hydroxyl functional groups in plasma polymerized thin films. *Plasma Process. Polym.* **2014**, *11*, 888–896, doi:10.1002/ppap.201400016.

176. Finke, B.; Luethen, F.; Schroeder, K.; Mueller, P.D.; Bergemann, C.; Frant, M.; Ohl, A.; Nebe, B.J. The effect of positively charged plasma polymerization on initial osteoblastic focal adhesion on titanium surfaces. *Biomaterials* **2007**, *28*, 4521–4534, doi:10.1016/j.biomaterials.2007.06.028.

177. St-Georges-Robillard, A.; Ruiz, J.C.; Petit, A.; Wang, H.T.; Mwale, F.; Elkin, B.; Oehr, C.; Lerouge, S.; Wertheimer, M.R. Adhesion of U-937 monocytes on

different amine-functionalised polymer surfaces. *Plasma Process. Polym.* **2012**, *9*, 243–252, doi:10.1002/ppap.201100128.

178. Mangindaan, D.; Kuo, W.H.; Chang, C.C.; Wang, S.L.; Liu, H.C.; Wang, M.J. Plasma polymerization of amine-containing thin films and the studies on the deposition kinetics. *Surf. Coatings Technol.* **2011**, *206*, 1299–1306, doi:10.1016/J.SURFCOAT.2011.08.046.

179. Choukourov, A.; Kousal, J.; Slavínská, D.; Biederman, H.; Fuoco, E.R.; Tepavcevic, S.; Saucedo, J.; Hanley, L. Growth of primary and secondary amine films from polyatomic ion deposition. *Vacuum* **2004**, *75*, 195–205, doi:10.1016/J.VACUUM.2004.02.006.

180. Millhouse, E.; Jose, A.; Sherry, L.; Lappin, D.F.; Patel, N.; Middleton, A.M.; Pratten, J.; Culshaw, S.; Ramage, G. Development of an in vitro periodontal biofilm model for assessing antimicrobial and host modulatory effects of bioactive molecules. *BMC Oral Health* **2014**, *14*, 1–11, doi:10.1186/1472-6831-14-80/FIGURES/4.

181. Ramage, G.; Lappin, D.F.; Millhouse, E.; Malcolm, J.; Jose, A.; Yang, J.; Bradshaw, D.J.; Pratten, J.R.; Culshaw, S. The epithelial cell response to health and disease associated oral biofilm models. *J. Periodontal Res.* **2017**, *52*, 325–333, doi:10.1111/JRE.12395.

182. Muchova, M.; Balacco, D.L.; Grant, M.M.; Chapple, I.L.C.; Kuehne, S.A.; Hirschfeld, J. Fusobacterium nucleatum Subspecies Differ in Biofilm Forming Ability in vitro. *Front. Oral Heal.* **2022**, *3*, 853618, doi:10.3389/FROH.2022.853618.

183. Guggenheim, B.; Gmür, R.; Galicia, J.C.; Stathopoulou, P.G.; Benakanakere, M.R.; Meier, A.; Thurnheer, T.; Kinane, D.F. In vitro modeling of host-parasite interactions: The "subgingival" biofilm challenge of primary human epithelial cells. *BMC Microbiol.* **2009**, *9*, 1–12, doi:10.1186/1471-2180-9-280/TABLES/3.

184. Livak, K.J.; Schmittgen, T.D. Analysis of relative gene expression data using

real-time quantitative PCR and the 2-ΔΔCT method. *Methods* **2001**, *25*, 402–408, doi:10.1006/meth.2001.1262.

185. Hempel, U.; Hintze, V.; Möller, S.; Schnabelrauch, M.; Scharnweber, D.; Dieter, P. Artificial extracellular matrices composed of collagen i and sulfated hyaluronan with adsorbed transforming growth factor β1 promote collagen synthesis of human mesenchymal stromal cells. *Acta Biomater.* **2012**, *8*, 659–666, doi:10.1016/j.actbio.2011.10.026.

186. Stalder, A.F.; Kulik, G.; Sage, D.; Barbieri, L.; Hoffmann, P. A snake-based approach to accurate determination of both contact points and contact angles. *Colloids Surfaces A Physicochem. Eng. Asp.* **2006**, *286*, 92–103, doi:10.1016/J.COLSURFA.2006.03.008.

187. Dai, X.J.; Plessis, J. Du; Kyratzis, I.L.; Maurdev, G.; Huson, M.G.; Coombs, C. Controlled amine functionalization and hydrophilicity of a poly(lactic acid) fabric. *Plasma Process. Polym.* **2009**, *6*, 490–497, doi:10.1002/ppap.200800216.

188. France, R.M.; Short, R.D.; Dawson, R.A.; MacNeil, S. Attachment of human keratinocytes to plasma co-polymers of acrylic acid/octa-1,7-diene and allyl amine/octa-1,7-diene. *J. Mater. Chem.* **1998**, *8*, 37–42, doi:10.1039/A705098D.

189. Calderon, J.G.; Harsch, A.; Gross, G.W.; Timmons, R.B. Stability of plasma-polymerized allylamine films with sterilization by autoclaving. **1998**, doi:10.1002/(SICI)1097-4636(19981215)42:4.

190. Hamerli, P.; Weigel, T.; Groth, T.; Paul, D. Surface properties of and cell adhesion onto allylamine-plasma-coated polyethylenterephtalat membranes. *Biomaterials* **2003**, *24*, 3989–3999, doi:10.1016/S0142-9612(03)00312-0.

191. Blanksby, S.J.; Ellison, G.B. Bond dissociation energies of organic molecules. *Acc. Chem. Res.* **2003**, *36*, 255–263, doi:10.1021/ar020230d.

192. Roach, P.; Farrar, D.; Perry, C.C. Interpretation of protein adsorption: Surface-induced conformational changes. *J. Am. Chem. Soc.* **2005**, *127*, 8168–8173, doi:10.1021/JA042898O/ASSET/IMAGES/MEDIUM/JA042898ON00001.GIF.

193. Coad, B.R.; Jasieniak, M.; Griesser, S.S.; Griesser, H.J. Controlled covalent surface immobilisation of proteins and peptides using plasma methods. *Surf. Coatings Technol.* **2013**, *233*, 169–177, doi:10.1016/J.SURFCOAT.2013.05.019.

194. Ward, C.L.; Sanchez, C.J.; Pollot, B.E.; Romano, D.R.; Hardy, S.K.; Becerra, S.C.; Rathbone, C.R.; Wenke, J.C. Soluble factors from biofilms of wound pathogens modulate human bone marrow-derived stromal cell differentiation, migration, angiogenesis, and cytokine secretion Microbe-host interactions and microbial pathogenicity. *BMC Microbiol.* **2015**, *15*, 1–14, doi:10.1186/S12866-015-0412-X/FIGURES/5.

195. Vyas, K.S.; Wong, L.K. Detection of Biofilm in Wounds as an Early Indicator for Risk for Tissue Infection and Wound Chronicity. *Ann. Plast. Surg.* **2016**, *76*, 127–131, doi:10.1097/SAP.0000000000000440.

196. Komori, T. Regulation of osteoblast differentiation by runx2. In Proceedings of the Advances in Experimental Medicine and Biology; Springer, Boston, MA, 2010; Vol. 658, pp. 43–49.

197. Silvent, J.; Nassif, N.; Helary, C.; Azaïs, T.; Sire, J.Y.; Guille, M.M.G. Collagen Osteoid-Like Model Allows Kinetic Gene Expression Studies of Non-Collagenous Proteins in Relation with Mineral Development to Understand Bone Biomineralization. *PLoS One* **2013**, *8*, e57344, doi:10.1371/journal.pone.0057344.

198. Sugawara, Y.; Suzuki, K.; Koshikawa, M.; Ando, M.; Iida, J. Necessity of Enzymatic Activity of Alkaline Phosphatase for Mineralization of Osteoblastic Cells. *Jpn. J. Pharmacol.* **2002**, *88*, 262–269,

doi:10.1254/JJP.88.262.

199. Zohar, R.; Cheifetz, S.; McCulloch, C.A.G.; Sodek, J. Analysis of intracellular osteopontin as a marker of osteoblastic cell differentiation and mesenchymal cell migration. *Eur. J. Oral Sci.* **1998**, *106 Suppl 1*, 401–407, doi:10.1111/J.1600-0722.1998.TB02206.X.

200. Manolagas, S.C. Osteocalcin promotes bone mineralization but is not a hormone. *PLOS Genet.* **2020**, *16*, e1008714, doi:10.1371/JOURNAL.PGEN.1008714.

201. Alves, C.M.; Yang, Y.; Marton, D.; Carnes, D.L.; Ong, J.L.; Sylvia, V.L.; Dean, D.D.; Reis, R.L.; Agrawal, C.M. Plasma surface modification of poly(D,L-lactic acid) as a tool to enhance protein adsorption and the attachment of different cell types. *J. Biomed. Mater. Res. Part B Appl. Biomater.* **2008**, *87B*, 59–66, doi:10.1002/JBM.B.31068.

202. Hempel, U.; Hefti, T.; Dieter, P.; Schlottig, F. Response of human bone marrow stromal cells, MG-63, and SaOS-2 to titanium-based dental implant surfaces with different topography and surface energy. *Clin. Oral Implants Res.* **2013**, *24*, 174–182, doi:10.1111/J.1600-0501.2011.02328.X.

203. Pittenger, M.F. Mesenchymal stem cells from adult bone marrow. *Methods Mol. Biol.* **2008**, *449*, 27–44, doi:10.1007/978-1-60327-169-1_2/FIGURES/1_2.

Appendix A. XPS spectra of polymers

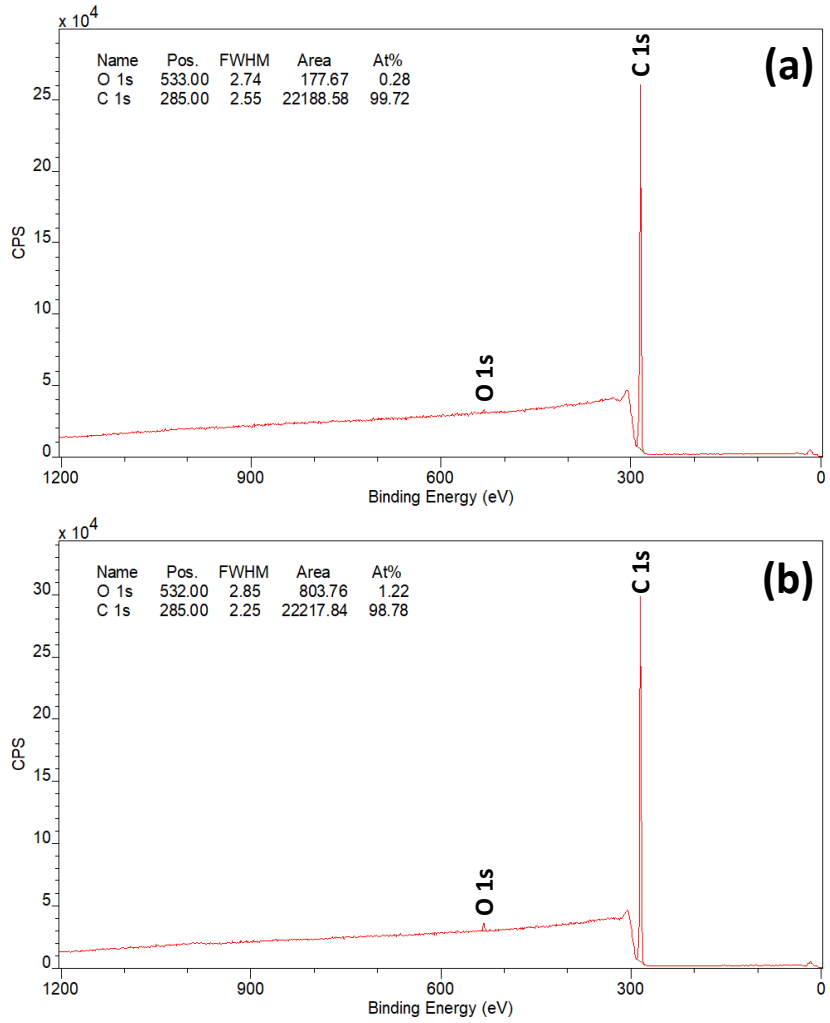

Figure A.1: XPS wide survey spectra of PP (a) before and (b) after TFBA derivatisation.

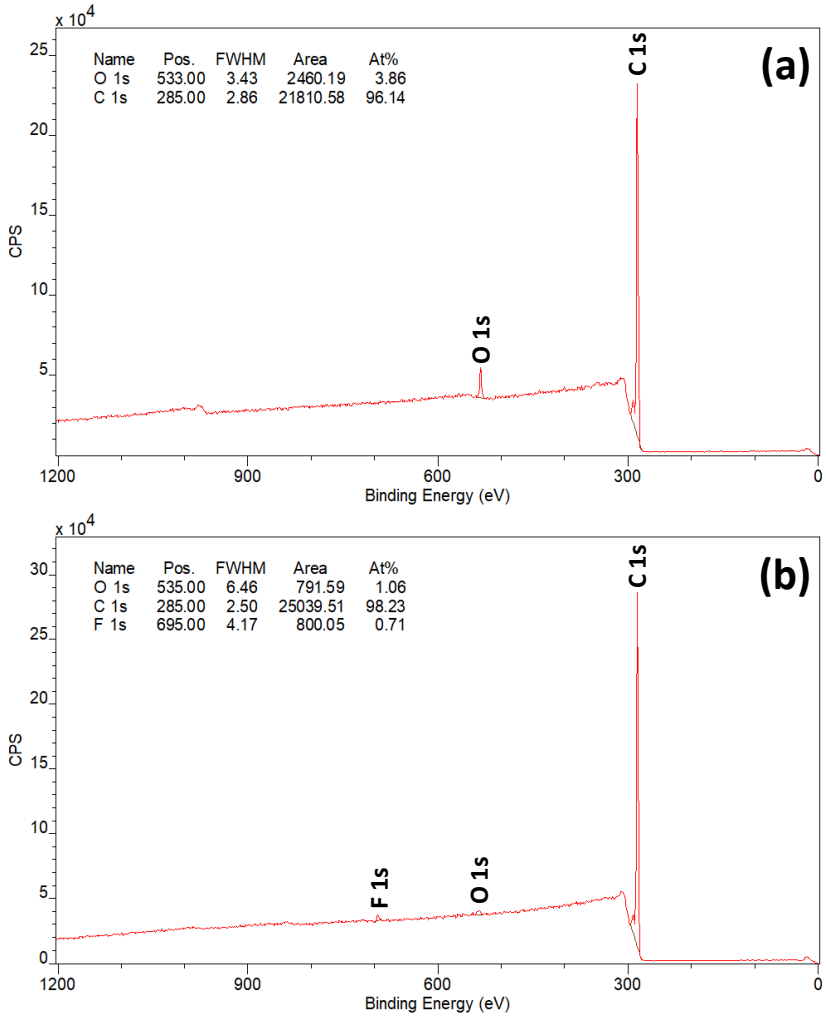

Figure A.2: XPS wide survey spectra of PS (a) before and (b) after TFBA derivatisation.

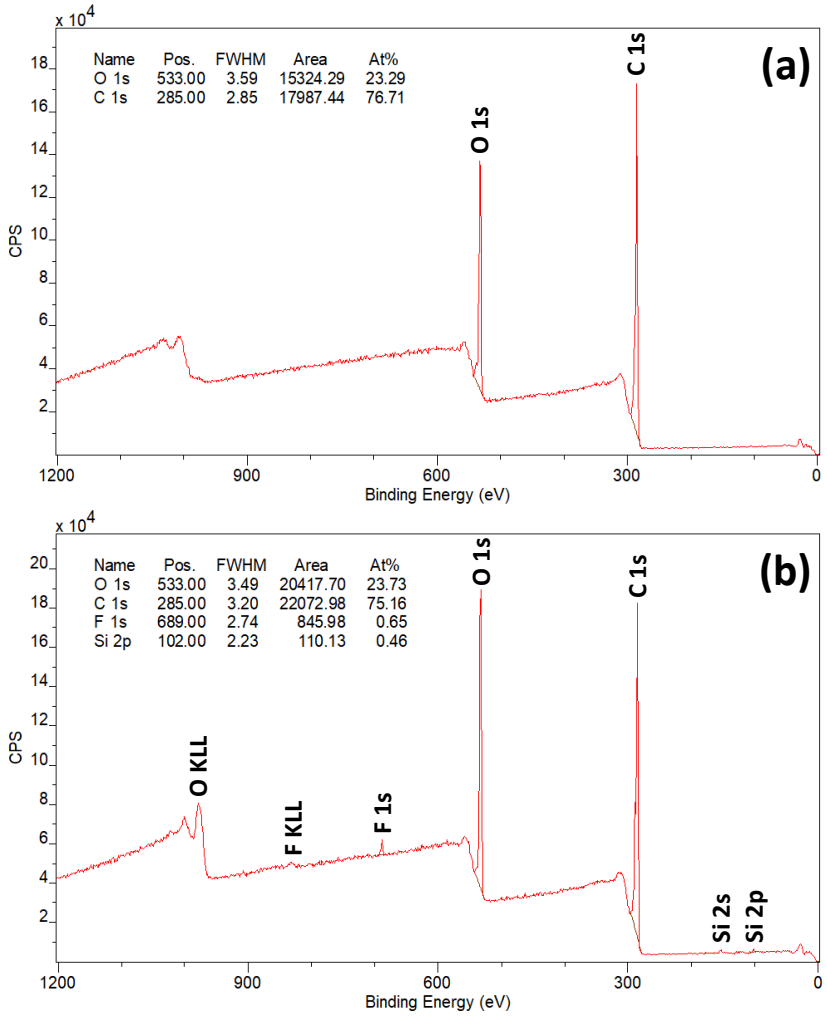

Figure A.3: XPS wide survey spectra of PET (a) before and (b) after TFBA derivatisation.

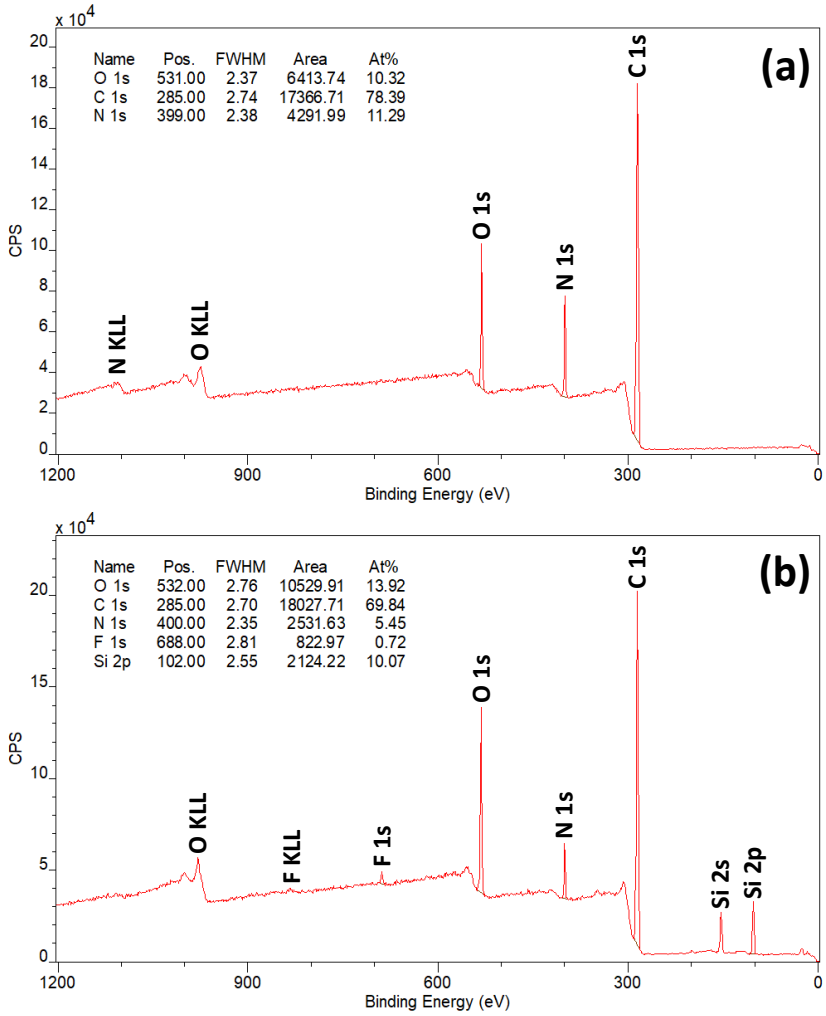

Figure A.4: XPS wide survey spectra of N6 (a) before and (b) after TFBA derivatisation.

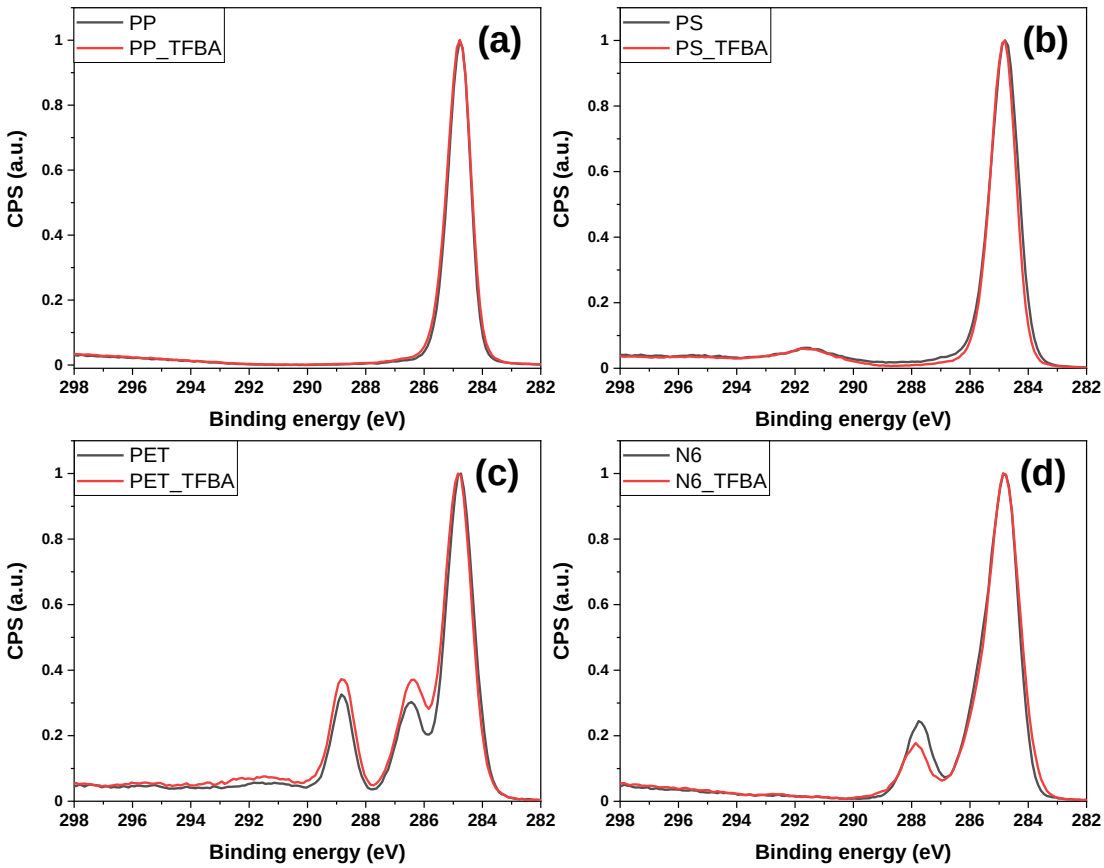

Figure A.5: XPS high-resolution normalised spectra of (a) PP, (b) PS, (c) PET, and (d) N6 before (black line) and after (red line) TFBA derivatisation.

Appendix B. XPS analyses of allylamine plasma polymer coatings made at UoLiv

AApp coatings were made at UoLiv by Dr. Stephane Simon and Prof. James Bradley in a different plasma reactor. The derivatisation of these coatings and the XPS analyses before and after derivatisation were performed at Lancaster University.

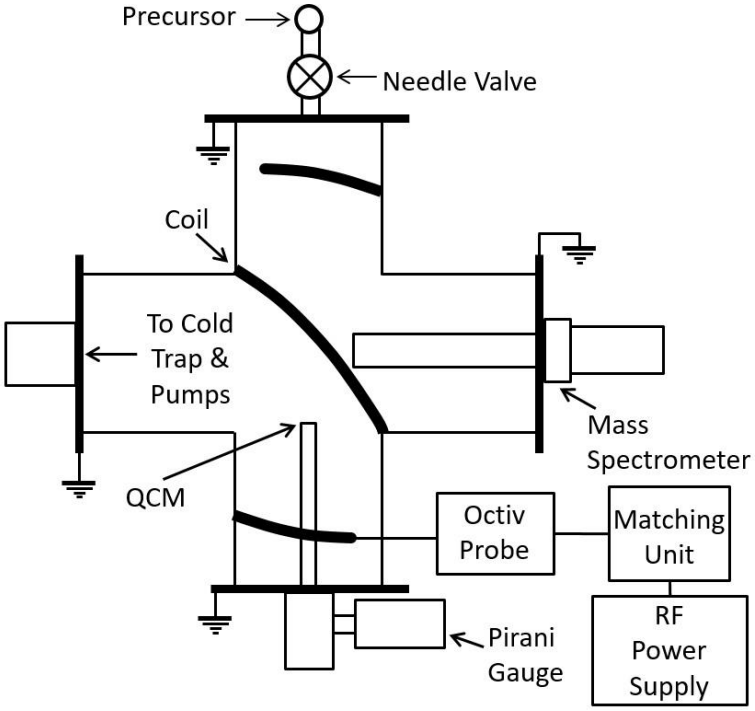

Figure B.1: Schematic diagram of the plasma reactor and experimental set-up used at the UoLiv to produce allylamine plasma polymer coatings.

Figure B.1 represents the schematic diagram of the plasma reactor used at the UoLiv where some AApp coatings were made for comparison with some made at Lancaster.

XPS analyses were performed before and after derivatisation for AApp3 (2.7 Pa – 20 W) and AApp4 (80 Pa – 5 W). Representative XPS wide scan spectra are shown in Figure B.2 for AApp3 and Figure B.3 for AApp4. High resolution spectra of carbon and fluorine are shown in Figure B.4.

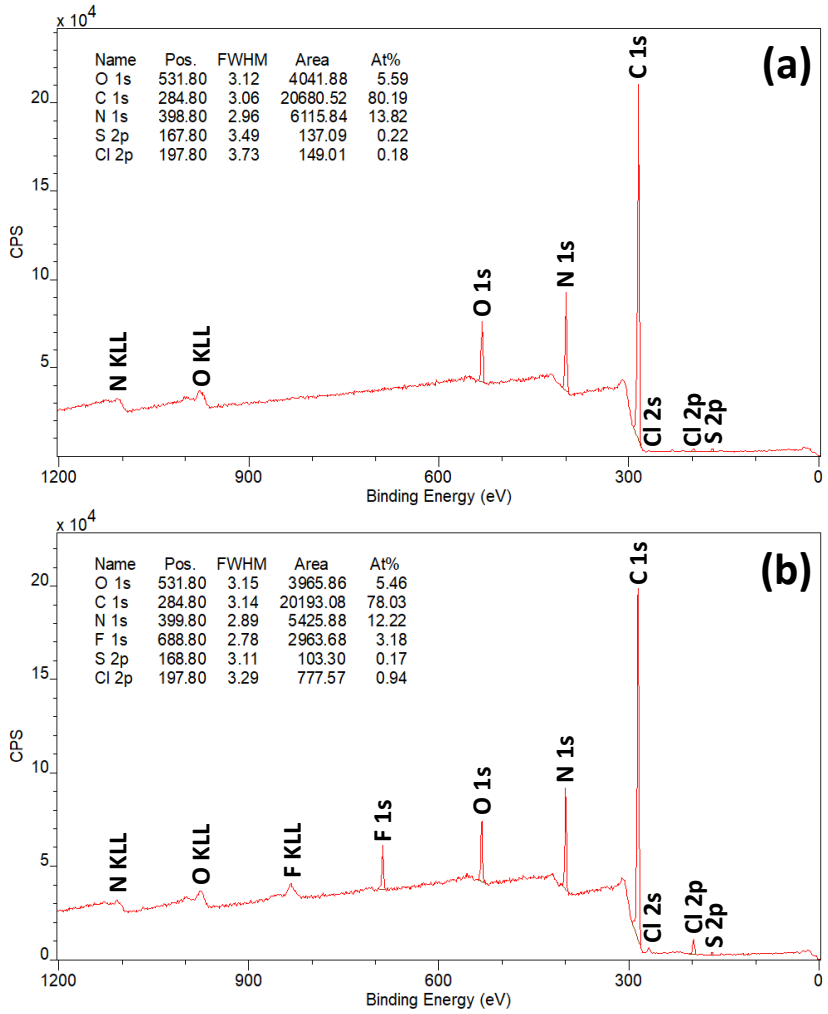

Figure B.2: Representative XPS wide scan spectra of AApp3 (2.7 Pa – 20 W) (a) before and (b) after TFBA derivatisation. Fluorine peak appears at 689 eV after derivatisation.

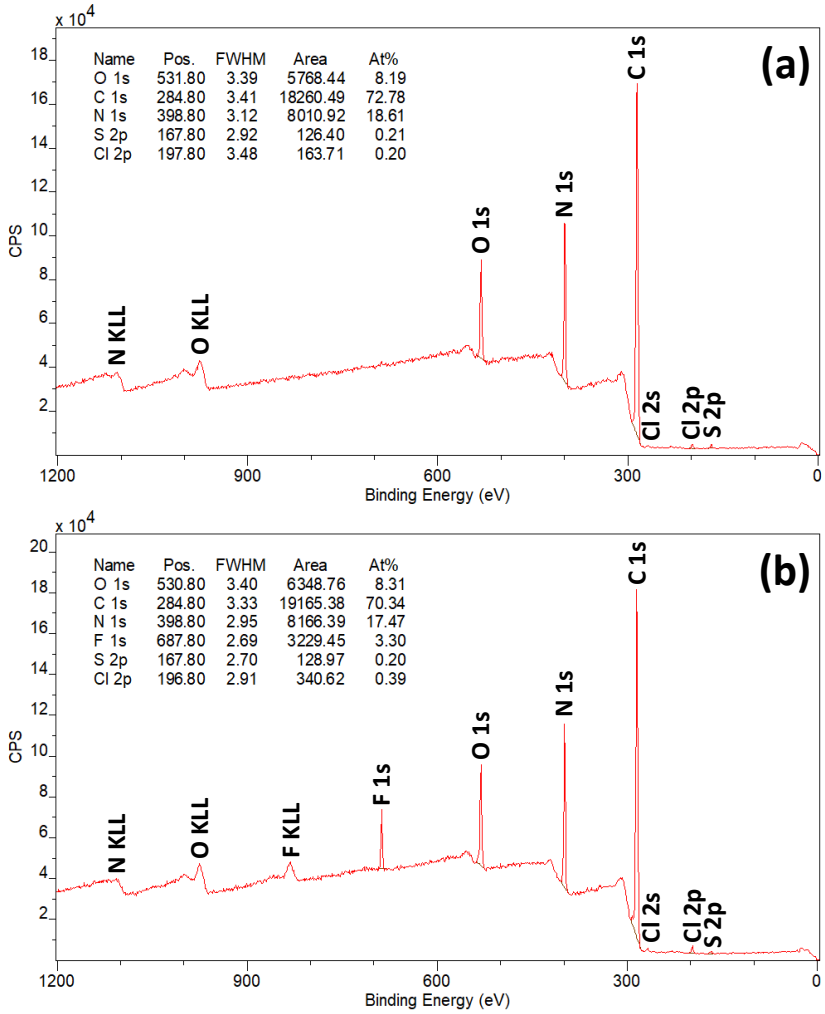

Figure B.3: Representative XPS wide scan spectra of AApp4 (80 Pa – 5 W) (a) before and (b) after TFBA derivatisation. Fluorine peak appears at 689 eV after derivatisation.

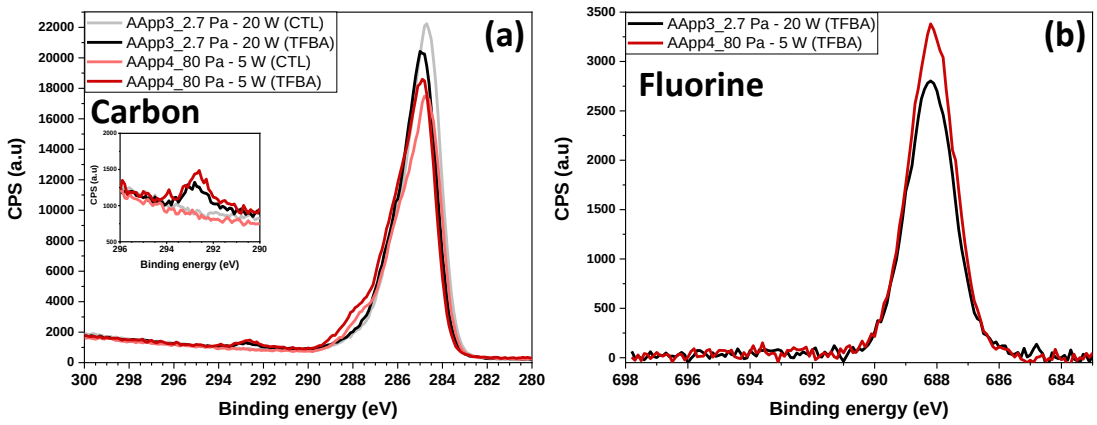

Figure B.4: (a) C1s with an insert graph corresponding to the CF_3 peak before (CTL) and after TFBA derivatisation, and (b) F1s high-resolution spectra after derivatisation of AApp coatings. C1s peaks are fitted with different carbon-nitrogen and carbon-oxygen environments. CF_3 environment clearly appeared after derivatisation for both coatings. The areas of CF_3 and F peaks are slightly higher for AApp4 compared to AApp3.

Appendix C. AFM analyses of the WPI fibrillar coatings

WPI fibrillar coatings were analysed by AFM images as shown in Figure C.1. Diameters *d* of WPI fibrils were *d* = 20.2 ± 2.5 nm for [WPI+PG0.1%] and *d* = 22.0 ± 1.7 nm for [WPI+PG0.5%], showing that fibril diameter seems unaffected by PG concentration as previously mentioned with the SEM images. Surface coverage was estimated to be about 33% and 49% for WPI+PG0.1% and WPI+PG0.5%, respectively (Figure C.2).

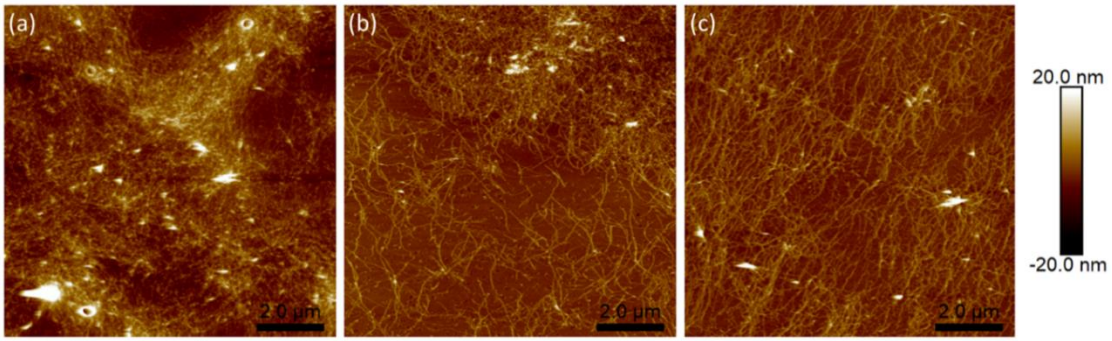

Figure C.1: AFM images of (a) WPI, (b) [WPI+PG0.1%] and (c) [WPI+PG0.5%] fibril coatings. XY scale bar: 2 µm. Z scale bar: (-20;+20) nm.

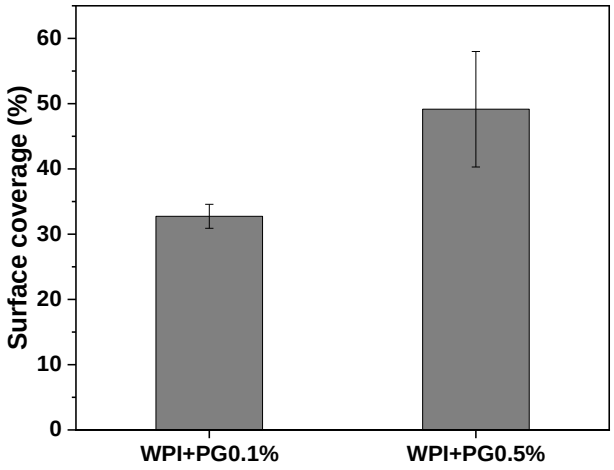

Figure C.2: AFM surface coverage associated to WPI+PG0.1% and WPI+PG0.5%.

Appendix D. SEM image of the biofilm used for the *in vitro* tests

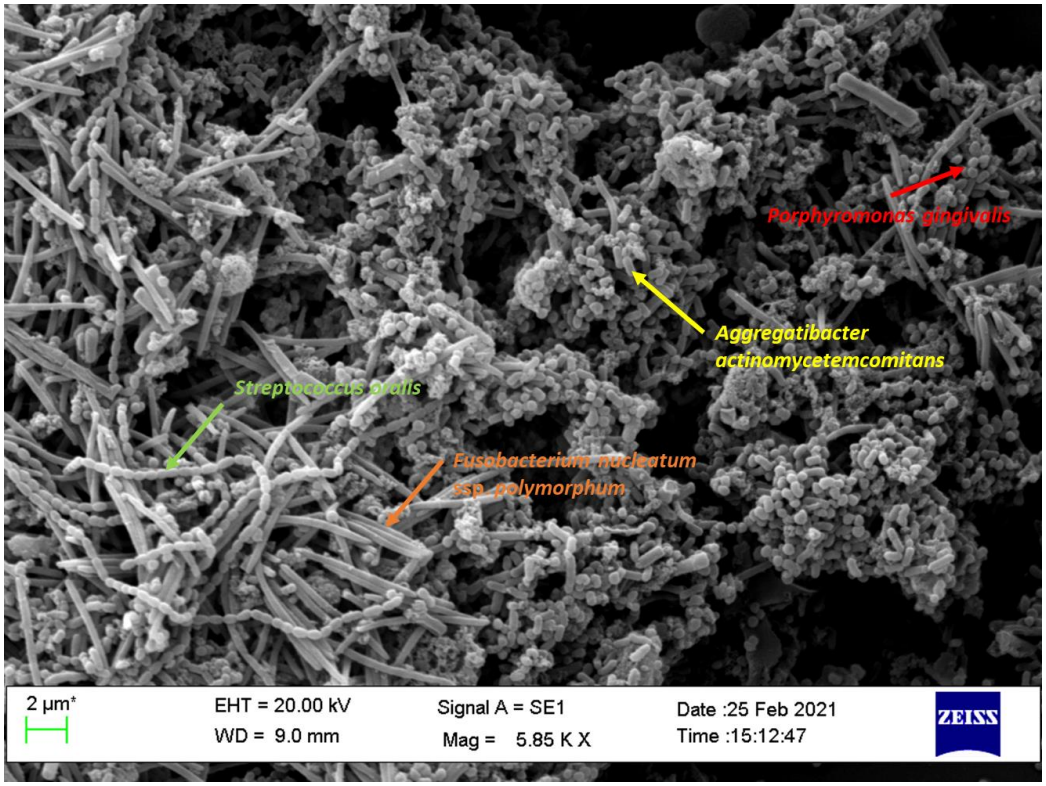

Figure D.1: SEM image of the biofilm used for the in vitro tests, constituted of 4 bacteria, namely Streptococcus oralis, Fusobacterium nucleatum esp. polymorphum, Aggregatibacter actinomycetemcomitans, and Porphyromonas gingivalis.

A biofilm image used in the study is shown in Figure D.1. The different bacteria that form the biofilm are all present in the oral cavity and can be responsible of different infections, for example:

- *Streptococcus oralis*: meningitis.
- *Fusobacterium nucleatum esp. polymorphum*: Lemierre's syndrome.
- *Aggregatibacter actinomycetemcomitans*: periodontitis.
- *Porphyromonas gingivalis*: gingivitis, periodontitis.

Appendix E. Minimum inhibitory concentration test of PG

This test was performed by Dr. Bethany Lee Patenall from Bath University whom I would like to acknowledge.

The minimum inhibitory concentration (MIC) of phloroglucinol was assessed against four species of bacteria: two Gram-positive species *Staphylococcus aureus* (*S. aureus*), *Enterococcus faecalis* (*E. faecalis*) and two Gram-negative species *Pseudomonas aeruginosa* (*P. aeruginosa*) and *Escherichia coli* (*E. coli*) to assess which species are theoretically more susceptible.

Following a clinical laboratory standards institute (CLSI) protocol, the MIC was determined at being between the lowest concentration of a drug which inhibited bacterial growth and the highest concentration of a drug with allowed for bacterial growth.

Bacterial growth corresponds to an increase in absorbance measurable at 600 nm. As the number of bacteria increase so will the absorbance reading. Shaking is used to promote turbidity, if shaking is not used bacteria are able to form biofilms.

Bacteria were maintained in 15% (v/v) glycerol freezer stocks at -80°C. As required they were streaked out onto appropriate media to obtain single colonies. *S. aureus* was grown on tryptic soy agar (TSA), *P. aeruginosa* and *E. coli* were grown on Luria-Bertani (LB) agar and *E. faecalis* on brain-heart infused (BHI) agar. Overnight (ON) cultures of bacteria were made by inoculating a single colony into 10 mL of Muller Hinton (MH) broth and incubated for 18 h at 37°C with shaking at 200 rpm.

For MIC experiment, subcultures were created to a starting optical density (OD) of 0.1 (~105 CFU/mL). Phloroglucinol (1% w/v) was serially diluted in MH broth in a 96 well plate to a final volume of 200 mL. 200 mL of MH broth was used as a negative control and 200 mL of subculture was used as a positive untreated control. This was done in triplicate. The plate was placed into Omege FLUROstar

plate reader at 37°C for 18 h with absorbance readings at 600 nm every 4 minutes and shaking at 200 rpm.

As shown in Figure E.1, *S. aureus* did not grow which is likely due to a dead strain. MIC for other strains *E. faecalis*, *P. aeruginosa* and *E. coli* was 2.5 mg/mL (1 in 4 PG dilution correspond to 2.5 mg/mL).

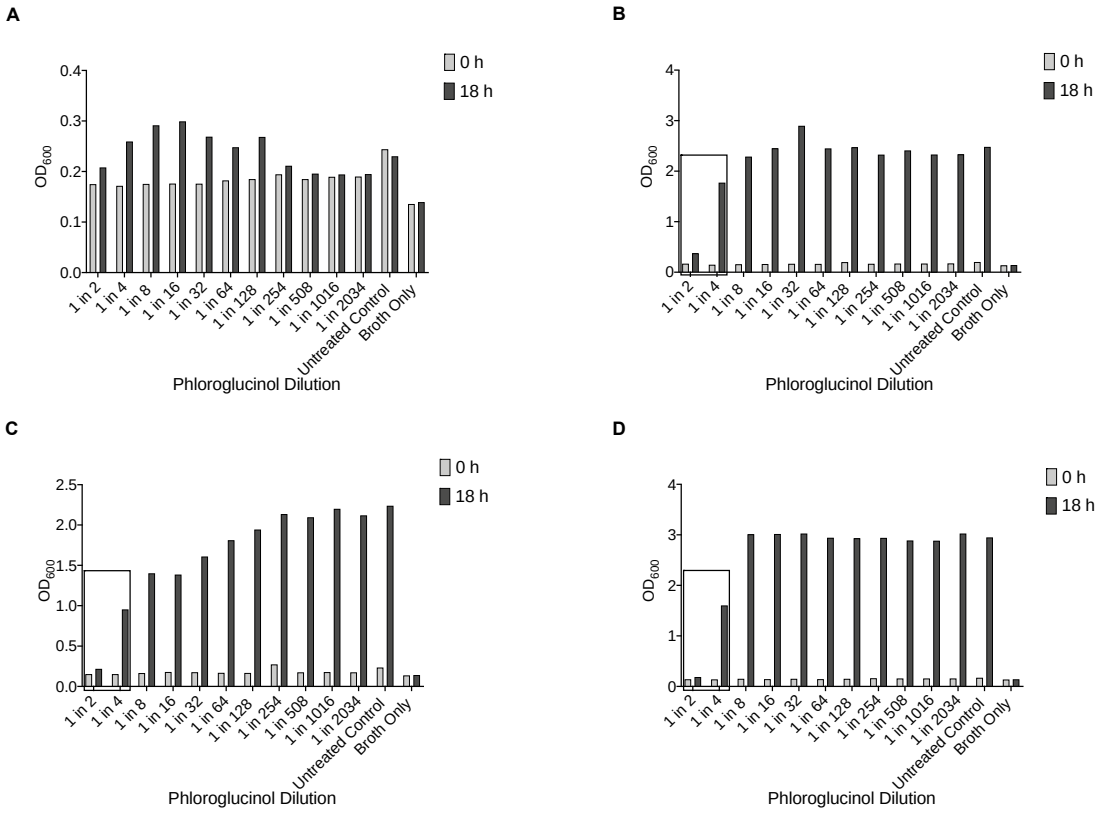

Figure E.1: Growth comparison at 0 h and 18 h for (A) S. aureus, (B) E. faecalis, (C) P. aeruginosa and (D) E. coli. MIC is highlighted in black boxes.